THERMODYNAMIC CHARACTERIZATION OF SALT COMPONENTS FOR MOLTEN SALT REACTOR FUEL

THERMODYNAMIC CHARACTERIZATION OF SALT COMPONENTS FOR MOLTEN SALT REACTOR FUEL

Proefschrift

ter verkrijging van de graad van doctor
aan de Technische Universiteit Delft,
op gezag van de Rector Magnificus prof. ir. K. C. A. M. Luyben,
voorzitter van het College voor Promoties,
in het openbaar te verdedigen op
maandag 1 februari 2016 om 10:00 uur

door

Elisa CAPELLI

MSc Nuclear Engineering
Politecnico di Milano
geboren te Ponte S. Pietro (BG), Italië.

This dissertation has been approved by the
promotor: Prof. dr. R.J.M. Konings

Composition of the doctoral committee:

Rector Magnificus	chairman
Prof. dr. R.J.M. Konings	Delft University of Technology

Independent members:

Prof. dr. ir. J. L. Kloosterman	Delft University of Technology
Prof. dr. ir. L. Luzzi	Politecnico di Milano, Italy
Prof. dr. H. A. J. Oonk	Universiteit Utrecht
Prof. dr. J. Sietsma	Delft University of Technology
Dr. R. Hania	NRG Petten

Other members:

Dr. O. Beneš	Institute for Transuranium Elements

The research described in this thesis was performed within a cooperation of the Institute for Transuranium Elements (ITU) of the Joint Research Centre (JRC) of the European Commission, P.O. Box 2340, 76125 Karlsruhe, Germany and the Department of Radiation Science and Technology, Faculty of Applied Sciences, Delft University of Technology, Melkeweg 15, 2629 JB Delft, The Netherlands. The work was supported by the EVOL project in the 7th Framework Programme of the European Commission (Grant number No. 249696).

Keywords: Molten Salt Reactor, molten salt, actinide fluorides, thermodynamics, phase diagram, heat capacity, enthalpy of mixing, vapour pressure

Printed by: Uitgeverij BOXpress || proefschiftmaken.nl

ISBN 978-946-2954-410

An electronic version of this dissertation is available at
`http://repository.tudelft.nl/`.

Se mi fosse dato di vivere senza la
possibilità di sognare e di lottare
per un sogno, bello quanto inutile,
sarei un uomo finito.

Giusto Gervasutti

CONTENTS

1

INTRODUCTION

The science of today is the technology of tomorrow.

Edward Teller

Every great advance in science has issued from a new audacity of imagination.

John Dewey

Nuclear power plants, which produce low CO_2 emission electricity [1] at competitive costs, can be part of the solution to global warming and a means of meeting the increasing energy demand from emerging and developed countries. In order to guarantee the future role of nuclear energy and improve the public perception, constant improvement of nuclear technology is needed. In particular, sustainability, safety and reliability, economic competitiveness and proliferation resistance are the four main areas of development believed to be necessary for the future success of nuclear energy.

In 2000 several countries have joined together to form the Generation IV International Forum (GIF). They identified the most important technical and societal challenges, which provided the basis for selecting six nuclear energy systems for further development [2]. Depending on their respective degree of technical maturity, the first Generation IV systems are expected to become available after 2030. Research and development activities needed to support the design and eventual deployment of those systems are underway in different countries worldwide [3]. This thesis focuses on one of the possible candidates for the next generation of nuclear power plants: the Molten Salt Reactor (MSR), which is described in the next section.

1

1.1. THE MOLTEN SALT REACTOR: TECHNOLOGY, ADVANTAGES AND OPEN CHALLENGES

Molten Salt Reactors were developed primarily at Oak Ridge National Laboratory (ORNL) beginning in the late 1940s. They were first designed for military purposes intended for a nuclear-powered aircraft [4] but recognized to be interesting also for the civilian nuclear development program. During almost 30 years of research, numerous technological challenges have been tackled and a small test reactor, called Molten Salt Reactor Experiment (MSRE) [5, 6], was built and operated successfully for several years. The experience acquired resulted in the design of a new conceptual breeder reactor, the Molten Salt Breeder Reactor (MSBR) [7]. Despite the success of this technology, the research program was terminated in the early 1970s and little advance was made until 2002. The selection of the MSR as one of the six Generation IV reactors has contributed to an increase of interest and a renaissance of research in this concept.

In the beginning, MSRs were designed as graphite-moderated reactors with a thermal neutron spectrum. Nowadays, the research has focused also on non-moderated designs, which have better reactivity performance and higher transmutation capability, converting minor actinides into shorter-lived and more tractable fission products. These studies have led to the design of two fast spectrum concepts: the Molten Salt Fast Reactor (MSFR) [8, 9] and the MOlten Salt Actinide Recycler & Transmuter (MOSART) [10, 11]. The latter concept is designed to efficiently burn the transuranic waste from spent Light Water Reactor (LWR) fuel without any uranium or thorium support. The former concept utilizes the ^{232}Th to ^{233}U fuel cycle, which produces several orders of magnitude less of transuranic wastes than a conventional once through cycle in a LWR. In addition many countries worldwide have research projects on this reactor technology [12], among them China (TMSR [13]), Japan (MSR-FUJI [14]), USA and India.

The very unique feature of the MSR technology is the liquid nature of the fuel. It consists of a molten salt mixture, in which the fissile and fertile isotopes are dissolved, circulating through the reactor core and the primary loop. A dual function is played by the salt, which serves both as a fuel and as a heat transfer medium. The heat generated by the fission reaction is transferred in a intermediate heat exchanger to a secondary liquid salt coolant and then to a power cycle facility. A schematic representation of the reactor is shown in Figure 1.1. The fuel salt is also extracted and circulated through a chemical processing plant, which is used to maintain the salt in a clean and operating condition, both removing fission products and adjusting fissile concentration.

A liquid fuel results in several advantages especially for the reactor safety. A comprehensive description of the MSR features can be found in literature [15–17] and the most important are summarized below.

- The meltdown scenario of the fuel is an irrelevant term. In accidental conditions, the fuel salt can be automatically drained to multiple storage tanks, geometrically sub-critical and provided with passive decay heat cooling systems.

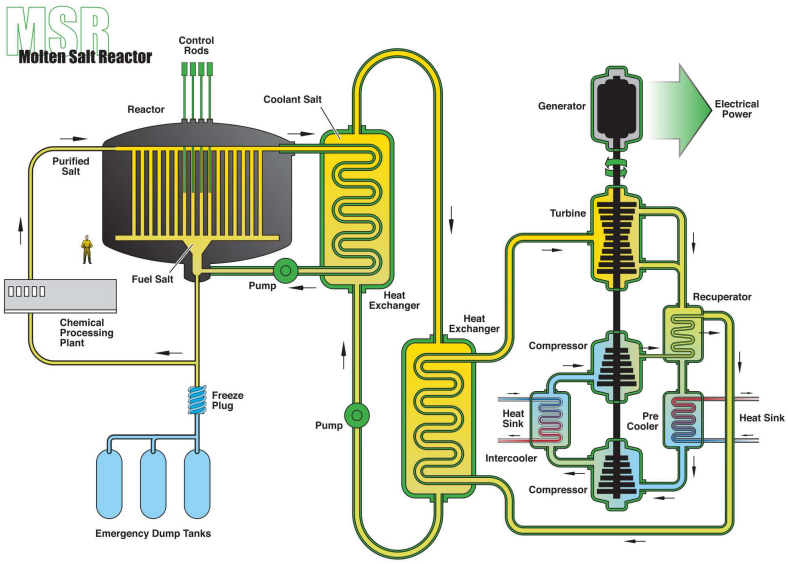

Figure 1.1: Schematic representation of MSR [2].

- The initial excess reactivity load is reduced by the on-line processing of the salt mixture. This permits to adjust the fissile concentrations on a continuous basis and remove the poisoning fission products, such as the Xe isotopes.
- The removal of the fission products has also the advantage of reducing the decay heat after reactor shut down.
- Safety is an area in which MSR performs very well due to the very strong negative temperature and void coefficients, especially for the non-moderated concept.
- The molten salt has a very low pressure due to their high boling point and low vapour pressure. The risk of reactor vessel break or salt leak due to high pressure is reduced.
- Most fission products quickly form stable fluorides, which would stay in the salt during any potential leak or accident. This prevents that volatile elements, such as Cs or I, are released from the fuel.

In essence, there are many benefits associated with the use of a liquid fuel, but this technology is still in the development phase. A number of technological challenges must be addressed and the safety approach must be established. The highest priority issues are in the area of (1) fuel development, (2) structural materials, (3) on-site fuel processing and (4) licensing procedure. The MSRE experience and the related research at ORNL has

produced a considerable amount of data on fluoride salts [18]. Nevertheless, fundamental research still needs to be conducted to determine thermodynamic and kinetic data on fuel salts and characterize the fission product behaviour. The main aim is the characterization of the fuel salt under normal and accidental conditions, providing the basis for the safety evaluation of the reactor. A nickel based alloy, called Hastelloy-N or INOR8 [19], was used as structural material in the MSRE. It was observed that when a suitable purification is performed on the initial fluoride salt, the corrosion is very small [20]. However, some issues remain open [21, 22], such as the formation of inter-granular cracking due to tellurium attack, and a material qualification is required for a long term use of the alloy. Corrosion can be mitigated by controlling the redox potential of the salt and research is being conducted on the molten salt chemistry to control it via the UF_4/UF_3 and treat the fuel salt. Finally, the different steps of the on-site fuel processing are currently under investigation including the engineering point of view to move from lab-scale to industrial scale.

It is worth to mention here that molten salts are excellent heat transfer media, therefore they are being considered in other advanced reactor concepts as well as for the conventional industry. For example, two types of solid-fuel liquid-salt cooled reactors are under investigation, the Advanced High-Temperature Reactor (AHTR) [23] and the Liquid Salt-cooled Fast Reactor (LSFR) [24]. The main advantages of molten salts as coolant compared with gas (which is used for the High-Temperature Reactors) are the better heat transfer (conductivity and heat capacity), the smaller size of the heat transfer loop and the increased safety mainly due to the low operating pressure.

1.2. MOLTEN SALT REACTOR FUEL

A fundamental step for the design and safety assessment of the MSR is the selection of the reference molten salt fuel composition. In fact, it influences nearly all the other design choices by defining the operation parameters (temperature and pressure) and the reprocessing scheme. The answer is not unique but depends on the application considered. Different properties must be taken into account in the context of neutronics (i.e. cross-section, moderation capability), chemistry (i.e. corrosion, fuel reprocessing), thermal and transport properties (i.e melting point, vapour pressure, heat capacity, density) and economics. The class of compounds that best fulfill the above mentioned criteria (at this step mainly low melting point and low capture cross section) for the MSR fuel are fluorides, which are considered as primary choice. Possible alternatives are also chlorides salts but the technology is less developed and they were not considered in this study.

A summary of the possible salt compositions for the various MSR designs is reported in Table 1.1. The first carrier salt proposed in 1960s was the so-called FLIBE, which is a mixture of enriched (>99.9%) ^{7}LiF and BeF_2. Both elements have a very low neutron capture cross section and are stable toward reduction by the structural material. When the neutron economy is not so strict as is the case for the fast spectrum designs, different fuel options are available and may include other elements such as NaF or CaF_2. These compounds were not considered in the early designs and experimental data on these systems are lacking.

Table 1.1: Reference salt compositions for the different MSR concepts.

Reactor type	Feed	Neutron spectrum	Reference salt
MSRE [6]	^{238}U,^{235}U (^{233}U)[a]	Thermal	^{7}LiF-BeF_2-ZrF_4-UF_4
MSBR [7]	^{232}Th, ^{233}U	Thermal	^{7}LiF-BeF_2-ThF_4-UF_4
MSFR [8, 9]	^{232}Th, ^{233}U	Fast	^{7}LiF-ThF_4 -UF_4
MSFR [25]	TRU [b]	Fast	^{7}LiF-ThF_4-UF_4-(Pu-MA)F_3
MOSART [10, 11]	TRU [b]	Fast	^{7}LiF-NaF-BeF_2-(Pu-MA)F_3
TMSR [13]	^{232}Th, ^{233}U	Thermal	^{7}LiF-BeF_2-ThF_4-UF_4
MSR-FUJI [14]	^{232}Th, ^{233}U	Thermal	^{7}LiF-BeF_2-ThF_4-UF_4

[a] After six months, the reactor was fuelled with ^{233}U.
[b] Transuranic mixture: 87.5% Pu, 6.3% Np, 5.3% Am and 0.9% Cm in the form of fluorides. It corresponds to the composition of a conventional LWR fuel after discharge and 5 years storage.

As mentioned before, it is extremely important to have detailed information on the physico-chemical properties of molten salts for the design and safety assessment of the reactor concept. The most important can be summarized as follows:

- **Melting temperature.** This is one of the key points in the choice of fuel and coolant. A low melting point decreases the risk of freezing as well as the risk of solid precipitates, which could cause local high concentration of fissile material. In order to keep an adequate margin of safety, it is required to operate at least 50 K above the melting point. A lower melting point allows a lower operating temperature of the reactor reducing the corrosion rate of the structural material.

- **Vapour pressure and boiling point.** The low vapor pressure of the molten salt fuel system is a beneficial parameter with regard to engineering issues as the system can operate at low pressure. This is also a very important advantage for the safety of the reactor as it reduces the main driving force of potential radioactivity release during accidents and of composition changes of the salt due to higher evaporation of one component in comparison with the others. The liquid range of the salt must include a wide margin towards evaporation/boiling.

- **Actinide solubility.** The salt must dissolve enough fissile material at operation temperature to be critical without formation of solid precipitates. Special attention is required in case of the trivalent elements (PuF_3 or the minor actinides) as their solubility in ThF_4-containing matrix is rather limited.

- **Heat capacity and heat transport properties.** A high heat capacity has the advantage that more energy can be stored reducing the amount of salt of the primary cooling circuit. Moreover, the system is less sensible to thermal fluctuations, providing additional time to react in case of irregularities. In addition to heat capacity, other properties such as viscosity, thermal conductivity and density are required for heat transfer calculation. Since the fuel mixture serves also as coolant, its efficiency as heat transfer medium must be carefully evaluated.

1

1.3. DEVELOPMENT OF A THERMODYNAMIC DATABASE ON FLUORIDE SALTS

Many of the above mentioned physico-chemical characteristics of liquid salts can be described by thermodynamic models. Potential fuel salt /coolant systems for the MSR have been critically reviewed and the development of an extensive thermodynamic database describing the most relevant systems is ongoing at Institute for Transuranium Elements of the Joint Research Centre (JRC-ITU) since several years. Typically the systems contain alkaline and alkaline-earth fluorides as matrix and ThF_4, UF_4, and PuF_3 as fertile and fissile materials. An overview of the status of the database is given in Figure 1.2, where the systems studied in the framework of this thesis are highlighted. The database is continuously extended and improved taking into consideration further relevant components and novel experimental data.

The generation of a reliable and consistent thermodynamic model is very important for material science. Considering a multi-components system, such as the molten salt fuel mixture, the amount of data that would be required for a complete description of every single system is enormous. Thermodynamic modeling is then indispensable to solve a problem like the optimization of the fuel composition. Once a reliable database is created, thermochemical equilibrium calculations can be performed, allowing the prediction of the thermodynamic properties and the evaluation of the safety margins for all potential fuel mixtures.

The thermodynamic model basically collects the thermodynamic description of all the systems, from pure compounds to binary and higher order mixtures. In other words, optimised thermodynamic functions are assigned for each phase as function of composition, temperature and pressure. The main outcome of thermodynamic modeling is the assessment of phase diagrams, which are a visual representation of the equilibrium state of a system. The basic relations between thermodynamics and phase equilibria were established more than a century ago by J.W. Gibbs [26], but only recently computer calculations of multicomponents phase equilibria are possible. In order to obtain the phase diagrams the CALPHAD *(CALculation of PHAse Diagram)* approach [27] is used, which is based on the minimization of the total Gibbs energy of all the phases that are considered in the equilibrium. Depending on the system and on the physico-chemical properties of the phase, a suitable thermodynamic model is selected and used to describe the temperature and composition dependence of the Gibbs energy function. The models contain adjustable parameters for binary and ternary systems which can be optimized based on experimental data. In fact, the assessment methodology includes a critical review of all data available in literature on the specific system and may reveal which further experiments are needed. The strength of the CALPHAD method is that data obtained from calculations are self-consistent and that, for example, the descriptions obtained for binary systems can be used to extrapolate to ternary or higher order systems. On the other hand, this also means that any modification of a constitutive subsystem affects the description of the multi-component system and therefore an accurate description of unary and binary systems is crucial. A more detailed description of the thermodynamic mod-

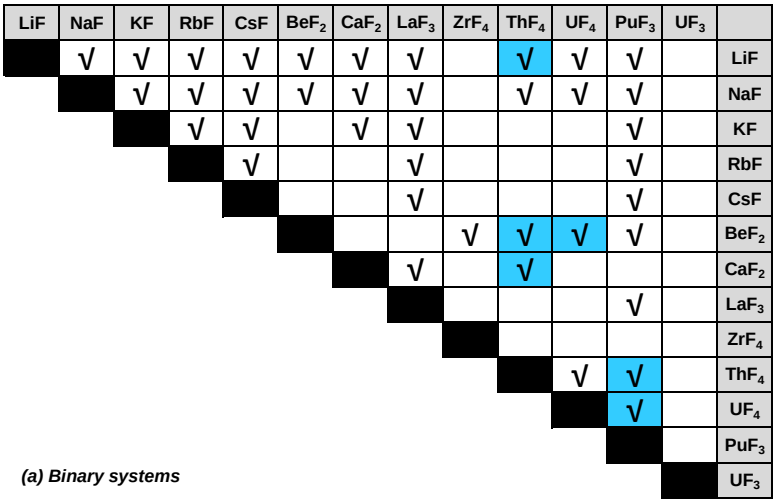

(a) Binary systems

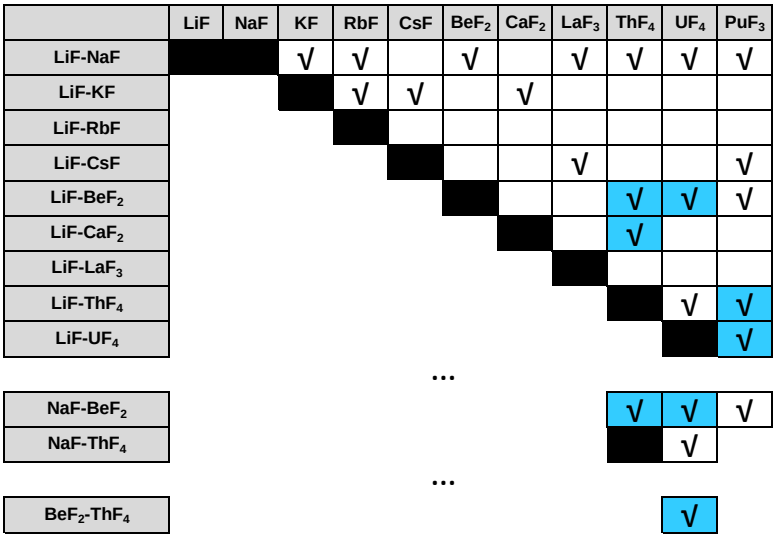

(b) Ternary systems

Figure 1.2: Database on fluoride salts developed at Institute for Transuranium Elements (ITU) of the Joint Research Centre (JRC). The assessed binary (a) and ternary (b) phase diagram are indicated in two scheme, where the systems studied in the framework of this thesis are highlighted in blue.

eling and the models used for the description of the thermodynamic functions is given in the following chapters.

As emphasized in this section, thermodynamic modeling is a very powerful tool. However, little can be done in absence of experimental data. The accuracy of a thermodynamic description strongly depends on the number and on the quality of data available. The type of measurements that can be used for the assessment are mainly of three kind: measurements quantitatively related to the Gibbs energy (i.e. enthalpy, entropy, heat capacity, chemical potential), phase equilibrium data that describes the shape of binary and ternary phase diagram and qualitatively data, such as the structural determination of a phase. Calorimetric methods are among the most used techniques to obtain those type of data. As an example, measurements by Differential Scanning Calorimeter (DSC) [28] allow the determination of temperature and enthalpy of transitions, heat capacity and enthalpy of mixing. However, these techniques are limited when dealing with quantities associated to the partial Gibbs energy, such as activity and activity coefficients. These data can be obtained from galvanic cells or from direct measurements of the vapour pressure. Finally, structural studies (i.e. X-ray diffraction, neutron diffraction, Raman spectroscopy) can be also used as source of auxiliary information, such as the stable phases or the short-ordering in the liquid solution.

Dedicated experimental procedures have been developed for performing these studies due to the complex chemistry of the compounds investigated. Fluoride salts are among the most stable compounds but at high temperatures and in presence of moisture the vapors can be very corrosive against the materials used in the employed instruments, such as the Pt/Ir used for thermocouples. Therefore, to preserve the integrity of the instruments the sample must be encapsulated [29, 30]. Furthermore, fluoride salts are very sensitive to oxygen and water. The handling of fluorides must be done in a protective atmosphere and the compounds must generally be purified beforehand. In fact, use of fluoride salts with a minimum content of water and impurity (oxides and/or oxyfluorides) is essential for the correct determination of their thermodynamic properties.

1.4. THESIS SYNOPSIS

The scope of this thesis is to provide a thermodynamic description on the most relevant systems for the Molten Salt Fast Reactor fuel. As briefly described, the approach adopted to investigate the salts is a combination of experimental measurements and thermodynamic modeling. New data were measured to extend the knowledge on the basic systems and a consistent database containing all the important systems was created. Based on the results obtained and the calculations performed, the goal was to identify several optimal fuel compositions for the reactor applications. The main body of the present thesis is divided into three parts, as schematically shown in Figure 1.3.

The first part focuses on the characterization of the binary mixture LiF-ThF_4, which is considered as the key system for the MSFR concept. The only experimental data available on this system were obtained in 1960s by Thoma *et al.* [31], who combined thermal analysis and X-ray diffraction to give a description of the LiF-ThF_4 phase diagram. Given

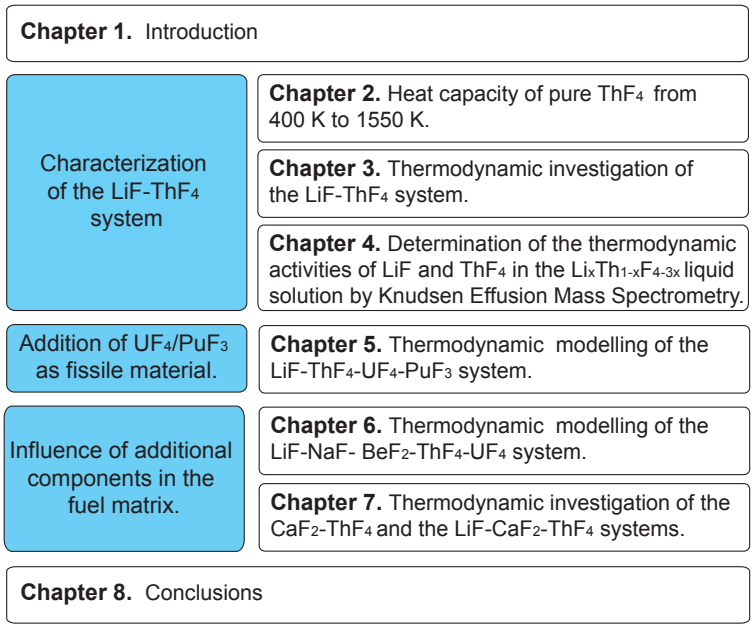

Figure 1.3: Scheme of the thesis layout.

the importance of this system that is the basis for all the studied higher order systems, we decided to carry out an extensive study to characterize it as best as possible. Chapter 2 focusses on the determination of the heat capacity of pure ThF_4 both in the solid and liquid phase. Despite its importance for different applications, no data were published in literature above room temperature. This is probably related to the challenging procedure to obtain highly pure ThF_4 compound, which is essential for a reliable determination of its heat capacity. In Chapter 3, the new assessment of the LiF-ThF_4 phase diagram is presented. New equilibrium data for the binary system were obtained in this study using the DSC technique and confirmed the stability of the $LiThF_5$ phase. In addition, the enthalpy of mixing of the $Li_xTh_{1-x}F_{4-3x}$ liquid solution was measured for the first time using a novel method developed for the same DSC technique. Finally, the vapor pressure of pure compounds LiF and ThF_4 and the vapor pressure of the $Li_xTh_{1-x}F_{4-3x}$ liquid solution was investigated using the Knudsen Effusion Mass Spectrometry (Chapter 4). The data obtained were then used to calculate the thermodynamic activities of LiF and ThF_4 in the liquid solution. All the sets of data were correlated with the developed thermodynamic model as discussed in the concluding chapter (Chapter 8).

The second part of the thesis considers the addition of fissile material to the binary LiF-ThF_4 mixture. In fact, for the start-up of the reactor, an initial load of fissile material is required, which can be either uranium or plutonium in the form of fluorides. The thermodynamic assessment of the LiF-ThF_4-UF_4-PuF_3 system has been performed and the description is presented in Chapter 5. Two binary systems, ThF_4-PuF_3 and UF_4-PuF_3,

and two ternary systems, LiF-ThF_4-PuF_3 and LiF-UF_4-PuF_3, have been assessed for the first time. Moreover, some selected experimental measurements have been performed to confirm the model developed that has been used to identify the most promising compositions for the MSFR fuel. The obtained results can also be extended to the case of a TRU fuelled reactor as the minor actinides are present in low concentrations and, in a first approximation, have a similar thermodynamic behaviour as PuF_3.

To improve the physico-chemical properties of the fuel mixture, additional components may be added to the salt matrix and their influence is analyzed in the third part of the present work. Different options are available as additive depending on the neutron economy of the reactor. The most obvious, and the only option in case of a thermal neutron spectrum, is BeF_2 and mixtures containing BeF_2 were studied extensively at ORNL [32]. On the other hand, in case of the MSFR, possible alternatives are NaF and CaF_2. While mixtures containing NaF were recently studied by Beneš *et al.* [33], in this work we have first considered the combined effect of NaF and BeF_2 addition, which is described in Chapter 6. The assessment of two binary and all ternary sub-systems of the LiF-NaF-BeF_2-ThF_4-UF_4 system were performed. Concerning CaF_2-containing systems, no data are available in literature. In order to evaluate the influence of CaF_2 addition to the mixture, a basic study of the thermodynamic properties of CaF_2-ThF_4 and LiF-CaF_2-ThF_4 was needed and it is presented in Chapter 7. The phase diagram of the binary system CaF_2-ThF_4 was determined by coupling the phase equilibrium determination and the identification of the present phases by X-ray diffraction. Then, the ternary phase diagram, LiF-CaF_2-ThF_4, was extrapolated and optimized based on measured ternary phase equilibria.

Finally, a summary of the results and the main outcomes are discussed in Chapter 8. All the experimental data collected are correctly described by the thermodynamic database and its capability to provide reliable prediction of the unknown properties has been demonstrated. Thermochemical equilibrium calculations were performed using the developed database. This allows the evaluation of the performance of several mixtures predicting their properties and thus the optimization of the fuel composition. A reference selection of promising salt compositions is finally presented.

REFERENCES

[1] *Comparison of lifecycle greenhouse gas emission of various electricty generation sources,* WNA report, http://www.world-nuclear.org/ (2011).

[2] *A Technology Roadmap for Generation IV Nuclear Energy System,* U.S. DOE Nuclear Energy Research Advisory Committee and the Generation IV International Forum (2002).

[3] *Technology Roadmap Update for Generation IV Nuclear Energy Systems,* OECD Nuclear Energy Agency for the Generation IV International Forum (2014).

[4] E. S. Bettis, R. W. Schroeder, G. A. Cristy, H. W. Savage, R. G. Affel, and L. F. Hemphill, *The Aircraft Reactor Experiment - Design and construction,* Nucl. Sci. Eng. **2**, 804 (1957).

[5] M. W. Rosenthal, R. B. Briggs, and P. R. Kasten, *Molten-Salt Reactor Program: Semi-annual Progress Report,* Tech. Rep. ORNL-4449 (1970).

[6] P. N. Haubenreich and J. R. Engel, *Experience with the Molten Salt Reactor Experiment,* Nucl. Appl. Technol. **8**, 118 (1970).

[7] E. S. Bettis and R. C. Robertson, *The design and performance features of a Single-Fluid Molten-Salt Breeder Reactor,* Nucl. Appl. Technol. **8**, 190 (1970).

[8] D. Heuer, E. Merle-Lucotte, M. Allibert, M. Brovchenko, V. Ghetta, and P. Rubiolo, *Towards the thorium fuel cycle with molten salt fast reactors,* Ann. Nucl. Energy **64**, 421 (2014).

[9] L. Mathieu, D. Heuer, R. Brissot, C. L. Brun, E. Liatard, J. Loiseaux, O. Meplan, E. Merle-Lucotte, A. Nuttin, J. Wilson, C. Garzenne, D. Lecarpentier, and E. Walle, *The Thorium Molten Salt Reactor: Moving on from the MSBR,* Prog. in Nucl. En. **48**, 664 (2006).

[10] *International Scientific Technical Centre, Moscow*, Tech. Rep. (July 2004) ISTC Project #1606 Final Report.

[11] V. Ignatiev, O. Feynberg, I. Gnidoi, A. Merzlyakov, A. Surenkov, V. Uglov, A. Zagnitko, V. Subbotin, I. Sannikov, A. Toropov, V. Afonichkin, A. Bovet, V. Khokhlov, V. Shishkin, M. Kormilitsyn, A. Lizin, and A. Osipenko, *Molten salt actinide recycler and transforming system without and with Th - U support: Fuel cycle flexibility and key material properties,* Ann. Nucl. Energy **64**, 408 (2014).

[12] J. Serp, M. Allibert, O. Beneš, S. Delpech, O. Feynberg, V. Ghetta, D. Heuer, V. Ignatiev, J. L. Kloosterman, L. Luzzi, E. Merle-Lucotte, J. Uhlíř, R. Yoshioka, and D. Zhimin, *The molten salt reactor MSR in generation IV: Overview and perspectives,* Prog. Nucl. Energ. **77**, 308 (2014).

[13] X. Hongjie, X. Cai, and W. Guo, *Thorium energy R&D in China,* ThEC13 conference, CERN, Ginevra (2013).

[14] K. Furukawa and et al., *Molten-Salt Reactor FUJI, in: Status of small reactor designs without on-site refueling*, Tech. Rep. IAEA TECDOC-1536 (2007).

[15] D. LeBlanc, *Molten salt reactors: A new beginning for an old idea,* Nucl. Eng. Des. **10**, 1644 (2010).

[16] R. Hargraves and R. Moir, *Liquid Fluoride Thorium Reactors,* Am. Sci. **98**, 304 (2010).

[17] R.Yoshioka, *Nuclear Energy Based on Thorium Molten Salt,* in *Molten Salt Chemistry: from Lab to Application*, edited by F. Lantelme and H. Groult (Elsevier, 2013) Chap. 23, pp. 471–496.

[18] *ORNL repository,* http://energyfromthorium.com/pdf/.

[19] H. E. McCoy, *The INOR - 8 story,* Oak Ridge Nat. Lab. Rev. **3**, 35 (1969).

[20] R. C. Robertson, *MSRE design and operation report- Part I*, Tech. Rep. ORNL-TM-728 (1965).

[21] V. Ignatiev and A. Surenkov, *Material performance in molten salts,* in *Comprehensive Nuclear Materials*, Vol. 5, edited by R. J. M. Konings (Elsevier, 2012) Chap. 10, pp. 221–250.

[22] H. E. McCoy, *Status of Materials Development for Molten-Salt-Reactors*, Tech. Rep. Report ORNL-TM-5920 (1978).

[23] C. W. Forsberg, P. F. Peterson, and R. A. Kochendarfer, *Design options for the Advanced High-Temperature Reactor,* Proceedings of the International Congress on Advances in Nuclear Power Plants (ICAPP), Anaheim, CA USA , (2008).

[24] C. W. Forsberg, P. F. Peterson, and D. F. Williams, *Practical aspects of Liquid-Salt-Cooled Fast-Neutron Reactors,* Proceedings of the International Congress on Advances in Nuclear Power Plants (ICAPP), Seoul, Korea , (2005).

[25] E. Merle-Lucotte, D. Heuer, C. L. Brun, L. Mathieu, R. Brissot, E. Liatard, O. Meplan, and A. Nuttin, *Fast thorium molten salt reactors started with plutonium,* Proceedings of the International Congress on Advances in Nuclear Power Plants (ICAPP), Reno, USA , (2006).

[26] J. W. Gibbs, *On the equilibrium of heterogeneous substances,* (Transaction of the Connecticut Academy of Arts and Sciences, 1874-1878).

[27] L. Kaufman and H. Bernstein, *Computer calculations of phase diagrams,* (Academic Press, New York, 1970).

[28] G. Höhne, W. Hemminger, and H. Flammersheim, *Differential Scanning Calorimeter,* (Springer, 1996).

[29] O. Beneš, R. J. M. Konings, C. Künzel, M. Sierig, A. Dockendorf, and L. Vlahovic, *The high-temperature heat capacity of the (Li, Na)F liquid solution,* J. Chem. Thermodyn. **41**, 899 (2009).

[30] O. Beneš, R. J. M. Konings, S. Wurzer, M. Sierig, and A. Dockendorf, *A DSC study of the $NaNO_3$–KNO_3 system using an innovative encapsulation technique,* Thermochim. Acta **509**, 62 (2010).

[31] R. E. Thoma, H. Insley, B. S. Landau, H. A. Friedman, and W. R. Grimes, *Phase equilibria in the fused salt systems LiF-ThF_4 and NaF-ThF_4,* J. Phys. Chem. **63**, 1266 (1959).

[32] C. F. Weaver, R. E. Thoma, H. Insley, and H. A. Friedman, *Phase Equilibria in Molten-Salt Breeder Reactor Fuels*, Tech. Rep. ORNL-TM-2896 (1960).

[33] O. Beneš, M. Beilmann, and R. J. M. Konings, *Thermodynamic assessment of the LiF–NaF–ThF_4–UF_4 system,* J. Nucl. Mater. **405**, 186 (2010).

2

HEAT CAPACITY OF ThF_4 FROM T = 400 K TO T = 1550 K

Elisa CAPELLI, Ondřej BENEŠ, Rudy J.M. KONINGS

The high temperature termodynamic behaviour of ThF_4 was studied for the first time in this work. The compound was purified using NH_4HF_2 as fluorinating agent and characterized using the Differential Scanning Calorimetry and X-ray Diffraction analysis. Both techniques demonstrated the high purity of the sample, which is particularly important for a reliable determination of the heat capacity. Drop calorimetry was used to measure the enthalpy increments for ThF_4 in the temperature range from 400 K *to 1550* K. *Based on the enthalpy data measured in this work and on the low temperature heat capacity data reported in literature, the high temperature heat capacity of the crystalline state was determined as:*

$$C_p(ThF_4, cr) \ / \ (\mathrm{J \cdot K^{-1} \cdot mol^{-1}}) = 91.011 + 7.891 \cdot 10^{-2}(T/\mathrm{K}) - 341290(T/\mathrm{K})^{-2},$$

and the heat capacity of the liquid state was found constant as:

$$C_p(ThF_4, l) \ / \ (\mathrm{J \cdot K^{-1} \cdot mol^{-1}}) = 163.6.$$

The enthalpy of fusion calculated from the obtained equations is in very good agreement with the value from DSC measurements on the same material.

Manuscript in preparation.

2.1. INTRODUCTION

Nuclear fuels containing thorium will probably play a role in the future generation of nuclear fission reactors. In fact, the thorium fuel cycle has the potential to reduce the production of long-lived transuranic waste and ensure long term sustainability of nuclear power. One of the possible future reactor concepts is the Molten Salt Reactor (MSR) [1], in which fissile and fertile materials are in the form of fluorides. Despite the importance of actinide fluorides for this type of reactor, data on their high-temperature thermodynamic behaviour are still incomplete.

The present paper focuses on the high temperature heat capacity of ThF_4, which is the only stable fluoride compound of thorium. ThF_4 is an inorganic compound, white coloured and hygroscopic. Its melting point was measured by different authors [2–5] and the selected value [6] is T = 1383 ± 3 K. The heat capacity of ThF_4 has been measured by Lohr *et al.* [7] in the low temperature range from 5 to 300 K, but no data are available in literature above room temperature. The only available information are preliminary enthalpy measurements by Dworkin from 1200 to 1420 K, which have not been published due to experimental difficulties encountered [8]. The results were compiled by Wagman *et al.* [9] to give two approximate equations respectively for the crystalline and liquid state. From the same data, the enthalpy of fusion was also derived.

Heat capacity functions, together with standard enthalpies of formation and entropies of formation, are essential properties to define the Gibbs energy of any phase. In other words, they are required to determine the stable phases in a system and to perform the thermodynamic assessment of any multi-component system. Moreover, the knowledge of the heat capacity is also required for practical aspects such as heat transfer calculations.

For all the reasons above, we decided to investigate the heat capacity of ThF_4. The first and fundamental step was the purification of the starting material, which is discussed in this paper as well. After demonstrating the high purity of the ThF_4 sample using the Differential Scanning Calorimetry (DSC) and X-ray Diffraction (XRD) analysis, the sample was encapsulated and measured. The enthalpy increments as function of temperature were determined by drop calorimetry and the results were used to calculate the heat capacity for both solid and liquid state of ThF_4. The high temperature heat capacity of the solid state was determined by simultaneous least square method considering the enthalpy data measured in this work and the low temperature heat capacity data by Lohr *et al.* [7]. Finally, the enthalpy of fusion was derived from the given equations and compared with the value obtained in our previous work [10].

2.2. EXPERIMENT

2.2.1. PURIFICATION OF ThF_4

The preparation of highly pure actinides fluorides is a challenging procedure. Compounds like ThF_4 or UF_4 are sensitive to water molecules as well as to oxygen and are likely to contain oxides and oxyfluorides impurities. The presence of these impurities in

the sample can be detected with calorimetric techniques and could in principle lead to imprecise experimental results.

Most of the methods developed for converting oxides impurities into fluorides are based on high-temperature fluorination using F_2 or HF gas. An alternative, which is less demanding in terms of technical equipment and safety constrains, is the use of the NH_4HF_2 compound as fluorinating agent. The method was first reported by Wani *et al.* [11] and it is based on the following chemical reactions for the oxides:

$$NH_4HF_2 \xrightarrow{\Delta} NH_3 + 2\,HF \tag{2.1}$$

$$ThO_2 + 4\,HF \longrightarrow ThF_4 + 2\,H_2O. \tag{2.2}$$

An excess of NH_4HF_2 was added to the commercial ThF_4 powder, obtained from Rhodia, and the mixture (about 1-2 g) was heated at 523 K for 12 hours. The reaction took place in a closed container, which is internally lined with nickel to avoid the formation of any corrosion product. Afterwards, two consecutive heating cycles (T= 673 K for 3 hours) were performed using an open container to allow the evaporation of residual ammonium and formed water. The furnace used can operate under continuous Ar/H_2 flow ensuring a low concentration of oxygen during the heat treatments. The purity of the obtained sample was checked by two different tecnhiques, respectively DSC and XRD analysis, which are described below.

Using the DSC method, the melting point of the compound was identified. For single components, the melting event is characterized by a single peak in the heat flow versus temperature signal. The onset of the peak corresponds to the melting temperature and its area to the enthalpy of fusion. Figure 2.1 shows the output signal for two different samples: the commercial ThF_4 before the purification and the same sample after purification. In the latter case a single peak was observed having an onset temperature of T = 1380 K, which is in close agreement to the literature value, within the instrument uncertainty of ± 5 K. Before purification, the presence of two peaks is a clear indication of some impurities, which affect the melting behaviour of ThF_4.

The purity of the sample was also checked by XRD analysis. After purification, the sample was heated up above its melting point and then cooled to room temperature with a slow cooling rate (~ 0.5 K/min). In this way, a better crystallization was achieved improving the quality of the final XRD spectra. The sample was measured at room temperature using a Bruker D8 X-ray diffractometer mounted in a Bragg-Brentano configuration with a curved Ge monochromator (1, 1, 1) and a ceramic copper tube (40 kV, 40 mA) equipped with a LinxEye position sensitive detector. After the measurement, structural analysis on the X-ray diffraction data was performed by Rietveld method using the FullProf suite [12]. ThF_4 crystallizes in the monoclinic system as most of the actinides tetrafluorides [13] in the space group C2/c (n°15). The published structure, reported by Benner and Muller [14] was used as basis for our analysis and the refined lattice parameters (a = 13.044(1) Å, b = 11.013(1) Å, c = 8.534(1) Å, β = 126.31 °) were found to be in good agreement with their results. The comparison between the measured pattern and the calculated pattern is shown in Figure 2.2. Considering the complexity of the monoclinic system, the result is very satisfactory and confirms the good quality of the ThF_4 compound. Moreover, no impurities were detected in the XRD pattern.

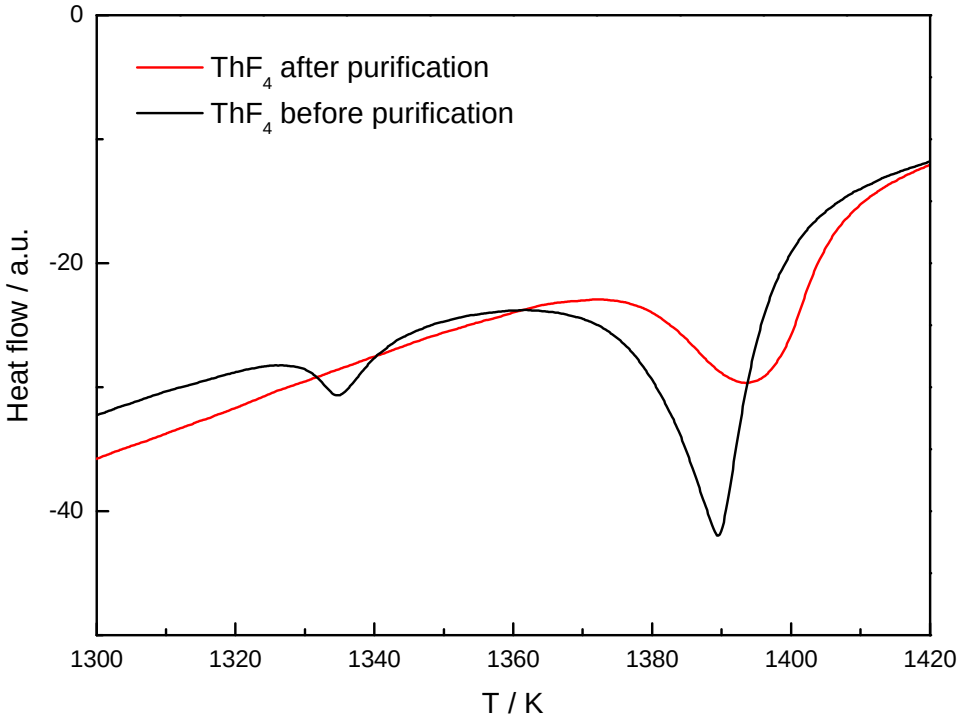

Figure 2.1: Comparison of the DSC output signal for the commercial ThF_4 before the purification and the same sample after purification.

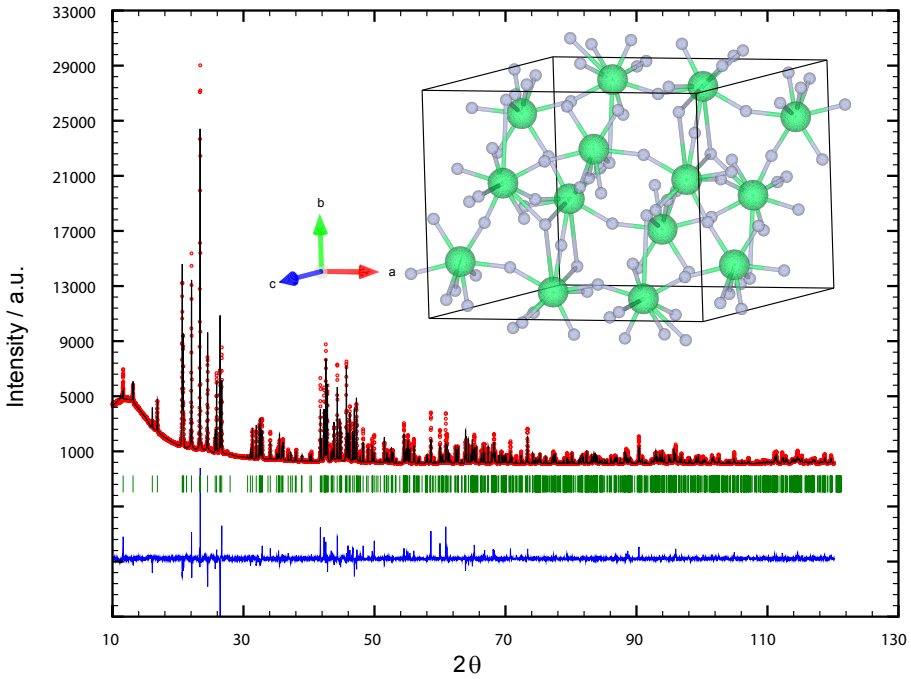

Figure 2.2: Comparison betweeen the observed (in red) and calculated (in black) X-ray diffraction pattern of ThF_4 compound. The difference between the two intensities is reported in blue and the Bragg reflections are marked in green. The inset figure shows a sketch of the ThF_4 structure.

From the purified ThF_4 batch, three samples were prepared as reported in Table 2.1. For each sample, a typical amount of 80-100 mg of ThF_4 was compressed into pellet and placed inside a nickel crucible. The crucibles were then closed by laser welding as described in detail in [15]. This avoids transport of fluoride vapours during the high temperature measurements and the consequent corrosion of the detectors of the instrument.

2.2.2. DROP CALORIMETRY

Enthalpy increments of solid and liquid phase of ThF_4 were measured in this work using drop calorimetry. The measurements were performed using a Setaram Multi Detector High Temperature Calorimeter (MDHTC-96 type) equipped with a drop sensor. During the experiment, a sample which is mantained at room temperature (T_1) is automatically dropped into a furnace with pre-set temperature (T_2). The additional heat required to re-equilibrate the furnace temperature is measured by a series of thermocouples and it is proportional to the enthalpy increment of the sample associated to the heating from T_1 to T_2. The heat capacity is then derived according to:

$$C_P = \left(\frac{\partial H}{\partial T}\right)_P . \tag{2.3}$$

Our drop calorimeter is equipped with an automatic multi-sample introducer which allows consecutive measurements of several samples without manual operations. Each experiment consists of seven drop events: three samples (encapsulated ThF_4) and four references (α-Al_2O_3 pieces). By alternating samples and references drops, the energy calibration is performed directly during the experiment and it is based on the very well defined heat capacity of sapphire [16]. Finally, the enthalpy increment of ThF_4 is derived substracting the contribution of nickel [17] from the total enthalpy increment. In drop calorimetry, it is very important to have a stable temperature signal before the sample or reference drop. Therefore, the temperature is stabilized over a 7-hours period before the first drop and for each successive drop a delay of 25 minutes is applied. The temperature calibration has been performed separately by measuring the melting temperatures of several reference materials (In, Sn , Pb, Zn, Al, Ag, Au).

Table 2.1: Samples characteristics: total mass m_{TOT}, mass of nickel m_{Ni}, mass of sample m_{ThF_4}, and molar ratio MM_{Ni}/MM_{ThF_4}.

Crucible	m_{TOT} (mg)	m_{Ni} (mg)	m_{ThF_4} (mg)	MM_{Ni}/MM_{ThF_4}
Crucible 1	340.5	238.5	102.0	12.27
Crucible 2	323.8	238.1	85.7	14.58
Crucible 3	334.5	236.3	98.1	12.66

2.3. RESULTS

2.3.1. SOLID PHASE HEAT CAPACITY

The high-temperature heat capacity of solid ThF_4 is reported for the first time in this study. Measurements were performed from 423 K to 1323 K with step of 50 K and the results are summarized in Table 2.2. The enthalpy increments reported are the average values of the different measurements performed at the given temperature and the error assigned corresponds to their standard deviation. We note here that the errors found are higher compared to the standard error of this technique, mainly due to the encapsulation of the sample. As it can be observed in Table 2.1 the mass of the encapsulation material Ni is far more than the mass of the sample ThF_4, resulting in a larger uncertainty of the results.

An equation for the crystalline state of ThF_4 was obtained by fitting simultaneously the enthalpy data measured in this work and the low-temperature heat capacity data by Lohr *et al.* [7] using the least square method. For the low-temperature data, only a limited number of points (10 points) were considered in the range from 200 K to 300 K, which was found as a good compromise to obtain a smooth transition between the two sets of data. The heat capacity at 298 K was used as a constraint and fixed to the experimental value of 110.78 $J \cdot K^{-1} \cdot mol^{-1}$ [7]. An error was assigned to each data point, for the enthalpy data the experimental error as reported in Table 2.2 and for the low temperature heat capacity data a fixed relative error of 0.1 % [7]. The obtained high temperature heat capacity of solid ThF_4 is described by the following polynomial form:

$$C_P = A + B \cdot (T/\mathrm{K}) + C \cdot (T/\mathrm{K})^{-2} \tag{2.4}$$

with the following coefficients:

$$\begin{aligned} A &= 91.011 \pm 7.579\ \mathrm{J \cdot K^{-1} \cdot mol^{-1}} \\ B &= 7.891 \cdot 10^{-2} \pm 1.91810^{-2}\ \mathrm{J \cdot K^{-1} \cdot mol^{-1}} \\ C &= -341290 \pm 166884\ \mathrm{J \cdot K^{-1} \cdot mol^{-1}}. \end{aligned} \tag{2.5}$$

The heat capacity fit is shown in the inset graph of Figure 2.3, in which the data for the low temperature heat capacity are also reported. Similarly, the corresponding enthalpy fit is shown in Figure 2.3 as a solid line. The agreement obtained with the experimental data is rather good, within the experimental error bars for almost all the points. As mentioned in the introduction, the only available data for the solid phase heat capacity of ThF_4 were reported by Wagman *et al.* [9]. They provided an approximate equation for the solid phase heat capacity using a computer-assisted least sums-least squares technique based on the preliminary data of Dworkin. The derived enthalpy plot is shown in Figure 2.3 as a dashed line.

2.3.2. LIQUID PHASE HEAT CAPACITY

The liquid phase of ThF_4 was investigated in the temperature range from 1448 K to 1523 K with steps of 25 K. Due to the temperature limit of the calorimeter, measurements at

Table 2.2: Enthalpy increments (H^T - H^{298}) of ThF_4 solid and liquid phase and their standard deviation as function of temperature T. The number of drops n is also reported.

T / K	H^T - H^{298} / J · mol^{-1}	Error / J · mol^{-1}	n
	Solid		
430.4	17170	1671	3
482.8	27011	3118	6
534.1	33541	6405	6
585.4	37291	205	2
636.7	47326	3286	5
687.1	55583	5975	3
737.3	61123	2220	3
787.7	70787	10692	5
837.6	90885	9212	6
887.7	84110	7206	6
937.4	97177	3942	3
987.6	107082	14119	6
1037.7	114857	13013	5
1087.7	106449	8169	7
1137.9	127639	4405	6
1187.9	137350	7984	5
1238.1	140134	16783	7
1288.2	143667	9835	6
1338.6	150342	14743	6
	Liquid		
1464.6	226847	17278	6
1490.2	221645	19563	6
1515.6	228512	7594	6
1540.9	238452	7535	3

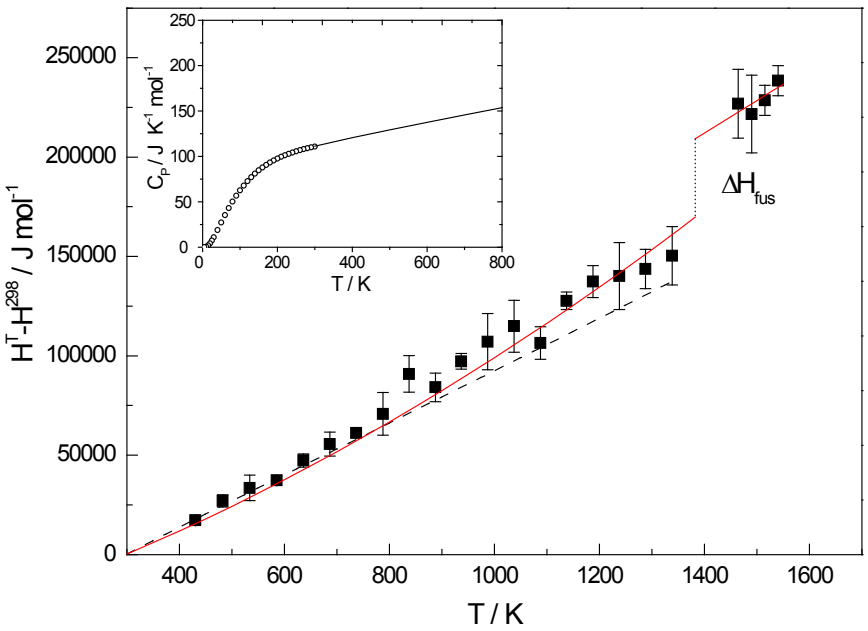

Figure 2.3: The enthalpy increments of the ThF_4 solid and liquid phase measured at different temperatures. Solid lines represent the fitted equations for both phases while the dotted line represents the enthalpy function calculated from the heat capacity equation by Wagman *et al.* [9]. Inset graph: Heat capacity of solid ThF_4 as function of temperature. (∘) Data at low temperature measured by Lohr *et al.* [7] (—) High temperature heat capacity fit obtained in this work.

higher temperatures could not be performed. Moreover, the crucibles are made of nickel which become soft at temperatures close to its melting point (1728 K) compromising their strength and the ability to contain the vapours. For these reasons, the temperature range of the measurements is very limited and further studies may be useful to extend the validity of the calculated equation. Same limitations are also found in other works on actinides fluorides [8, 18].

The results obtained in this study are reported in Table 2.2 and plotted in Figure 2.3. In agreement with previous works on the liquid heat capacity of fluoride salts [10, 19], a constant heat capacity with respect to temperature was considered. The measured enthalpy was fitted using a least squares linear fit and the obtained heat capacity is:

$$C_P = 163.6\,\mathrm{J\cdot K^{-1}\cdot mol^{-1}}. \tag{2.6}$$

This value is higher compared to the suggested value ($133.9\ \mathrm{J\cdot K^{-1}\cdot mol^{-1}}$) reported in literature [6]. However, we should mention here that the liquid heat capacity of ThF_4 has been recently re assessed in our work on the thermodynamic assessment of the LiF-ThF_4 phase diagram [10]. In order to reproduce the experimental values of the Li_3ThF_7 enthalpy of fusion, higher heat capacity of liquid ThF_4 was suggested and set to $170\ \mathrm{J\cdot K^{-1}\cdot mol^{-1}}$. Considering the uncertainty on this estimation, the present experimental result is in very good agreement with this assumption. Moreover, the new value of the liquid heat capacity for ThF_4 is similar to the experimentally determined liquid heat capacity of UF_4 found at $174.74\ \mathrm{J\cdot K^{-1}\cdot mol^{-1}}$ [8]. In fact, the two compounds have strong similarities as already observed for other thermodynamic properties [20, 21].

2.3.3. ENTHALPY OF FUSION

Based on the equations derived for the solid and liquid state of ThF_4, the enthalpy of fusion was calculated. The difference between the two enthalpy increment functions evaluated at the melting temperature of ThF_4 (1383 K) was found to be:

$$\Delta H_{fus}^{DROP} = 40.31\,\mathrm{J\cdot mol^{-1}}. \tag{2.7}$$

This value was compared with the experimentally determined enthalpy of fusion as measured by the DSC method and reported in our previous work [10]:

$$\Delta H_{fus}^{DSC} = 41.9 \pm 2.0\,\mathrm{J\cdot mol^{-1}}. \tag{2.8}$$

The two values are in good agreement within the instrument uncertainty, supporting the validity of the equations derived.

2.4. CONCLUSIONS

The aim of the present work was to determine the heat capacity of the ThF_4 compound, which has never been published before. A considerable effort was made to obtain highly pure ThF_4 samples and the result was achieved using NH_4HF_2 as fluorinating agent.

During the measurements we have observed that a small amount of impurities can significantly influence the thermodynamic properties of the compound and therefore it is important to have high purity material when performing this type of fundamental measurements. In this work, the purity was evaluated based on the XRD analysis and on the identification of the melting point of the compound. No impurities were detected and the melting point was found to be in agreement with literature within the instrument uncertainty.

Enthalpy measurements were performed in the temperature range from 400 K to 1550 K and two equations, respectively for the solid and liquid state of ThF_4 are given in this paper. The fit of the data for solid ThF_4 took into account also the low temperature heat capacity data by Lohr *et al.* [7] and provide a consistent description of the heat capacity function across the different temperature ranges. Finally, the enthalpy of fusion was calculated from the obtained equation and compared with the experimental value.

ACKNOWLEDGEMENTS

E.C. acknowledges the European Commission for support given in the frame of the program "Training and Mobility of Researchers". This work was supported by the EVOL project in the 7th Framework Programme of the European Commision (Grant agreement No.249696). The authors would like to thank D. Bouxière and G. Pagliosa for the collection of the X-ray data and P. E. Raison for the fruitful discussion on the XRD analysis.

REFERENCES

[1] *A Technology Roadmap for Generation IV Nuclear Energy System,* U.S. DOE Nuclear Energy Research Advisory Committee and the Generation IV International Forum (2002).

[2] W. J. Asker, E. R. Segmit, and A. W. Wylie, *The potassium thorium fluorides,* J. Chem. Soc. , 4470 (1973).

[3] B. Porter and E. A. Brown, *Melting points of inorganic fluorides,* J. Am. Ceram. Soc. **45**, 49 (1962).

[4] R. E. Thoma, H. Insley, B. S. Landau, H. A. Friedman, and W. R. Grimes, *Phase equilibria in the fused salt systems LiF-ThF_4 and NaF-ThF_4,* J. Phys. Chem. **63**, 1266 (1959).

[5] A. S. Dworkin and M. A. Bredig, *Miscibility of liquid metals with salts,* J. Phys. Chem. **75**, 2340 (1971).

[6] R. J. M. Konings, J. P. M. van der Meer, and E. Walle, *Chemical aspects of Molten Salt Reactor Fuel*, Tech. Rep. (2005) ITU-TN 2005/25.

[7] H. R. Lohr, D. W. Osborne, and E. F. Westrum, *Thermodynamic properties of thorium tetrafluoride from 5 to 300 K and the magnetic entropy of uranium tetrafluoride,* J. Am. Chem. Soc. **76**, 3837 (1954).

[8] A. S. Dworkin, *Enthalpy of uranium tetrafluoride from 298-1400 K: enthalpy and entropy of fusion,* J. Inorg. Nucl. Chem. **34**, 135 (1954).

[9] D. D. Wagman, R. H. Schumm, and V. B. Parker, *A computer assisted evaluation of the thermochemical data of the compounds of thorium,* (NBSIR-77-1300, 1977).

[10] E. Capelli, O. Beneš, M. Beilmann, and R. J. M. Konings, *Thermodynamic investigation of the LiF-ThF_4 system,* J. Chem. Thermodyn. **58**, 110 (2013).

[11] B. N. Wani, S. J. Patwe, U. R. K. Rao, and K. S. Venkateswarlu, *Fluorination of oxides of uranium and thorium by ammonium hydrogen fluoride,* J. Fluor. Chem. **44**, 177 (1989).

[12] J. Rodriguez-Carvajal, *Recent advances in magnetic structure determination by neutron powder diffraction,* Physica B **192**, 55 (1993).

[13] L. B. Asprey and R. G. Haire, *On the actinide tetrafluoride lattice parameters,* Inorg. Nucl. Chem. Letters **9**, 1121 (1973).

[14] G. Benner and B. G. Mueller, *Zur kenntnis binärer fluoride des ZrF_4 typs: HfF_4 und ThF_4,* Z. anorg. allg. Chem. **588**, 33 (1950).

[15] O. Beneš, R. J. M. Konings, S. Wurzer, M. Sierig, and A. Dockendorf, *A DSC study of the $NaNO_3$–KNO_3 system using an innovative encapsulation technique,* Thermochim. Acta **509**, 62 (2010).

[16] *Standard reference material no.720,* National Institutes of Standards and Technology (NIST): Gaithersburg, MD (1986).

[17] P. D. Desai, *Thermodynamic properties of nickel,* Int. J. Therm. **8**, 763 (1987).

[18] E. G. King and A. U. Christensen, *High-temperature heat content of uranium tetrafluoride*, Tech. Rep. Bur. Mines Rep. Invest. 5909 (1961).

[19] M. Beilmann, O. Beneš, E. Capelli, V. Reuscher, R. J. M. Konings, and T. Fanghänel, *Excess heat capacity in liquid binary alkali-fluoride mixtures,* Inorg. Chem. **52**, 2404 (2013).

[20] O. Beneš and R. J. M. Konings, *Thermodynamic assessment of the LiF–CeF_3–ThF_4–UF_4 system,* J. Nucl. Mater. **435**, 164 (2013).

[21] E. Capelli, O. Beneš, and R. J. M. Konings, *Thermodynamic assessment of the LiF-ThF_4–PuF_3-UF_4 system,* J. Nucl. Mater. **462**, 43 (2015).

3

THERMODYNAMIC INVESTIGATION OF THE LiF-ThF_4 SYSTEM

Elisa CAPELLI, Ondřej BENEŠ, Markus BEILMANN, Rudy J.M. KONINGS

A thermodynamic investigation of the LiF-ThF_4 system is presented in this study. The enthalpy of mixing of the (Li,Th)F_x liquid solution was measured for the first time using a method designed for conventional DSC technique. To verify the possibility to measure the mixing enthalpy with the used calorimeter, the known LiF-KF system was first investigated and compared to the literature data. After the successful test, this technique was applied to investigate the LiF-ThF_4 system and obtained novel results are presented in this study. Furthermore, using the DSC technique, new equilibrium data of the LiF-ThF_4 phase diagram were measured, confirming the stability of the $LiThF_5$ phase. The intermediate compound Li_3ThF_7 was synthesized and its enthalpy of fusion was determined. Considering the new experimental data, the LiF-ThF_4 system was re-optimized using a quasi chemical model for the description of excess Gibbs parameters of the liquid solution.

Parts of this chapter have been published in Journal of Chemical Thermodynamics **58**, 110 (2013) [1].

3.1. INTRODUCTION

The Molten Salt Reactor (MSR) is one of the six concepts considered in the Generation IV initiative. The MSR concept, developed in the 1960s in Oak Ridge National Laboratory, is based on a liquid fuel. The fissile material is dissolved in a molten salt mixture, circulating in the primary circuit which serves both as fuel and coolant. A specific reference configuration for the MSR has not been yet identified and this reactor can be designed considering both thermal or epithermal neutron spectra. One of the currently developed MSR concepts is the Molten Salt Fast Reactor (MSFR) [2], which combines the generic assets of fast neutron reactors with those related to molten fluoride salts as liquid fuel. The salt considered as primary candidate in this concept, is the binary system LiF-ThF_4 with the addition of ^{233}U or ^{239}Pu in the form of fluorides serving as startup fissile material.

For the safety assessment of a molten salt reactor it is extremely important to know the phase equilibria of the fuel during operating and off-normal conditions. Therefore, the aim of this study is to improve the knowledge of the thermodynamic properties of the LiF-ThF_4 system. The only up to date experimental data for the LiF-ThF_4 phase diagram were obtained by Thoma *et al.* [3]. Using thermal analysis coupled with X-ray analysis of the crystalline phases they found one congruently melting compound (Li_3ThF_7) and three incongruently melting compounds $Li_7Th_6F_{31}$, $LiTh_2F_9$ and $LiTh_4F_{17}$ [4]. A later study by the same authors [5] considers the intermediate compound $LiThF_5$ instead of $Li_7Th_6F_{31}$. However, the correct intermediate compound has not been yet clarified. The thermodynamic assessments published in the past [6, 7] were based on the phase diagram temperatures, which were at that time the only available data found in the literature.

In this study, new experimental data on the phase transitions were collected and the enthalpy of mixing of the (Li,Th)F_x liquid solution was studied using a new technique which was first tested on the LiF-KF system as presented in this work as well. Both experimental data sets were obtained using Differential Scanning Calorimetry (DSC), which is based on the detection of temperature changes between the sample and reference crucible upon heating. Furthermore, the intermediate compound Li_3ThF_7 was synthesized and its enthalpy of fusion was determined. Based on our new experimental data, a thermodynamic re-assessment of the LiF-ThF_4 system has been performed.

3.2. EXPERIMENT

3.2.1. MATERIALS

The samples used for all the experiments were prepared from pure lithium fluoride LiF and potassium fluoride KF, obtained from Alfa Aesar, and thorium tetrafluoride ThF_4, obtained from Rhodia (France). Since the fluorides exhibit tendency to absorb water molecules, the handling of samples has been done in argon glove boxes in which a very low concentration of water vapour is ensured. In order to remove the residual moisture, LiF and KF were subjected to a purification, which consist of a heating cycle at 350 °C for several hours in inert Argon atmosphere. The ThF_4 shows in addition a tendency to oxidize and a special purification process is required to turn the oxide impurities into

fluorides. The purification method adopted, described in literature [8], is based on the reaction with ammonium hydrofluoride NH_4HF_2, which serves as fluorinating agent. The mixture is heated in a closed stainless steel container lined with nickel and the reaction occurs during a heating cycle at 250°C for 12 hours. It is followed by a second cycle in an open nickel container to allow the evaporation of residual ammonium fluoride and formed water. Both heating cycles were performed in a furnace under Ar/H_2 flow to avoid oxygen presence. The purity of the thus prepared salts was checked first using the DSC method for the identification of melting point. The obtained results (T=1383 K) were in close agreement with the previously published data [9] with the discrepancy of 3 K which is within the error of the DSC technique. Furthermore, the purity was confirmed by x-ray analysis, which indicated pure phase with no contaminants.

The provenance and the purity of all initial materials is summarized in Table 3.1.

3.2.2. MIXING ENTHALPY DETERMINATION TECHNIQUE

A new method to measure the enthalpy of mixing of binary systems compatible with the available DSC equipment has been developed in this work. The DSC instrument used in this study is a SETARAM MDHTC96 and is made of a furnace for heating and cooling the sample at constant rate and a detector monitoring the heat flow change between the sample and reference crucibles. Both crucibles are surrounded by a series of interconnected S-type thermocouples, suited up to 1400°C. In order to avoid vapour release of analyzed sample during measurements, an encapsulation technique previously developed at ITU [10] was adopted.

The principle of the novel method is schematically shown in Figure 3.1. Before the experiment, the end-members (LiF, KF, ThF_4) were compressed into pellets and placed in the gas tight crucible. The compound with the lower melting point is placed in the bottom part and the two salts are separated by a thin nickel liner in order to avoid eutectic melting upon heating. A standard program consisting of four thermic cycles was used for each measurement. Upon the first heating the mixing enthalpy was determined, while the subsequent cycles were used for the phase diagram equilibria determination of the formed mixture. The heating cycles were performed with a constant rate of 10 K/min up to above melting temperature of higher melting end-member (up to T=1373 K and

Table 3.1: Provenance and purity of the materials used in this study.

Material	Supplier	Metallic purity
LiF	Alfa Aesar	99.99 w%[a]
KF	Alfa Aesar	99.99 w%[a]
ThF_4	Rhodia	98+ w%[b]
NH_4HF_2	Sigma Aldrich	99.999 w%[a]

[a] Given by the supplier.
[b] Minimal estimated purity, based on XRD analysis.

T=1523 K in case of LiF-KF system, resp. LiF-ThF_4 system). The mixing occurs during the first heating, when the first melting temperature is reached. At this stage the nickel separator sinks in the formed molten phase and the two salts come in contact. The total enthalpy of this thermal event consists of three contributions: the fusion enthalpies of the two end-members and the enthalpy of mixing.

Therefore, the enthalpy of mixing is obtained from the total DSC signal subtracting the fusion contributions of the end-members. Since relatively large quantity must be subtracted from the total signal measured, the accuracy of the technique is highly dependent on the precision of the sensitivity determination. It was observed that the sensitivity of the apparatus is slightly different for various measurement runs, therefore a method with internal silver standard as described in [11] was applied. Using such a setup the standard material is placed in the reference crucible and measured in the same cycle with the sample. In this way it is possible to calculate the detector sensitivity of each measurement individually. To justify this technique a series of test measurements were performed prior to measurements including pure LiF and pure KF with well established fusion enthalpies, using anhydrous NaCl as second standard. The values for LiF and KF obtained from our test campaign are respectively 27850 J·mol^{-1} and 28320 J·mol^{-1}, in a good agreement with NIST-JANAF values [12]: 27100 J·mol^{-1} for LiF and 27200 J·mol^{-1} for KF.

A typical DSC output of one of the measured LiF-ThF_4 compositions using the silver standard placed in the reference crucible is shown in Figure 3.2. The first single peak corresponds to the sum of the fusion enthalpy of LiF, fusion enthalpy of ThF_4 and mixing enthalpy of the formed solution, whereas the second peak with opposite direction refers to melting of silver standard. Note that although both signals are endothermic, the opposite direction is due to different positioning in sample, resp. reference crucibles. Wether the complete mixing occurred upon LiF melting is confirmed by no peak appearance at the melting temperature of pure ThF_4. The corresponding cooling curve shows again the signal related to melting of silver standard and liquidus and solidus points of the formed solution.

3.3. RESULTS

3.3.1. MIXING ENTHALPY OF THE (LI,K)F LIQUID SOLUTION

The technique to measure mixing enthalpies of liquid solutions as described in the previous section was first demonstrated by the determination of the LiF-KF mixing enthalpy as this binary mixture has been already studied in the past [13, 14] and most recently by Hong and Kleppa [15] at T=1360 K and T=1176 K.

In this work, in total nine intermediate compositions were prepared and measured using the DSC technique. The mixing enthalpy was determined for T=1121 K (melting point of LiF) and the results are reported in Table 3.2. The errors were calculated based on the sensitivity uncertainty obtained from the calibration process and considering the accuracy of the fusion enthalpy data of the mixing end-members. Quantitatively, the uncertainty is larger compared to work of Hong and Kleppa [15], but in their study the

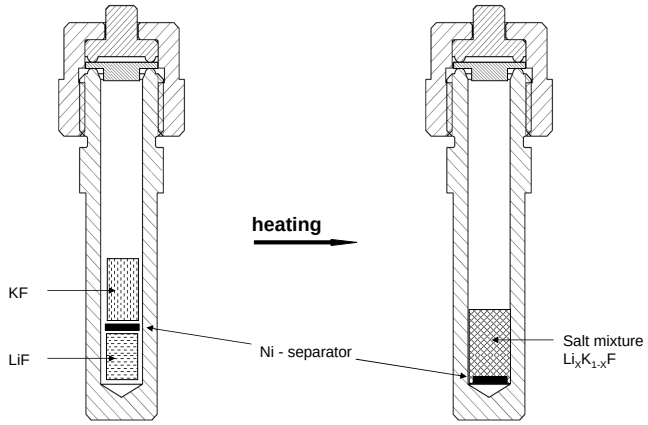

Figure 3.1: Schematic representation of the technique to measure the enthalpy of mixing.

mixing enthalpy was measured directly whereas in our work, as described in the previous section, the subtraction of the fusion enthalpy contributions from the total signal measured was necessary. Nevertheless, the comparison with the existing literature data which is given in Figure 3.3 shows a good agreement and justifies that the presented technique is suitable for obtaining reliable data.

3.3.2. MIXING ENTHALPY OF (LI,TH)F_x LIQUID SOLUTION

Prior to the mixing enthalpy measurements the fusion enthalpy of pure ThF_4 was experimentally determined by the DSC technique, giving ΔH_{fus}=41.9±2.0 kJ·mol^{-1}. This value is in excellent agreement with the previously reported value ΔH_{fus}=41.8 kJ·mol^{-1} [9] and was used in this work to assess the mixing properties. We have to note here that for the current analysis we considered no temperature dependence of the ThF_4 fusion enthalpy. This assumption was checked by the DSC analysis of the cooling curves as strong supercooling of ThF_4 was observed at cooling rate 10 K/min, giving supercooled melting temperature of 1194 K, thus 189 K lower than equilibrium value. Careful analysis revealed almost the same peak area as for the heating curve and since the same agreement was observed for silver standard, it suggests no temperature dependence of ThF_4 fusion enthalpy in this temperature range.

The determination of the mixing enthalpy of the LiF-ThF_4 system was more complex than in case of the LiF-KF system as the end-members have very different melting

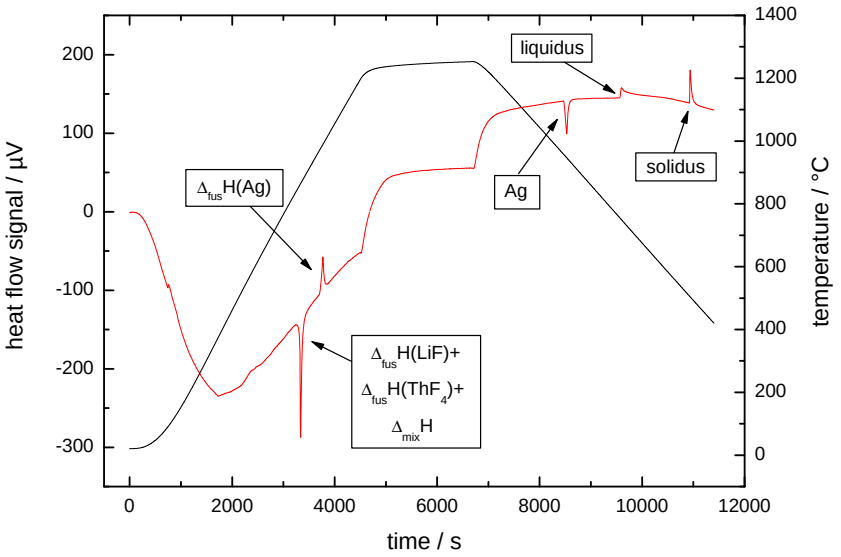

Figure 3.2: A DSC output of the measurement of the LiF-ThF$_4$ mixing enthalpy using the novel technique.

Table 3.2: Mixing enthalpy of the LiF-KF system experimentally determined in this study at 1121 K.

X (KF)	$\triangle_{mix}$H/(J·mol^{-1})	Error^a /(J·mol^{-1})
0.4771	-4110	808
0.5609	-4350	800
0.4420	-4200	805
0.6542	-3950	814
0.1901	-2410	867
0.2669	-3660	823
0.8028	-3340	836
0.3415	-3940	814
0.9029	-2950	850

^{a} The error is based on the standard uncertainty determined during the calibration.

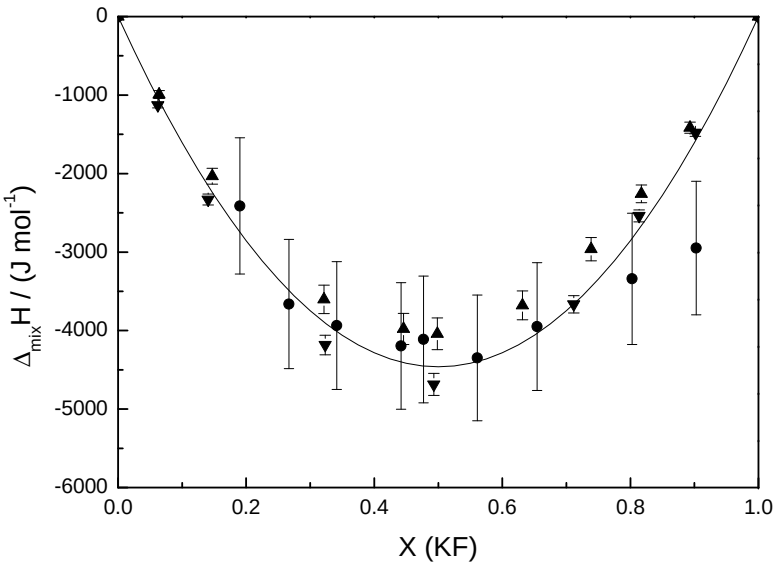

Figure 3.3: Mixing enthalpy of the LiF-KF system. (•) Data obtained in this study at T=1121 K. (▲) Data by Hong and Kleppa [15] at T=1360 K. (▼) Data by Hong and Kleppa [15] at T=1176 K. The line represent a regular fit of our data.

points. It was sometimes the case that the mixing did not occur in a proper way and a second peak was observed at the ThF_4 melting point indicating presence of some unreacted ThF_4. In general no data were deduced from such measurements. Due to these experimental complications a limited number of points was taken into account for the analysis, but showing consistent composition dependence. It also sometimes appeared that the quantitative analysis of the first peak at LiF melting point revealed contribution corresponding only to the LiF fusion heat. Possible explanation could be that the compounds stayed unmixed until the melting temperature of ThF_4 was reached, probably due to the position of the Ni-plate. At this point the mixing occurred and a single DSC peak corresponding to the sum of enthalpy of fusion of ThF_4 and mixing enthalpy was measured. Therefore two sets of data were obtained in this study, one referred to melting temperature of LiF, thus at T=1121 K, and the other one upon melting of ThF_4 at T=1383 K. The data are summarized in Table 3.3 and plotted in Figure 3.4, the errors identified in a same way as in the case of the LiF-KF system. The figure shows that the experimental data are significantly higher than the calculated mixing enthalpy from the previous assessment [7]. Hence, a re-assessment of the LiF-ThF_4 phase diagram considering these novel experimental data was suggested.

3.3.3. LiF-ThF_4 EQUILIBRIUM DATA

After the enthalpy of mixing determination the equilibrium data of the LiF-ThF_4 system were measured. The obtained values are reported in Table 3.4 and represent the average value of three consecutive heating cycles. For a given composition only the data which were within ± 10 K were considered. As shown in Figure 3.5 the data obtained in this study are generally in a good agreement with the data of Thoma *et al.* [3] reported previously. Our measurement suggests an existence of the $LiThF_5$ phase, instead of $Li_7Th_6F_{31}$, as a transition was observed in the composition range X_{ThF_4} = 0.46-0.5. Furthermore a behaviour of an unknown origin was observed in the composition range X_{ThF_4} = 0.6-0.7, where an unexpected transition at T=945 K was observed. A more careful analysis of the DSC spectra for all these four measurements has revealed small unreacted quantity of ThF_4 and hence these points were not taken into account for the modelling of the phase diagram.

Table 3.4: Phase diagram equilibria of the LiF-ThF_4 system obtained by DSC in this study.

X (ThF_4)	T^a / K	Equilibrium	X (ThF_4)	T^a / K	Equilibrium
0	1118.9	LiF m.p.	0.4703	874.3	Peritectic
0.0638	831.6	Eutectic	0.4703	1043.9	Peritectic
0.0638	1097.8	Liquidus	0.4703	1097.8	Liquidus
0.1052	836.1	Eutectic	0.4809	819.6	Eutectic
0.1052	1057.4	Liquidus	0.4809	871.6	Peritectic
0.1286	835.2	Eutectic	0.4809	1053.1	Peritectic
0.1286	1036.5	Liquidus	0.4809	1109.2	Liquidus

Continued on next page

Table 3.4 – *Continued from previous page*

X (ThF_4)	T[a] / K	Equilibrium	X (ThF_4)	T[a] / K	Equilibrium
0.182	835.9	Eutectic	0.4894	830.8	Eutectic
0.182	959.2	Liquidus	0.4894	872.0	Peritectic
0.2151	834.5	Eutectic	0.4894	1040.4	Peritectic
0.2151	889.7	Liquidus	0.4894	1121.6	Liquidus
0.250	831.3	congruent melting	0.5214	861.7	Peritectic
0.2774	832.4	Eutectic	0.5214	1038.1	Peritectic
0.3137	825.0	Eutectic	0.5214	1134.6	Liquidus
0.3137	873.9	Liquidus	0.6084	860.3	Peritectic
0.3208	828.0	Eutectic	0.6084	945.2	Unknown
0.3208	881.1	Liquidus	0.6084	1048.4	Peritectic
0.3412	826.3	Eutectic	0.6084	1162.2	Liquidus
0.3412	870.5	Peritectic	0.6211	853.1	Eutectic
0.3412	973.4	Liquidus	0.6211	945.2	Unknown
0.361	834.3	Eutectic	0.6211	1049.0	Peritectic
0.361	879.5	Peritectic	0.6211	1159.1	Liquidus
0.361	982.8	Liquidus	0.6487	942.4	Unknown
0.3752	827.8	Eutectic	0.6487	1047.6	Peritectic
0.3752	875.3	Peritectic	0.6487	1171.4	Liquidus
0.3752	991.0	Liquidus	0.6573	935.1	Unknown
0.3907	831.8	Eutectic	0.6573	1059.4	Peritectic
0.3907	875.8	Peritectic	0.6573	1194.5	Liquidus
0.3907	1001.8	Liquidus	0.7143	1028.0	Peritectic
0.4103	831.9	Eutectic	0.7143	1181.4	Peritectic
0.4103	879.2	Peritectic	0.7143	1230.1	Liquidus
0.4103	991.3	Liquidus	0.7809	1188.0	Peritectic
0.4377	831.4	Eutectic	0.7809	1274.6	Liquidus
0.4377	873.4	Peritectic	0.8417	1159.3	Peritectic
0.4377	1064.6	Liquidus	0.8417	1296.7	Liquidus
0.4423	833.4	Eutectic	0.9083	1138.0	Peritectic
0.4423	880.2	Peritectic	0.9083	1328.5	Liquidus
0.4423	1057.5	Liquidus	1	1386.0	ThF_4 m.p.
0.4703	824.5	Eutectic			

[a] Maximum temperature error is 10 K.

Table 3.3: Enthalpy of mixing of the LiF-ThF_4 system experimentally determined in this study at T=1121 K and T=1383 K.

X (ThF_4)	$\triangle_{mix}$ H/ (J·mol^{-1})	Error[a]/(J·mol^{-1})
	Data at T=1121 K	
0.3137	-8810	812
0.4423	-10140	832
0.1052	-4850	843
0.2151	-7570	805
0.2774	-8760	795
	Data at T=1383 K	
0.1286	-4970	270
0.1820	-5807	360

[a] The error is based on the standard uncertainty determined during the calibration.

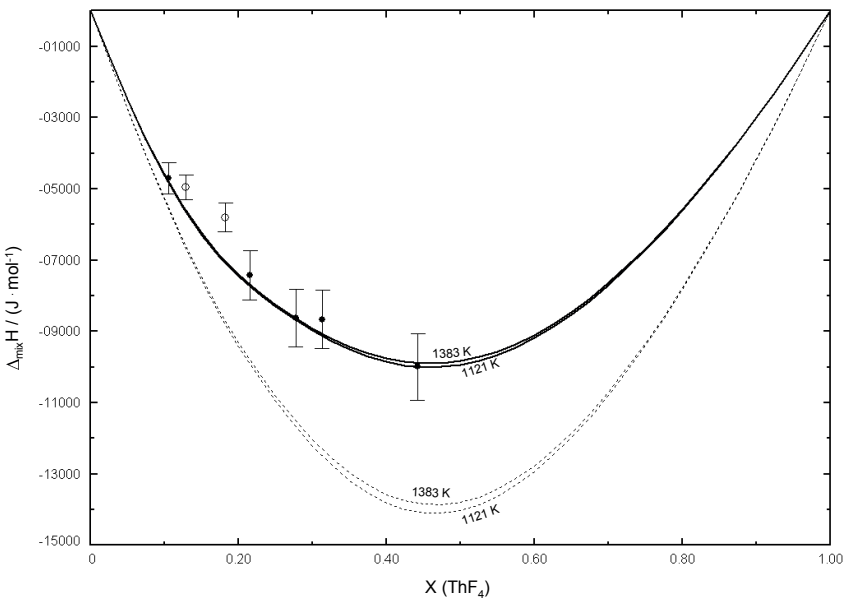

Figure 3.4: Enthalpy of mixing of the LiF-ThF_4 system. (•) Data obtained in this study at T=1121 K. (○) Data obtained in this study at T=1383 K. Solid line: Calculated enthalpy of mixing from the assessment performed in this work. Dotted line: Calculated enthalpy of mixing from the previous assessment [7].

3.3.4. Li_3ThF_7 COMPOUND

The LiF-ThF_4 system consists of four intermediate phases in the solid state. While the melting points and some information on the crystal structure of these compounds are available, the thermodynamic properties have not been completely determined. In this work, the congruently melting compound Li_3ThF_7 was synthesized by mixing stoichiometric quantities of purified LiF and ThF_4. To achieve complete reaction between these end-members the prepared mixture was heated in a closed crucible above the melting of ThF_4. The purity of the thus synthesized compound was checked by X-ray technique for the crystalline structure and by DSC technique for the melting point identification. Both analyses confirmed high purity of the sample. One clear peak was observed in the DSC spectra, confirming the congruently melting behaviour of the compound at T=831 K. The heat of fusion of the Li_3ThF_7 compound, was experimentally determined as $\triangle H_{fus}$=54.8±8.0 kJ·mol^{-1}, in a good agreement with the literature data by Gilbert [16] who found $\triangle H_{fus}$=58.4 kJ·mol^{-1}.

3.4. THERMODYNAMIC MODELLING

Using the thermodynamic data obtained in this study, the LiF-ThF_4 phase diagram has been re-assessed. The optimization was done according to Calphad method using a Factsage software [17]. An assessment of a phase diagram requires knowledge of the Gibbs energy functions of all phases considered in a system. For pure compounds, the Gibbs energy function is defined as:

$$G(T) = \triangle_f H^0(298) - S^0(298)\,T + \int_{298}^{T} C_P(T)\,\mathrm{d}T - T\int_{298}^{T} \frac{C_P(T)}{T}\,\mathrm{d}T \tag{3.1}$$

where $\triangle_f H^0(298)$ is the standard enthalpy of formation and $S^0(298)$ is the standard absolute entropy, both referring to a temperature of 298.15 K. $C_P(T)$ is the heat capacity as a function of temperature.

3.4.1. PURE COMPOUNDS

The thermodynamic functions for pure LiF and pure ThF_4 were derived from literature, respectively from [7] and [9] with different estimation of the heat capacity of liquid ThF_4 as discussed further. The thermodynamic functions of intermediate compounds were not known and were estimated or obtained by optimization. The heat capacities of these compounds were estimated by Neumann-Kopp rule from its LiF and ThF_4 end members. Based on the experimental equilibrium data obtained in this study the intermediate compound $LiThF_5$ instead of the $Li_7Th_6F_{31}$ compound was considered during the assessment. Table 3.5 reports all the thermodynamic data used in this study.

3.4.2. LIQUID SOLUTION

The Gibbs energy function of a solution is described by the following equation:

$$G(T) = x_A \cdot G_A + x_B \cdot G_B + x_A RT\ln x_A + x_B RT\ln x_B + \triangle G^{xs} \tag{3.2}$$

Table 3.5: Thermodynamic data for pure compounds and intermediate compounds used in this study for the phase diagram assessment: $\Delta_f H^0(298)$ (kJ·mol^{-1}), $S^0(298)$ (J·K^{-1}·mol^{-1}) and heat capacity coefficients C_p (J·K^{-1}·mol^{-1}).

Compound	$\Delta_f H^0(298)$	$S^0(298)$	a	b·T	c·T^2	d·T^{-2}
LiF (s)	-616.931	35.660	43.309	$1.631\cdot10^{-2}$	$5.047\cdot10^{-7}$	$-5.691\cdot10^{6}$
LiF (l)	-598.654	42.962	64.183			
ThF_4(s)	-2097.900	142.05	122.173	$8.37\cdot10^{-3}$		$-1.255\cdot10^{6}$
ThF_4(l)	-2103.654	101.237	170[a]			
Li_3ThF_7(s)[a]	-3943.210	268.1	252.100	$5.730\cdot10^{-2}$	$1.514\cdot10^{-6}$	$-2.962\cdot10^{6}$
$LiThF_5$(s)[a]	-2711.425	189.89	165.482	$2.468\cdot10^{-2}$	$5.047\cdot10^{-7}$	$-1.824\cdot10^{6}$
$LiTh_2F_9$(s)[a]	-4807.970	337.29	287.655	$3.305\cdot10^{-2}$	$5.047\cdot10^{-7}$	$-3.079\cdot10^{6}$
$LiTh_4F_{17}$(s)[a]	-9003.500	624.0	532.001	$4.979\cdot10^{-2}$	$5.047\cdot10^{-7}$	$-5.589\cdot10^{6}$

[a] optimized in this study

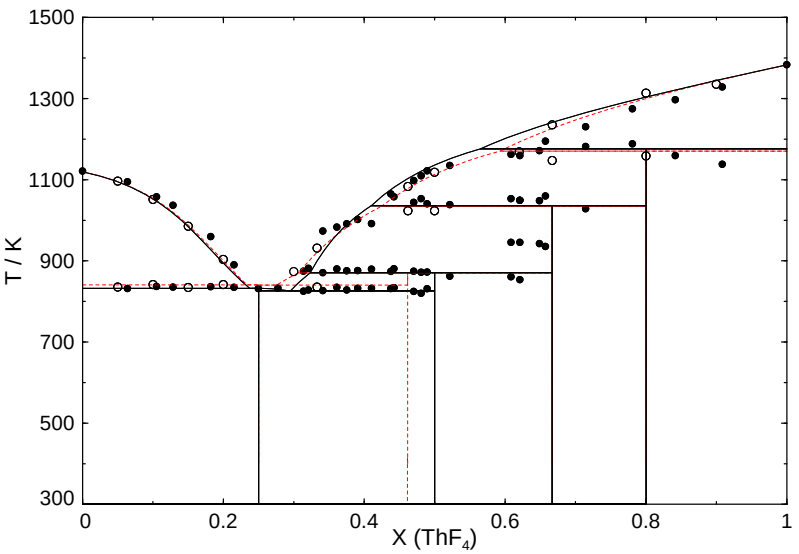

Figure 3.5: The LiF-ThF_4 phase diagram optimized in this study (solid line) in comparison with our previous version (dotted line) [7]. (•) Data measured in this work; (○) Data obtained by Thoma *et al.* [3].

where G_A and G_B are the molar Gibbs energies of the end-members, x_A and x_B are mole fractions of mixed end-members and $\triangle G^{xs}$ is the excess Gibbs energy function. For the description of the (Li,Th)F_x liquid solution the quasi-chemical model that is used at ITU for fluoride salt database was adopted. The excess Gibbs parameters described by the used quasi-chemical model are the Gibbs energy changes $\Delta g_{LiTh/F}$ for the second nearest neighbor (SNN) pair-exchange reaction:

$$(Li-F-Li)+(Th-F-Th)=2(Li-F-Th) \qquad \Delta g_{LiTh/F} \tag{3.3}$$

The $\Delta g_{AB/F}$ parameter for given reaction can be expanded as a polynomial such as:

$$\Delta g_{LiTh/F} = \Delta g^0_{LiTh/F} + \sum_{(i+j)\geqq 1} g^{ij}_{LiTh/F} \chi^i_{LiTh/F} \chi^j_{ThLi/F} \tag{3.4}$$

where $\Delta g^0_{LiTh/F}$ and $g^{ij}_{LiTh/F}$ are composition independent coefficients (although possibly temperature dependent) obtained from the optimization of the experimental data for the binary LiF-ThF_4 liquid solution. The $\chi_{LiTh/F}$ term is a composition variable and is defined as

$$\chi_{LiTh/F} = \left(\frac{X_{LiLi}}{X_{LiLi} + X_{LiTh} + X_{ThTh}} \right). \tag{3.5}$$

The quasi-chemical model used in this study was presented by Pelton *et al.* [18] and Chartrand *et al.* [19] and one of the big advantages of this model is to freely permit the choice of the composition of maximum short range ordering in a binary system thus very well suited for the description of ionic liquids. The selection is done by the definition of cation-cation coordination numbers $Z^{Li}_{LiTh/FF}$ and $Z^{Th}_{LiTh/FF}$ and is of importance to perform thermodynamic optimization as the excess Gibbs function of the solution tends to have its minimum here. The values of cation-cation coordination numbers that have been used in this study are reported in Table 3.6. These coordination numbers correspond exactly to one point where one expects maximum short range ordering, and thus are composition independent.

Once the cation-cation coordination numbers are selected the anion-anion coordination numbers are defined according to the following equation in order to maintain the electro-neutrality in the system.

$$\frac{q_{Li}}{Z^{Li}_{LiTh/FF}} + \frac{q_{Th}}{Z^{Th}_{LiTh/FF}} = \frac{q_F}{Z^F_{LiTh/FF}} + \frac{q_F}{Z^F_{LiTh/FF}} \tag{3.6}$$

Table 3.6: Cation-cation coordination numbers of the liquid.

A-cation	B-cation	Z^A_{AB}	Z^B_{AB}
Li^+	Li^+	6	6
Th^{4+}	Th^{4+}	6	6
Li^+	Th^{4+}	2	6

The q_{Li}, q_{Th} and q_F terms in the above given formula are the absolute charges of various ions, thus I, IV and -I respectively. The excess Gibbs parameters of the (Li,Th)F_x liquid solution optimized in this study are given below keeping the same notation as proposed by Chartrand and Pelton [20].

$$\Delta g_{LiTh/FF} = -10883 + \chi_{LiTh/F}(-6697 + 2.93T) + \chi_{ThLi/F}(-20930 + 19.25T) \quad \mathrm{J \cdot mol^{-1}} \quad (3.7)$$

3.4.3. LiF-ThF_4 PHASE DIAGRAM

Considering the new experimental data for the mixing enthalpy of the (Li,Th)F_x liquid solution, the new LiF-ThF_4 equilibrium data and the fusion enthalpy of Li_3ThF_7 the LiF-ThF_4 phase diagram has been re-optimized and the result is shown in Figure 3.5. The figure compares the obtained phase diagram with the previous version [7] which was based solely on the equilibrium data of Thoma *et al.* [3]. The system is characterized by five invariant equilibria; two eutectics and three peritectics. The exact temperatures and compositions are reported in Table 3.7 with comparison to the previous assessment. While the peritectic temperatures are almost identical the two eutectics are slightly lower in order to agree with new experimental equilibrium data and in order to reproduce the experimentally determined melting temperature of the Li_3ThF_7 compound found at 831 K.

The liquidus line shows a good agreement in the LiF rich region, however some discrepancies between the two versions are found in the middle range of the phase diagram. Although both liquidus descriptions are within experimental errors of the measurements, the higher liquidus line found in the current assessment is due to higher entropy of mixing which was better optimized taking into account the measured enthalpy of mixing. The calculated enthalpy and entropy of mixing for the (Li,Th)F_x liquid solution are reported in Figures 3.4 and 3.6 for T=1121 K and T=1383 K, the former quantity in excellent agreement with the experimental data obtained in this study. The mixing enthalpy shows a very regular profile, whereas the entropy shows a strong inflection at around the 1:1 ratio with higher values in the LiF region. Such behaviour is typical for systems that have some short range ordering which is preferential at certain concentrations. The entropy of mixing derived from our assessment correlates very well with the NMR studies performed on the same system by Bessada *et al.* [21]. They found a high concentration of free F^- ions at the LiF rich region while at ThF_4 side their studies confirmed bridging of these fluoride ions with ThF_4 clusters increasing ordering of the system and consequently decreasing the entropy.

Based on the experimental equilibrium data and the mixing enthalpy data the excess Gibbs energy of the (Li,Th)F_x liquid solution was optimized as shown above. It was however not possible to reproduce the measured fusion enthalpy of the congruently melting Li_3ThF_7 intermediate compound without optimizing the heat capacity of the pure liquid ThF_4 which is not known experimentally. Initially the suggested 133.9 $\mathrm{J \cdot K^{-1} \cdot mol^{-1}}$ value [9] was considered, but this value appears to be underestimated, e.g. in comparison to the experimentally determined heat capacity of liquid UF_4 found at 174.74 $\mathrm{J \cdot K^{-1} \cdot mol^{-1}}$. With such low value the calculated fusion enthalpy of Li_3ThF_7 was 80.8 $\mathrm{kJ \cdot mol^{-1}}$, thus much higher than the experiment. Therefore, the heat capacity of liquid ThF_4

was optimized to target the measured fusion enthalpy of Li_3ThF_7. It was found that increasing the ThF_4 heat capacity to 170 $J{\cdot}K^{-1}{\cdot}mol^{-1}$ gives fusion enthalpy of Li_3ThF_7 58.4 $kJ{\cdot}mol^{-1}$ which is in excellent agreement to the value of Gilbert [16] and the measured value in this study.

3.5. CONCLUSIONS

It has been demonstrated in this study that the conventional DSC technique can be applied to determine mixing enthalpies of liquid solutions. Using the presented approach the mixing enthlapy of the (Li,Th)F_x liquid solution was measured for the first time and these data were subsequently used to re-optimize the LiF-ThF_4 phase diagram. It has been shown that for the thermodynamic assessment of a binary system the mixing enthalpy data are of big importance as they lead to better description of the Gibbs energy function of the liquid solution and thus of the mixing entropy. Furthermore it has been shown that it is always fruitful to have more than just one set of experimental data for a studied system, especially when there is large number of unknown parameters which are subject of optimization during the performance of a thermodynamic assessment. In the present case this has been demonstrated by consideration of the measured fusion enthalpy of the congruently melting Li_3ThF_7 compound which we believe lead to more realistic estimate of the heat capacity of the liquid ThF_4. Further experiments are recommended to confirm the value of this quantity.

ACKNOWLEDGEMENT

M.B. and E.C. acknowledge the European Commission for support given in the frame of the program "Training and Mobility of Researchers". The authors want to thank Rhodia for providing the ThF_4 sample. This work was supported by the EVOL project in the FP7 work programme of the European Commission (Grant agreement no. 249696).

Table 3.7: Invariant equilibria in the LiF-ThF_4 system.

Equilibrium	*This study*		*Previous study [7]*	
	T / K	X (ThF_4)	T / K	X (ThF_4)
Eutectic	832	0.238	841	0.234
Eutectic	826	0.294	840	0.276
Congruent melting	832	0.250	842	0.250
Peritectic	870	0.323	870	0.307
Peritectic	1038	0.411	1035	0.426
Peritectic	1176	0.565	1170	0.592

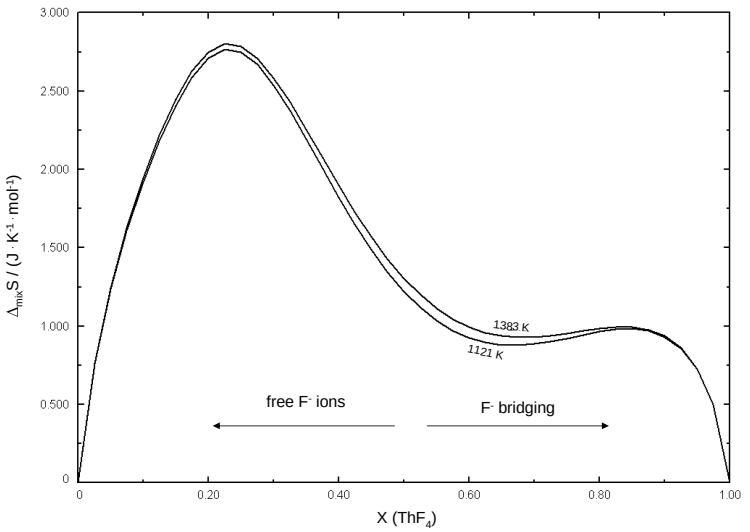

Figure 3.6: The mixing entropy of the (Li,Th)F$_x$ liquid solution calculated from the thermodynamic assessment of the LiF-ThF$_4$ system for T=1121 K and T=1383 K.

REFERENCES

[1] E. Capelli, O. Beneš, M. Beilmann, and R. J. M. Konings, *Thermodynamic investigation of the LiF-ThF_4 system,* J. Chem. Thermodyn. **58**, 110 (2013).

[2] S. Delpech, E. Merle-Lucotte, D. Heuer, M. Allibert, V. Ghetta, C. Le-Brun, X. Doligez, and G. Picard, *Reactor physics and reprocessing scheme for innovative molten salt reactor system,* J. Fluor. Chem. **130**, 11 (2009).

[3] R. E. Thoma, H. Insley, B. S. Landau, H. A. Friedman, and W. R. Grimes, *Phase equilibria in the fused salt systems LiF-ThF_4 and NaF-ThF_4,* J. Phys. Chem. **63**, 1266 (1959).

[4] L. A. Harris and G. D. White, *X-Ray analyses of the solid phases in the system LiF-ThF_4,* J. Phys. Chem. **63**, 1974 (1959).

[5] R. E. Thoma, *Advances in Molten Salt Chemistry,* (Plenum Press, 1975) Chap. 6, p. 275.

[6] J. van der Meer, R. J. M. Konings, M. H. G. Jacobs, and H. A. J. Oonk, *A miscibility gap in LiF-BeF_2 and LiF-BeF_2-ThF_4,* J. Nucl. Mat. **344**, 94 (2005).

[7] O. Beneš, M. Beilmann, and R. J. M. Konings, *Thermodynamic assessment of the LiF–NaF–ThF_4–UF_4 system,* J. Nucl. Mater. **405**, 186 (2010).

[8] B. N. Wani, S. J. Patwe, U. R. K. Rao, and K. S. Venkateswarlu, *Fluorination of oxides of uranium and thorium by ammonium hydrogen fluoride,* J. Fluor. Chem. **44**, 177 (1989).

[9] R. J. M. Konings, J. P. M. van der Meer, and E. Walle, *Chemical aspects of Molten Salt Reactor Fuel*, Tech. Rep. (2005) ITU-TN 2005/25.

[10] O. Beneš, R. J. M. Konings, S. Wurzer, M. Sierig, and A. Dockendorf, *A DSC study of the $NaNO_3$–KNO_3 system using an innovative encapsulation technique,* Thermochim. Acta **509**, 62 (2010).

[11] O. Beneš, D. Sedmidubský, M. Beilmann, O. S. Valu, E. Capelli, M. Salanne, S. Nichenko, and R. J. M. Konings, *A comprehensive study of the heat capacity of CsF from 5 K to 1400 K,* J. Chem. Thermodyn. **57**, 92 (2013).

[12] M. W. Chase Jr.(ed.), *NIST-JANAF Thermochemical Tables Fourth Edition,* J. Phys. Chem. Ref. Data, Monograph **9**, (1998).

[13] R. A. Gilbert, *Enthalpies of mixing in the molten lithium fluoride-potassium fluoride system,* J. Phys. Chem. **67**, 1143 (1962).

[14] J. L. Holm and O. J. Kleppa, *Enthalpies of mixing in binary liquid alkali fluoride mixtures,* J. Chem. Phys. **49**, 2425 (1968).

[15] K. C. Hong and O. J. Kleppa, *Enthalpies of mixing in some binary liquid alkali fluoride mixtures,* J. Chem. Thermodyn. **8**, 31 (1976).

[16] R. A. Gilbert, *Heat of fusion of 3LiF·ThF_4*, J. Chem. Eng. Data **7**, 388 (1962).

[17] C. W. Bale and et al., *Factsage Software,* (v. 6.2).

[18] A. D. Pelton, P. Chartrand, and G. Eriksson, *The Modified Quasi-chemical Model: Part IV. Two sublattice quadruplet approximation,* Metall. Trans. **32A**, 1409 (2001).

[19] P. Chartrand and A. D. Pelton, *The Modified Quasi-chemical Model: Part III. Two sublattice,* Metall. Trans. **32A**, 1397 (2001).

[20] P. Chartrand and A. D. Pelton, *Thermodynamic evaluation and optimization of the LiF-NaF-KF-MgF_2-CaF_2 system using the modified quasi-chemical model,* Metall. Trans. **32A**, 1385 (2001).

[21] C. Bessada, A. Rakhmatullin, A. L. Rollet, and D. Zanghi, *Lanthanide and actinide speciation in molten fluorides: A structural approach by NMR and EXAFS spectroscopies,* J. Nucl. Mater. **360**, 43 (2007).

4

DETERMINATION OF THE THERMODYNAMIC ACTIVITIES OF LiF AND ThF_4 IN THE $Li_xTh_{1-x}F_{4-3x}$ LIQUID SOLUTION BY KEMS

Elisa CAPELLI, Ondřej BENEŠ, Jean-Yves COLLE, Rudy J.M. KONINGS

Knudsen Effusion Mass Spectrometry (KEMS) has been used to investigate the vapour pressure over the molten LiF-ThF_4 salt and determine the thermodynamic activity of LiF and ThF_4 in the liquid solution. As part of the study, the vaporization of pure LiF and pure ThF_4 was examined and the results were compared with the literature values finding a good agreement. Next, the vapour pressure of the $Li_xTh_{1-x}F_{4-3x}$ liquid solution was investigated by measuring four samples having different compositions ($X_{LiF} \sim$ 0.2, 0.4, 0.6, 0.8 mol%). In order to determine the thermodynamic activities, the vapour pressure of LiF and ThF_4 species over the liquid solution, as calculated from our results, were compared with the vapour pressure over the pure LiF(l) and pure ThF_4(l) systems. A strong deviation from the Raoult's law was observed, more evident in case of LiF species, in agreement with the predictions by our thermodynamic model.

Parts of this chapter have been published in Physical Chemistry Chemical Physics **17**, 30110 (2015) [1].

4.1. INTRODUCTION

The binary system LiF-ThF_4 is a key system for various designs of the Molten Salt Reactor (MSR). The MSR is one of the most promising future fission reactor technologies, selected by the Generation IV Forum, in which the fissile and fertile materials are dissolved into a molten salt mixture. Recent designs [2, 3] are based on a fast neutron spectrum reactor and on the thorium fuel cycle, therefore a crucial component is ThF_4 which is dissolved mainly in the ^{7}LiF solvent. In view of this fact, an extensive study is being conducted on the physico-chemical properties of the binary mixture LiF-ThF_4 in order to determine the operation parameters and the safety limit of this technology. With respect to the reactor safety, one of the key parameter to be assessed is the vapour pressure of the salt mixture. A low pressure system offers the advantage of reducing the main driving force of radioactivity release during accidents and it is a beneficial parameter with regard to engineering issues. Furthermore, in a multi-component salt higher evaporation of one component in comparison with the others causes a change in the final composition of the mixture leading to a change in its thermodynamic properties. Since the salt composition is usually optimized to have the lowest liquidus temperature, a change in the concentrations would lead to an increase of the melting temperature and could approach the safety limit.

Vapour pressure measurements can be used to determine the activity of a species (such as LiF or ThF_4) in a mixture, which is a measure of the thermodynamic stability of a system. These thermodynamic functions are extremely important in the development of thermodynamic models and they are particularly important in the context of the electrochemistry of the fuel salt. In fact, MSRs design includes a reprocessing of the fuel salt, mainly for separation of fissile material, actinides and fission products. Some of the steps of the global reprocessing scheme are based on the redox processes [4] and thus on the electrochemical properties and the activities of the different elements and the solvent (LiF-ThF_4).

The aim of the present work is to evaluate the vapour pressure over the molten LiF-ThF_4 salt and determine the thermodynamic activities of the end-member species in the liquid solution. The system was investigated using Knudsen Effusion Mass Spectrometry, which is a very well suited technique to measure high-temperature thermodynamic properties of condensed and gaseous phases. As first step, we have studied the vaporization of pure LiF and pure ThF_4 focusing on the liquid phase. Rather good agreement was found between our results and the literature value. Next, the vapour pressure of the $Li_xTh_{1-x}F_{4-3x}$ liquid solution was investigated by measuring four samples with different compositions ($X_{LiF} \sim$ 0.2, 0.4, 0.6, 0.8 mol%). The vapour pressure of LiF and ThF_4 species over the liquid solutions were compared with the vapour pressure over the pure LiF(l) and pure ThF_4(l). From the observed difference with the ideal behaviour, the thermodynamic activity of LiF and ThF_4 in the $Li_xTh_{1-x}F_{4-3x}$ liquid solution were determined.

4.2. EXPERIMENT

4.2.1. SAMPLE PREPARATION

All the samples measured in this work were prepared from pure lithium fluoride LiF, obtained from Alfa Aesar, and pure thorium fluoride ThF_4, obtained from Rhodia. Since fluorides are very sensitive to water molecules, the materials were stored in a protective atmosphere and the preparation of the samples was done completely inside an argon glove box, where a low level of oxygen and water is ensured (typically below 5 ppm). Moreover, both compounds have been subjected to pre-treatments to ensure the high purity of the starting materials. In case of LiF compound, it consists of a heating cycle at 623 K for several hours under inert argon flow in order to remove the residual moisture, if present. Different treatment is required for ThF_4 that shows an additional tendency to oxidize and form oxyfluorides. A purification technique was applied using NH_4HF_2 as fluorinating agent as described in detail elsewhere [5]. The purity of both compounds was then checked by identification of the melting point using the Differential Scanning Calorimeter (DSC), as described in our previous works [5, 6]. The samples were encapsulated to prevent possible reactions with water/oxygen and protect the instrument from corrosive fluoride vapours. The results were in close agreement with the literature value, within ± 5 K.

In total six samples have been prepared as listed in Table 4.1, in which the exact composition and the liquidus temperature of each sample, as measured by DSC, are reported. Typically, an amount of salt about 30-50 mg was loaded into a nickel crucible and placed in the Knudsen cell for the measurement.

4.2.2. SETUP AND MEASUREMENTS

The experimental setup used in this work consists of a Knudsen effusion cell coupled to a quadrupole mass spectrometer, as shown in Figure 4.1. The facility is specifically designed for radioactive materials and irradiated fuel samples and it is described in detail elsewhere [7]. The Knudsen cell (cell dimensions: h=21 mm, ∅=11 mm, orifice dimensions: d=0.25 mm, ∅=0.5 mm) is made of tungsten with an inserted internal liner made of pure nickel in order to avoid possible corrosion by the fluoride vapours. Prior the

Table 4.1: Composition and liquidus temperature of the samples measured in this work.

Sample	Molar fraction ThF_4	Molar fraction LiF	Liquidus temperature (K)
LiF	0	1	1121.2
$Li_{0.8}Th_{0.2}F_{1.6}$	0.200	0.800	893.8
$Li_{0.6}Th_{0.4}F_{2.2}$	0.391	0.609	1044.6
$Li_{0.4}Th_{0.6}F_{2.8}$	0.598	0.402	1200.0
$Li_{0.2}Th_{0.8}F_{3.4}$	0.796	0.204	1303.0
ThF_4	1	0	1383.2

measurement, the chamber is evacuated to high vacuum (10^{-8} – 10^{-9} kPa) so that no interference between atmosphere and sample gas molecules occurs. The cell is heated to high temperature using a tungsten-coil heating element and seven cylindrical shields, both in tungsten and tantalum, are placed around the cell to provide the required thermal isolation. The molecular beam emerging from the effusion orifice on the top of the cell is ionized by a cross electron beam and then analyzed by a quadrupole mass spectrometer.

Two main signals are measured during an investigation by the KEMS technique: the intensities of ion currents originating from the ionization of the evaporated gaseous species and the Knudsen cell temperature. The latter is measured using a pyrometer, which had been calibrated by determining the melting points (visible on the MS signal) of several standard materials (Zn, Cu, Fe, Pt, Al_2O_3). Furthermore, a calibration of the electron energy was performed prior the measurements by identifying the ionization potential of different gaseous and metal species (Ar, Kr, Xe, Zn, In, Ag).

A standard procedure was used for all the measurements performed, applying an electron ionization energy of 33.5 eV and a temperature ramp of 10 K/min. The use of a continuous temperature increase, instead of isothermal steps, allows a good description over the widest possible temperature range in a relative short time. Nevertheless, equilibrium conditions are reached during the measurements as suggested by the reproducibility of the literature values for Ag, LiF and ThF_4. The temperature was increased until both sample and standard material were quantitatively vaporized. Moreover, the possible reaction products between fluorine and tungsten were monitored but none of these masses were detected indicating that no corrosion occurred during the measurements. For the pure substances, appearance potentials measurements were also performed to identify dissociation processes. The intensity of each species was measured during two consecutive runs performed at constant temperature (1250 K for LiF and 1293 K for ThF_4) and increasing the electron energy from 0.9 to 63.4 eV with step of 0.5 eV. The complete available energy range was scanned in order to have more information on the ionization process.

4.2.3. MASS SPECTRAL ANALYSIS

Under quasi equilibrium conditions (small ratio between the orifice cross section and the vaporising surface) and low pressure conditions, the partial pressure p_A of the species A at the temperature T results from the following relation:

$$p_A = KT\frac{1}{\sigma_A}\sum_i \frac{1}{\gamma_i} I_i \tag{4.1}$$

where K is the calibration factor, σ_A is the electron impact ionization cross section of the species A, $\sum_i (1/\gamma_i) I_i$ is the sum of intensities of the ion currents i originating from the molecule A considering the efficiency (γ_i) of the Secondary Electron Multiplier (SEM) for each ion mass.

The calibration factor K is determined based on the quantitative evaporation of a known amount of a standard material, in our case silver, placed in the Knudsen cell dur-

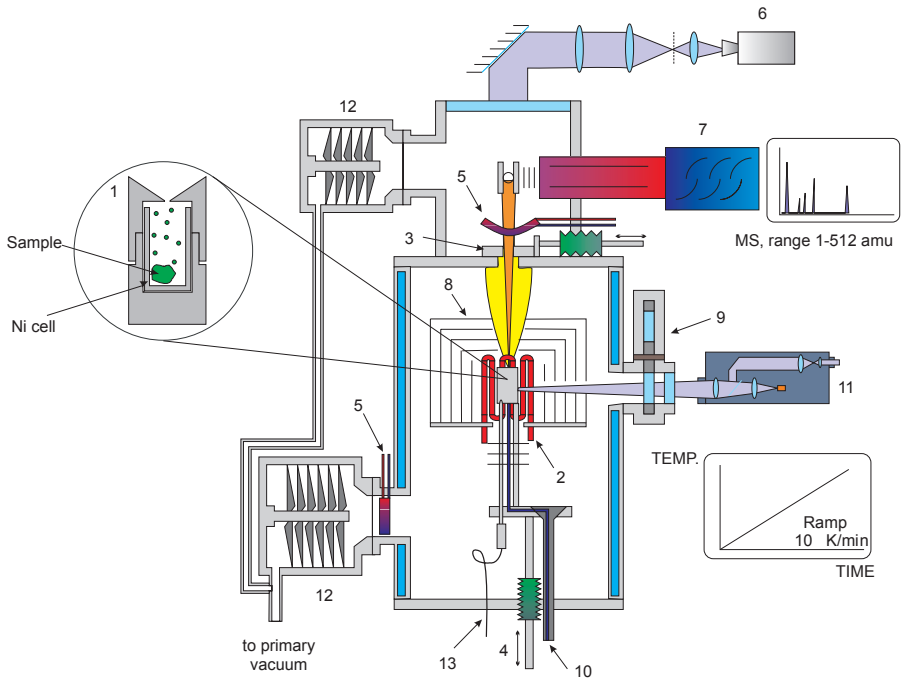

Figure 4.1: The KEMS experimental setup used in this work. Main components: (1) Knudsen cell with Ni liner; (2) tungsten resistant coil; (3) molecular beam chopper; (4) facilities to lift the cell for fast heating/cooling; (5) liquid nitrogen trap to reduce background signal; (6) CCD camera to align the cell orifice and the chopper diaphragm; (7) quadrupole mass spectrometer; (8) thermal shield; (9) revolving protection windows; (10) inlet gas capillary; (11) linear pyrometer; (12) turbo molecular pump; (13) removable W/Re thermocouple.

ing the measurements. The mass loss rate of silver $\mathrm{d}m/\mathrm{d}t$ is given by the Hertz-Knudsen equation as follows:

$$\frac{\mathrm{d}m}{\mathrm{d}t} = \frac{p_{Ag} \cdot S \cdot C \cdot \sqrt{M_{Ag}}}{\sqrt{2\pi \cdot R \cdot T}} \tag{4.2}$$

where p_{Ag} is the vapour pressure of silver, T is the temperature, M_{Ag} is the molar mass of silver, R is the universal gas constant, S is the effusion orifice surface and C is the Clausing factor. The latter term is the correction for an orifice with short but finite channel as reported by Santeler [8]. By integration over the measurement time of the Hertz-Knudsen equation combined with Eq. 4.1 for p_{Ag}, it is possible to determine the calibration factor K.

$$K = \frac{\sigma_{Ag} \cdot \gamma_{Ag} \cdot \sqrt{2\pi \cdot R} \cdot \Delta m}{S \cdot C \cdot \sqrt{M_{Ag}} \cdot \sum_n (I_{Ag} \cdot T^{1/2}) \cdot \Delta t_n} \tag{4.3}$$

where σ_{Ag} is the electron impact ionization cross section of silver, γ_{Ag} is the efficiency of secondary electron multiplier for silver, Δm is the total mass evaporated and the term $\sum_n (I_{Ag} \cdot T^{1/2}) \cdot \Delta t_n$ is the integrated product between the intensity of silver ion current and the temperature along the time of the experiments. In addition to this method, the calibration factor can be determined using the well-known vapour pressure of silver [9].

IONIZATION CROSS SECTIONS AND EFFICIENCIES OF SEM

As described in the previous section, the determination of the absolute vapour pressure requires the knowledge of the efficiency of the SEM for each recorded ion and the electron impact ionization cross section of the molecular species. A detailed explanation on the estimation of these properties as applied in this work is given in this section.

The efficiency of the secondary electron multiplier depends on the mass of the species detected and is usually approximed, as suggested by Grimley [10], to:

$$\gamma_i = \delta \, M_i^{-1/2} \tag{4.4}$$

where δ is a constant and M_i is the molar mass of the species i. Using Eq. 4.4 the normalized SEM gains γ_i/γ_{Ag} for the species Th^+, ThF^+, ThF_2^+, ThF_3^+ were determined as 0.68, 0.66, 0.63, 0.61 respectively. However, this approximation is good only for mass numbers greater than 50 amu and in case of the lighter species (Li^+, LiF^+, Li_2F^+) could not be applied. For that reason, the normalized SEM gains γ_i/γ_{Ag} for the species Li^+, LiF^+, Li_2F^+ and $Li_3F_2^+$ (0.87, 1.47, 1.66 and 2.48) were taken from Yamawaki *et al.* [11] and for more details of obtaining these values we refer to that study.

The second important term is the electron impact ionization cross section, which depends on the electron energy. For single atoms, the ionization cross sections have been computed by Mann [12, 13] and are available for a large range of energy. In this work, the SIGMA software [14], which is based on Mann's values, has been used for the calculation of the atomic cross sections. The case of molecules is more complex and the

additivity rule postulated by Otvos and Stevenson [15] is generally used. Following this rule, the cross section of a molecule is calculated as sum of the cross sections of the single components. However, this "simple" approach is not giving good estimations in case of complex molecules, such as ThF_4 in the present case. If we consider as an example the similar SiF_4 molecule, a clear contradiction of the additivity rule has been observed. In fact, for the series SiF, SiF_2, SiF_3 and SiF_4, the ionization cross section decreases with increasing number of fluorine atoms ($\sigma_{SiF_4} < \sigma_{SiF_3} < \sigma_{SiF_2} < \sigma_{SiF}$). This discrepancy was explained by Deutsch *et al.* [16] as an effect of the molecular bonding and weighting factors have to be introduced to take this effect into account. A modified additivity rule [17] has been proposed for the calculation of total electron impact cross sections of molecules of the form AB_n, as given by the following equation:

$$\sigma^+(AB_n) = [r_A^2/r_B^2]^{\alpha}[\xi_A/(\xi_A + n\xi_B)]\sigma_A^+ + [nr_B^2/r_A^2]^{\beta}[n\xi_B/(\xi_A + n\xi_B)]n\sigma_B^+ \tag{4.5}$$

where r_A and r_B are the atomic radii, taken from the table of Desclaux [18], ξ_A and ξ_B are the effective number of atomic electrons and σ_A and σ_B are the atomic ionization cross sections calculated at the correct ionization energy. The exponents α and β are explicitly dependent on r_A, r_B, ξ_A and ξ_B and they are determined empirically (see details in [17]).

Since no experimental data on the electron impact ionization cross section of ThF_4 have been found in literature, the value was calculated based on Eq. 4.5 and using parameters reported in Table 4.2. In this case the dependency of the cross section on energy is expressed solely by the energy dependence of the individual atomic ionization cross section, as follows:

$$\sigma^+(ThF_4) = 0.44\ \sigma_{Th}^+ + 2.08\ \sigma_F^+. \tag{4.6}$$

This relation gives, for the ionization energy used in our measurement, a total ionization cross section for ThF_4 of $\sigma_{ThF_4} = 8.9184 \cdot 10^{-16}$ cm^2. In case of the LiF related species, the ionization cross section normalized to silver σ_i/σ_{Ag} for the monomer, dimer and trimer was estimated to be 0.61, 0.71 and 0.85 as reported by Yamawaki *et al.* [11] for a similar ionization energy as used in this study.

THERMODYNAMIC CALCULATIONS

Calculations of thermochemical data for pure LiF and pure ThF_4 were performed using both second law and third law approaches. Second law enthalpies of reaction (vapor-

Table 4.2: Effective number of electrons, atomic radii from the tables of Desclaux [18] and ionization cross-section at 33.5 eV (used in this study) calculated from SIGMA software [14].

Atom	Effective number of electron	Atomic radius (cm)	Ionization cross-section (cm^2)
Th	22	$19.37 \cdot 10^{-9}$	$16.6974 \cdot 10^{-16}$
F	7	$3.81 \cdot 10^{-9}$	$0.7329 \cdot 10^{-16}$

ization or sublimation) $\Delta_r H^0_T$ are obtained based on the equilibrium constant measurement in a certain range of temperature, as given by the equation:

$$\Delta_r H^0_{T_M} = -R \frac{\mathrm{d}(\ln K^{eq}_T)}{\mathrm{d}(1/T)} \tag{4.7}$$

where R is universal gas constant, K^{eq}_T is the equilibrium constant of the vaporization reaction and T_M is the mean temperature of the measurement. For a simple vaporization process, such as A(s)=A(g) or A(l)=A(g), the equilibrium constant is given by the following equation:

$$K^{eq}_T = \frac{a(g)}{a(s)} \ \ resp. \ \ \frac{a(g)}{a(l)} \tag{4.8}$$

in which $a(g)$, $a(s)$ and $a(l)$ are activities of the gas phase, the solid phase and the liquid phase respectively. Since activities of solids and liquids in equilibrium are equal to unity, K^{eq}_T becomes:

$$K^{eq}_T = \frac{P(g)}{P_0} \tag{4.9}$$

where $P(g)$ is the equilibrium pressure and P_0 is the standard pressure (10^5 Pa). Thus, a plot of $ln(P(g)/P_0)$ versus $1/T$ gives a linear relation with a slope $\Delta_r H^0_{T_M}$/R. The reaction enthalpy refers to the average temperature ($1/T$) of the measurements and it is converted to the reaction enthalpy at the standard temperature $\Delta_r H^0_{298}$ by using the reported C_p function for the different phases. The enthalpy of fusion was also considered to calculate the sublimation enthalpy from the liquid state data.

The third law approach is based on similar equations but requires in addition the knowledge of the standard entropy function S^0_T for all the phases. The enthalpy of the reaction at the standard temperature is given by the following equation:

$$\Delta_r H^0_{298} = -RT\ln K^{eq}_T + T\Delta fef_T \tag{4.10}$$

where fef_T is the free energy function which is defined for each phase as:

$$fef_T = \frac{-G^0_T + H^0_{298}}{T} = S^0_T - \frac{H^0_T - H^0_{298}}{T} \tag{4.11}$$

This results in an enthalpy of reaction for each data point and the average is taken from all the data. The thermodynamic functions for the third law calculation were taken from [19] for the LiF and from [20] and [21] for ThF_4 solid and gas phases. In case of the ThF_4 liquid phase, the data have been taken from our previous work [22] where they have been revised.

4.3. RESULTS

4.3.1. VAPOUR PRESSURE OF PURE LiF

The lithium fluoride vaporization has been studied by different authors during the past years using different techniques, such as the Miller and Kusch method [23] (re-plotted by Scheefee *et al.* [24]), the KEMS technique [11, 25–27], a double-oven apparatus [28] and the torsion-effusion method [29]. As established by all the authors, the LiF vapour system contains monomer, dimer and trimer species but some discrepancies on their relative amounts have been found owing to assumptions concerning the electron-impact ionization cross section and the ion-neutral precursor assignment.

In this work, four main ions were observed in the mass spectrum, namely Li^+, LiF^+, Li_2F^+, $Li_3F_2^+$, in accordance with the literature works. The attribution of the measured molar mass to the respective ion was confirmed by the identification of the correct isotopic ratio (natural abundance: ^{7}Li 92.41% and ^{6}Li 7.59%). For each ion species, the ionization efficiency curve at fixed temperature was also recorded as illustrated in Figure 4.2. Based on these results, the appearance energies of the ions were determined and they are listed in Table 4.3 in which the measured values are compared with literature. As mentioned before, although the LiF vapour system has been the subject of numerous investigations, there is disagreement in literature on the identity of the neutral precursors of each ions. In particular, the ions Li^+ and LiF^+ could be produced by different mechanisms from monomer, dimer or from both species. Since our measurements showed no clear inflection in the linear portion of the ionization efficiency curves, thus indicating no dissociation of molecules,as first attempt we considered that both ions (Li^+ and LiF^+) are generated only from the monomer. Using this approach, the resulting dimer pressure was found to be considerable lower than the literature value. Therefore, a different fragmentation path was tested, as given in one of the most recent work on LiF compound performed by Bonnell *et al.* [27]. Using a phase-sensitive mass spectral analysis, they report for similar ionization energy the following ion-precursor combinations: Li^+ [90.4% LiF - 9.6% Li_2F_2], LiF^+ [18% LiF -71% Li_2F_2- 11% Li_3F_3], Li_2F^+ [99.5% Li_2F_2- 0.5% Li_3F_3] $Li_3F_2^+$ [100% Li_3F_3]. This fragmentation path is not in disagreement with our experimental results when considering that most of the processes (i.e for LiF^+: simple ionization LiF + e^- → LiF^++ 2e^- and fragmentation Li_2F_2 + e^- → LiF^+ + LiF+ 2e^-) are probably within few eV [30] and a better energy resolution is needed to identify the slope changes. Applying the precursor partition as reported by Bonnell *et al.* [27], the best agreement with literature was observed for both monomer and dimer pressure, thus it was considered in all the calculations in this work. It is important to notice that although there are some uncertainties in the assignment of the neutral precursors to the ions, the different assumptions do not strongly influence neither the total vapor pressure of the salt (mainly given by the monomer) nor the activities (providing a consistent analysis for all the measurements).

The experimental data measured in this work are shown in Figure 4.3, where the vapour pressure of all the gaseous species LiF, Li_2F_2, Li_3F_3 are reported. Two LiF samples were measured under the same experimental conditions and the comparison confirms the reproducibility of the measurement. The results have been compared with the data

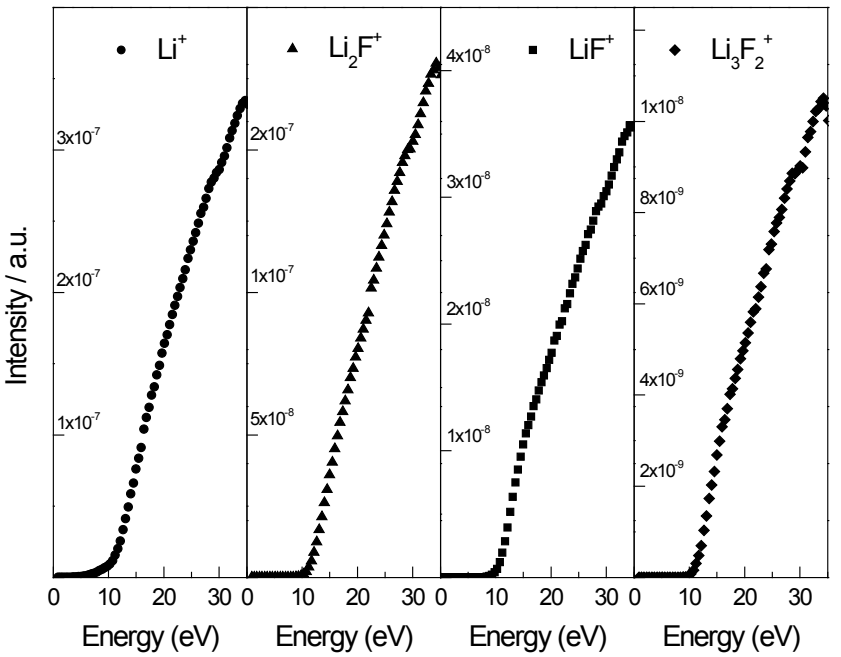

Figure 4.2: Ionization efficiency curves measured for the ions Li^+, LiF^+, Li_2F^+, $Li_3F_2^+$. The intensity of the signal is reported as function of the calibrated energy in the range between 0 and 35 eV.

Table 4.3: Appearance energy of the ion species detected by the mass spectrometer

Reaction	Appearance energy (eV)	
	Measured	*Literature*
$LiF + e^- \rightarrow Li^+ + F + 2e^-$	11.5 ± 0.5	11.5 [28], 11.8 [26] and 11.4 [11]
$LiF + e^- \rightarrow LiF^+ + 2e^-$	11.8± 0.5	11.3 [28], 11.8 [26] and 11.1 [11]
$Li_2F_2 + e^- \rightarrow Li_2F^+ + F + 2e^-$	11.3± 0.5	11.5 [28], 13.0 [26] and 11.7 [11]
$Li_3F_3 + e^- \rightarrow Li_3F_2^+ + F + 2e^-$	12.3± 0.5	12.3 [26] and 11.4 [11]
$ThF_4 + e^- \rightarrow Th^+ + 4\,F + 2e^-$	33.0± 0.5	39 [31]
$ThF_4 + e^- \rightarrow ThF^+ + 3\,F + 2e^-$	29.1± 0.5	30 [31]
$ThF_4 + e^- \rightarrow ThF_2^+ + 2\,F + 2e^-$	21.1 ± 0.5	23.2 [31] and 21.0 [32]
$ThF_4 + e^- \rightarrow ThF_3^+ + F + 2e^-$	13.4 ± 0.5	14.5 [31] and 13.5 [32]

calculated from the FactSage software [33] based on the JANAF Tables [19] and the agreement is very good except for the trimer species. Such a discrepancy may arise from the low ion currents of the trimer, but we must note that our result is in line with the results obtained by other authors.

The vapour pressure data of liquid phase of LiF (from 1121 K to 1352 K) were fitted using a least-square method and the following equations were found to represent the monomer, dimer and trimer pressure:

$$\textbf{Monomer:}\quad \ln(P/\text{Pa}) = (25.893 \pm 0.124) - (28064 \pm 159)(T/\text{K})^{-1} \tag{4.12}$$

$$\textbf{Dimer:}\quad \ln(P/\text{Pa}) = (24.886 \pm 0.055) - (27707 \pm 69)(T/\text{K})^{-1} \tag{4.13}$$

$$\textbf{Trimer:}\quad \ln(P/\text{Pa}) = (19.305 \pm 0.161) - (24566 \pm 203)(T/\text{K})^{-1}. \tag{4.14}$$

In addition, the enthalpy of sublimation have been calculated for all the LiF gaseous species using the second and third law methods, as described in Section 4.2.3. The results are summarized in Table 4.4. A very good agreement between second and third law calculations was observed for the monomer while a slightly higher discrepancy was observed for dimer and trimer. Moreover, the results fit very well within the literature values.

4.3.2. VAPOUR PRESSURE OF PURE ThF_4

There are three studies on the vapour pressure of ThF_4(s) and ThF_4(l), performed by Darnell *et al.* [36], Lau *et al.* [32] and Nagarajan *et al.* [37]. The composition of the vapour phase is very simple, consisting of only ThF_4(g) in the monomeric form. The observed ions in the mass spectrum of the vapour effusing from the cell were Th^+, ThF^+, ThF_2^+ and ThF_3^+ and the appearance potentials of these ions, as measured in this work (Figure 4.4), are listed in Table 4.3. No evidences were found during the measurement for the presence of ThO_2 or $ThOF_2$ impurities in the salt.

The measurements were performed from 1000 K to 1457 K when the complete evaporation of the sample was reached. Figure 4.5 shows the results obtained, which are in good agreement with the literature. The total vapor pressure of solid and liquid ThF_4 can be represented by the following equations:

$$\begin{aligned} &\textbf{Solid:}\quad \ln(P/\text{Pa}) = (36.045 \pm 0.101) - (43493 \pm 124)(T/\text{K})^{-1} \\ &\textbf{Liquid:}\quad \ln(P/\text{Pa}) = (29.386 \pm 0.124) - (34858 \pm 180)(T/\text{K})^{-1}. \end{aligned} \tag{4.15}$$

Also in the case of ThF_4 compound, the enthalpy of sublimation was determined by second and third law. The calculations gave $\Delta_s H^0_{298} = 359.25 \pm 2.6$ kJ/mol from second law method and $\Delta_s H^0_{298} = 353.8 \pm 2.5$ kJ/mol from third law method, similar to the selected literature value [38] of $\Delta_s H^0_{298} = 349.3 \pm 2$ kJ/mol.

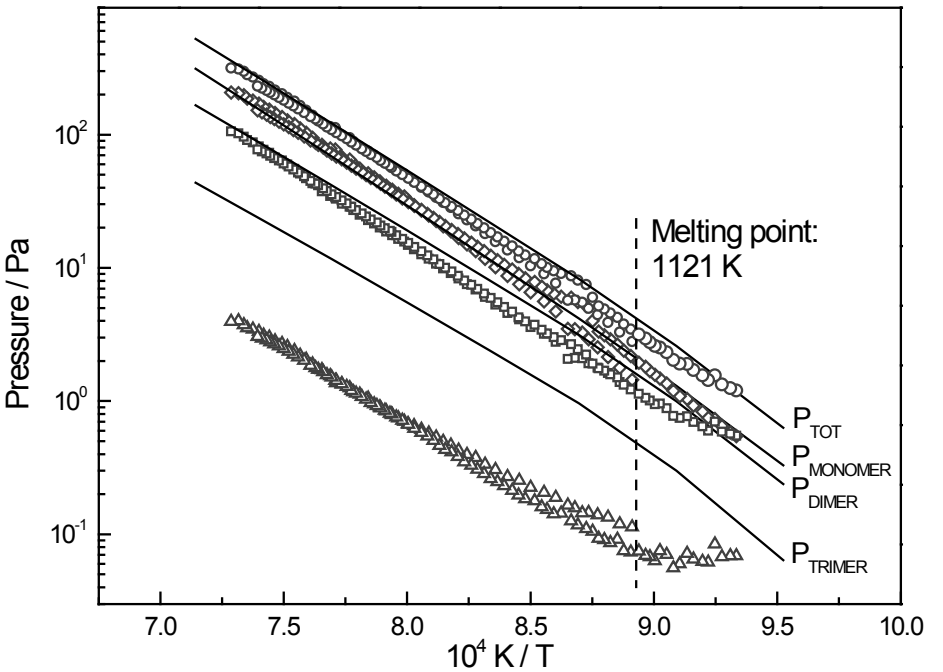

Figure 4.3: Vapour pressure of lithium fluoride LiF. (∘) Total pressure over LiF measured in this work. (⋄) Data measured in this work for the monomer species. (□) Data measured in this work for the dimer species. (△) Data measured in this work for the trimer species. (—) Data calculated using FactSage software based on JANAF Table [19].

Table 4.4: Enthalpy of sublimation $\Delta_s H^0_{298}$ (kJ/mol) of LiF(s) at 298.15 K for the three found gaseous species.

Researchers	$\Delta_s H^0_{298}$ (LiF)	$\Delta_s H^0_{298}$ (Li_2F_2)	$\Delta_s H^0_{298}$ (Li_3F_3)
Yamawaki *et al.* [11](1982)[a]	284.5 ±6.7	309.6 ± 7.1	326.7±18.4
Yamawaki *et al.* [11] (1982) [b]	283.3 ±7.1	301.2 ± 7.1	349.9
Grimley *et al.* [26] (1978) [a]	272.2 ±2.1	308.1 ± 1.7	337.4±1.3
Snelson *et al.* [34] (1969)[a]	285.2 ±4.6	337.2 ± 5.4	428.4±6.7
JANAF Tables [19] (1968)	276.1	291.1	333.6
Glushko Tables [35] (1982)	277.4 ± 3		
Present work [a]	277.9 ±1.5	316.6 ±1	333.5 ±1.5
Present work [b]	277.48 ±2	301.6 ±8.2	360.3 ±18.4

[a] Second law calculation
[b] Third law calculation

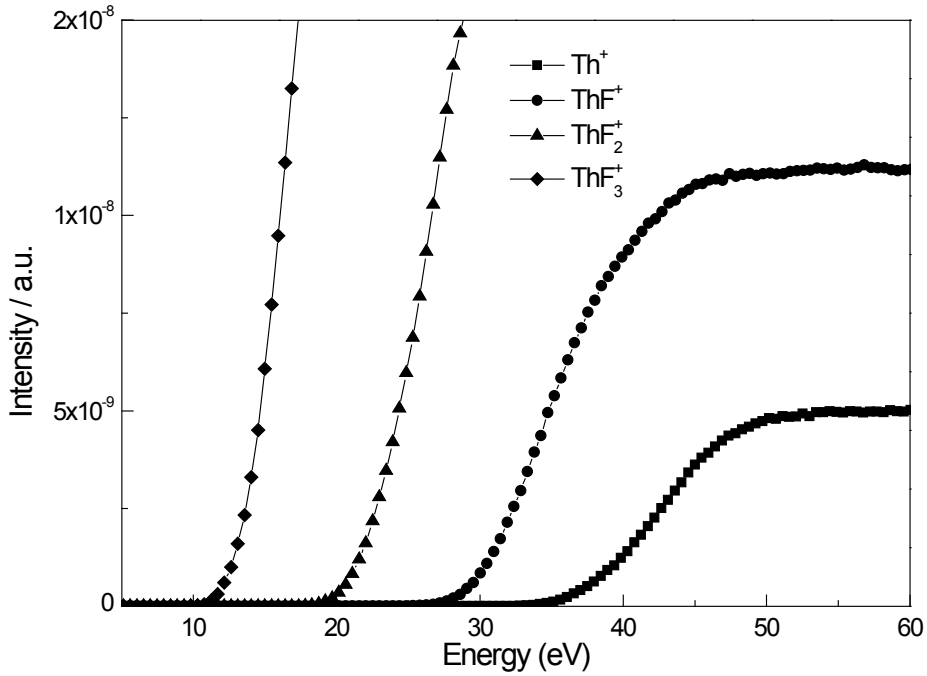

Figure 4.4: Ionization efficiency curves measured for the ions Th^+, ThF^+, ThF_2^+, ThF_3^+. The intensity of the signal is reported as function of the calibrated energy in the range between 0 and 60 eV.

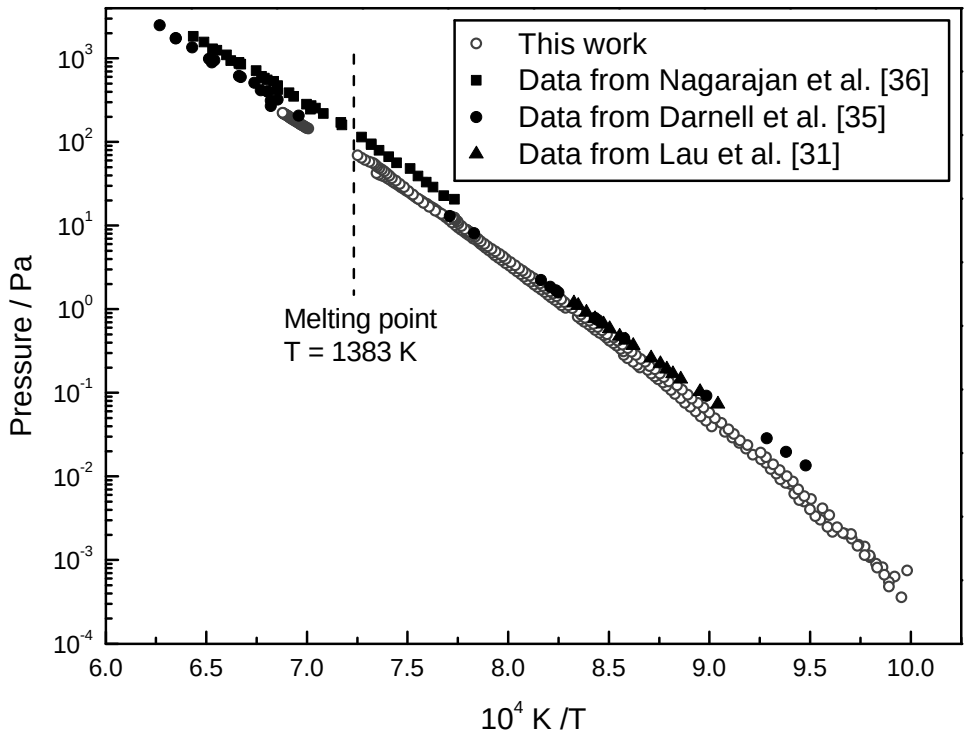

Figure 4.5: Vapour pressure of thorium tetrafluoride ThF_4. ○ Data measured in this work. ■ Data from Nagarajan *et al.* [37]. • Data from Darnell *et al.* [36]. ▲ Data from Lau *et al.* [32].

4.3.3. VAPOUR PRESSURE OF THE $Li_xTh_{1-x}F_{4-3x}$ LIQUID SOLUTION

The vapour pressure of the $Li_xTh_{1-x}F_{4-3x}$ liquid solution was studied in this work for the first time. In order to understand the behaviour in the whole composition range, four binary mixtures were prepared with mole fractions in steps of 0.2 mol and they were measured under the same experimental conditions as the end-members. The mass spectrum of all the samples showed the presence of the same ions, Li^+, LiF^+, Li_2F^+, Th^+, ThF^+, ThF_2^+, ThF_3^+ in addition to the reference signal Ag^+, with different relative intensities. The $Li_3F_2^+$ signal was too low to be detected in most of the cases and no evidences for formation of Li-Th molecules in the gaseous phase were found by scanning the complete range of molar masses. We note here that as reported in literature [39], the formation of an intermediate compound in the gas phase has been observed for several ionic halide systems and often the main ion formed after electron impact is Li^+. In this case, it is not straightforward to separate the contribute to the ion signal from $Li_xTh_yF_{4y+x}$ (g) and from LiF (g), respectively. In absence of any experimental evidence on the formation of such compounds, none was consider in our analysis.

As an example, the temperature function of the mass spectrum of $Li_{0.4}Th_{0.6}F_{2.8}$ is shown in Figure 4.6, in which only the major isotopes are reported for clarity reasons.Since ourmethod does not allow the determination of the backgroundsignal and the sample signal simultaneously, no background treatment has been performed. However, background intensities are very small in comparison to the overall signal in the temperature range considered for the analysis. It is important to notice that all the signals, except the reference, dropped after the complete vaporization at the same temperature/time giving a strong indication of the complete mixing between the end-members LiF and ThF_4. The maximum temperature reached is around 1450 K, determined by complete vaporization of the salt in very low pressure conditions. In different conditions, for instance at ambient pressure, the salts are far from their boiling points and the complete vaporization would occur at higher temperatures.

The vapour pressure of the liquid mixtures was calculated in the range of temperature between the liquidus temperature of the binary mixture and the maximum temperature reached (complete vaporisation of the sample). All the data have been analysed using the same approach and the equations obtained for the partial pressure of the major species, LiF and ThF_4, are summarized in Table 4.5. The plot of the vapour pressure measured as function of the composition of the liquid is shown in Figure 4.7 for the LiF and ThF_4 species.

Using the data obtained in this study for pure compounds and binary mixtures, the thermodynamic activities of both species in the liquid solution were determined. In general, the activity of one species is given by the relation:

$$a_i = \frac{P_i(soln)}{P_i(end-member)} \tag{4.16}$$

where $P_i(soln)$ is the vapour pressure of the species i in the solution and $P_i(end-member)$ is the vapour pressure of the end-member species i. Following this relation, the activities of LiF and ThF_4 have been calculated as function of the molar fraction and temperature. The reference state for pure ThF_4 is the supercooled liquid, as derived by

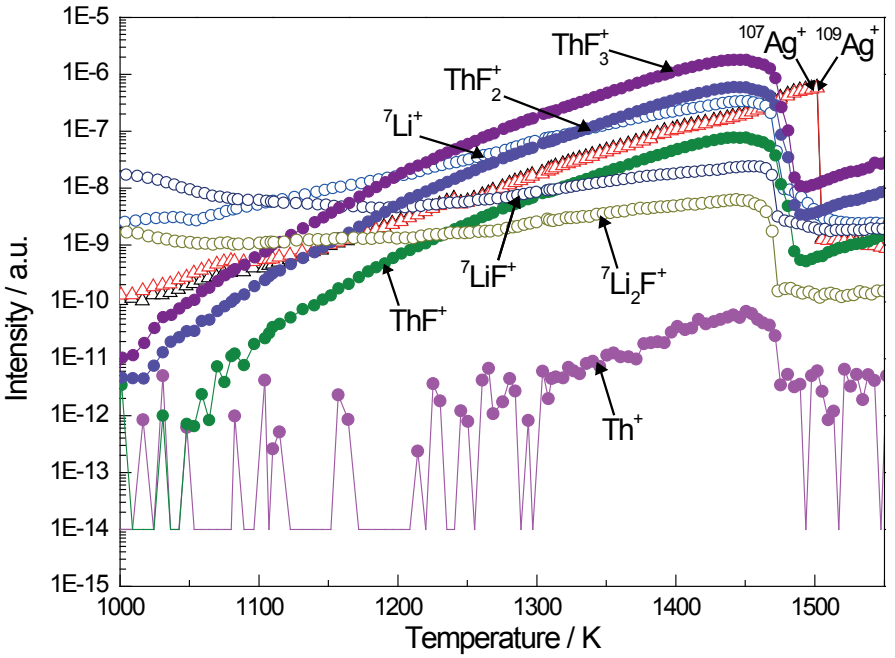

Figure 4.6: The ion intensities versus temperature obtained for the intermediate composition $Li_{0.4}Th_{0.6}F_{2.8}$. The main species recorded are: Li^+, LiF^+, Li_2F^+ (○), Th^+, ThF^+, ThF_2^+, ThF_3^+ (•) plus the reference signal Ag^+ (△). Only the intensities of the most intensive isotope is given in each case.

Table 4.5: Vapor pressure equations for the LiF and ThF_4 species over the LiF-ThF_4 liquid solution.

Sample name	Species	Vapor pressure equation	Temperature interval
$\mathbf{Li_{0.8}Th_{0.2}F_{1.6}}$	LiF	ln (P/Pa) = (21.428±0.128) - (23940±161) (T/K)	1302 - 1443 K
	ThF_4	ln (P/Pa) = (41.451±0.140) - (53818±180) (T/K)	
$\mathbf{Li_{0.6}Th_{0.4}F_{2.2}}$	LiF	ln (P/Pa) = (22.916±0.221) - (25439±274) (T/K)	1202-1432 K
	ThF_4	ln (P/Pa) = (33.046±0.062) - (40905±127) (T/K)	
$\mathbf{Li_{0.4}Th_{0.6}F_{2.8}}$	LiF	ln (P/Pa) = (19.742±0.094) - (23783±122) (T/K)	1123-1441 K
	ThF_4	ln (P/Pa) = (29.643±0.128) - (35886±168) (T/K)	
$\mathbf{Li_{0.2}Th_{0.8}F_{3.4}}$	LiF	ln (P/Pa) = (17.755±0.223) - (22455±32) (T/K)	1122- 1443 K
	ThF_4	ln (P/Pa) = (26.411±0.322) - (31232±444) (T/K)	

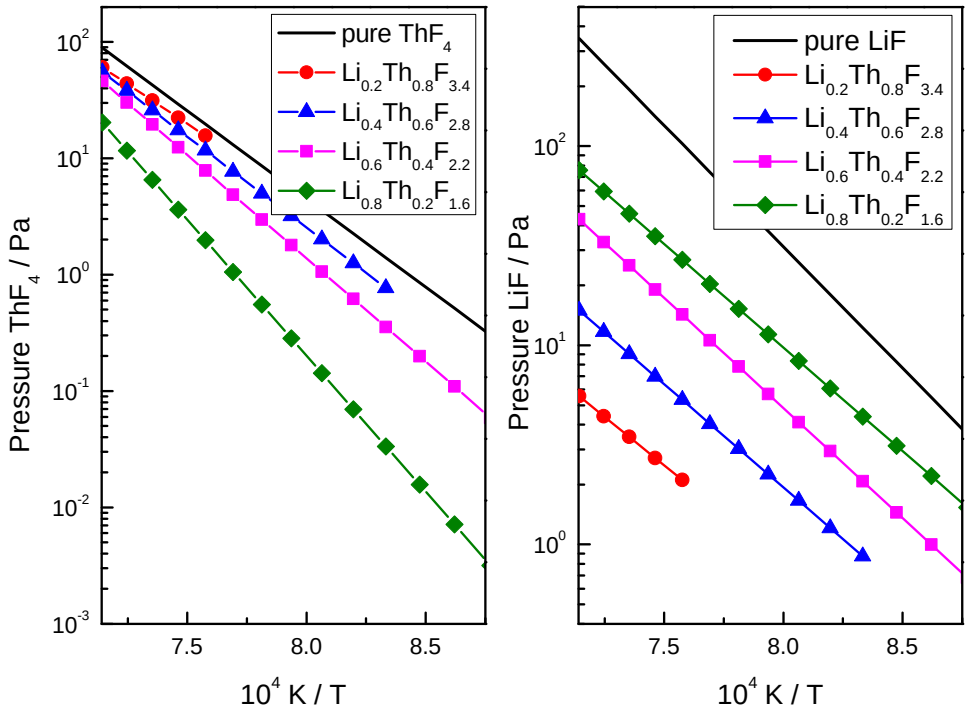

Figure 4.7: **Right graph:** Comparison between the LiF vapour pressure (monomer) for the pure LiF liquid phase and for the $Li_xTh_{1-x}F_{4-3x}$ liquid solution. **Left graph:** Comparison between the ThF_4 vapour pressure for the pure ThF_4 liquid phase and for the $Li_xTh_{1-x}F_{4-3x}$ liquid solution. The vapour pressure of ThF_4 has been extrapolated for temperature lower than the melting point from the equation of the liquid state.

extrapolation from the equation of the vapour pressure of the liquid phase (Eq. 4.15). The results are plotted for three selected temperature 1200 K, 1300 K and 1400 K in Figure 4.8. In case of the LiF species, an alternative method to calculate the thermodynamic activity was also applied. In fact when both monomer and dimer are present in the salt vapor, the activity can be calculated directly from ion intensities [40], as given by the following equation:

$$a = \frac{(I_{Li^+} / I_{LiF_2^+})_{pure}}{(I_{Li^+} / I_{LiF_2^+})_{mixt}} \tag{4.17}$$

where I_{Li^+} and $I_{LiF_2^+}$ are the intensities of the ion Li^+ and LiF_2^+ for the pure component and for the mixed samples. This method, which is in principle applicable only when the ion intensities Li^+ and LiF_2^+ result solely from the LiF and Li_2F_2 respectively, offers the advantage to give the value of the thermodynamic activities without necessity of pressure calibration. The results obtained with this method are in fair agreement with the activities calculated from absolute vapour pressure and the comparison between the two methods was used to estimate the uncertainty on the activity determination. For each measurement, the average deviation of the two methods was calculated and the maximum of those values (about 18 %) was considered, in a first approximation, as the error of the thermodynamic activities of LiF and ThF_4.

The results on the activity of the end members LiF and ThF_4 in the $Li_xTh_{1-x}F_{4-3x}$ liquid solution are shown in Figure 4.8. The dashed lines in the figure represent the behaviour of the activities for an ideal solution which is given by the Raoult's law:

$$a_i = X_i \tag{4.18}$$

where X_i is the molar fraction of the gaseous species i. The results clearly show a strong deviation from the ideality of the $Li_xTh_{1-x}F_{4-3x}$ liquid solution, more evident in case of LiF species. There is a strong connection between the microscopic structure and the deviation of the vapour pressure from the ideality. In ideal mixtures, the assumption is that at the microscopic level the intermolecular forces between two different molecules (LiF -ThF_4) are equal to those between similar molecules (LiF-LiF and ThF_4-ThF_4, respectively). The lesser the extent to which these criteria are true the greater the deviations of the partial pressures from their linear dependency on the mole fractions. The significant deviation from ideality of the studied system has been observed also for the enthalpy of mixing, as reported in our previous work [5].

For comparison, the solid lines in Figure 4.8 represent predictions from the thermodynamic model developed for the LiF-ThF_4 system [5]. This assessment was performed considering the available experimental data on the binary system, that were the phase diagram temperatures, the enthalpy of fusion of the Li_3ThF_7 compound and the enthalpy of mixing of the liquid solution. Considering this fact, the agreement obtained between predictions and experiments is rather good. An higher discrepancy is observable in case of the LiF species, especially with increasing temperature, but the agreement is very good for the ThF_4 species. It can thus be concluded that the model correctly predicts the general behaviour of the thermodynamic activities as function of composition and this confirms that the thermodynamic model predicts the mixture properties correctly.

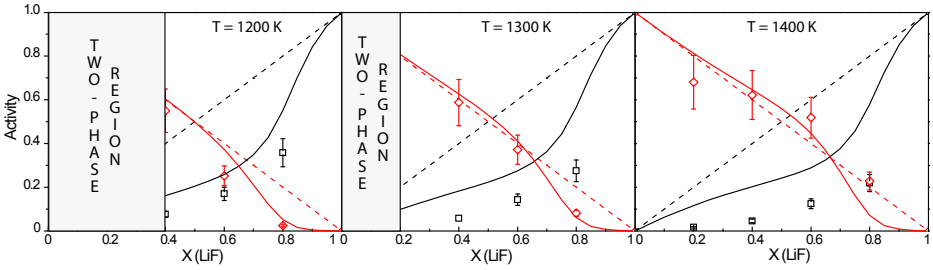

Figure 4.8: Activities of LiF and ThF_4 in the $Li_xTh_{1-x}F_{4-3x}$ liquid solution as function of LiF molar fraction at T = 1200 K, 1300 K and 1400 K. The results are reported in red for the ThF_4 species and in black for the LiF species. Dotted lines: Ideal behaviour of activity as calculated from Raoult's law. Solid lines: Activities calculated based on the thermodynamic model developed [5]. (□) Measured activity of LiF. (◇) Measured activitiy of ThF_4.

4.4. CONCLUSIONS

This work presents the determination of the thermodynamic activities of LiF and ThF_4 in the $Li_xTh_{1-x}F_{4-3x}$ liquid solution. Knudsen Effusion Mass Spectrometry has been successfully applied to measure fluoride samples at high temperatures. First the end-members LiF and ThF_4 were investigated and next some selected intermediate compositions. The results for the end-members were found to be in very good agreement with the literature data for appearance potential, vapour pressure and enthalpy of sublimation. Afterwards, the same experimental procedure was applied to four different compositions of the $Li_xTh_{1-x}F_{4-3x}$ liquid solution and its vapour pressure was determined for the first time. Based on these measurement the thermodynamic coefficients of LiF and ThF_4 in the $Li_xTh_{1-x}F_{4-3x}$ liquid solution were determined.

As mention in the introduction, these type of the data are of great interest to evaluate the safety and the performance of the MSR fuel as well as to evaluate the reprocessing scheme. The experimental results confirm that the $Li_xTh_{1-x}F_{4-3x}$ liquid solution has low vapour pressure and it is therefore compatible with a low operating pressure of the reactor. Moreover, the experimental results fit well with the predictions based on the previously published thermodynamic model [5], confirming the reliability of the developed database.

ACKNOWLEDGEMENTS

E.C. acknowledges the European Commission for support given in the frame of the program "Training and Mobility of Researchers". This work was supported by the EVOL project in the 7th Framework Programme of the European Commision (Grant agreement No.249696).

REFERENCES

[1] E. Capelli, O. Beneš, J.-Y. Colle, and R. J. M. Konings, *Determination of the thermodynamic activities of LiF and ThF_4 in the $Li_xTh_{1-x}F_{4-3x}$ liquid solution by Knudsen effusion mass spectrometry,* Phys. Chem. Chem. Phys. **17**, 30110 (2015).

[2] S. Delpech, E. Merle-Lucotte, D. Heuer, M. Allibert, V. Ghetta, C. Le-Brun, X. Doligez, and G. Picard, *Reactor physics and reprocessing scheme for innovative molten salt reactor system,* J. Fluor. Chem. **130**, 11 (2009).

[3] A. Nuttin, D. Heuer, A. Billebaud, R. Brissot, C. L. Brun, E. Liatard, J. M. Loiesaux, L. Mathieu, O. Meplan, E. Merle-Lucotte, H. Nifenecker, and F. Perdu, *Potential of thorium molten salt reactors: detailed calculations and concept evolution with a view to large scale energy production,* Prog. Nucl. Energ. **46**, 77 (2005).

[4] S. Delpech, *Possible routes for pyrochemical separation: Focus on the reductive extraction in fluoride media,* Pure Appl. Chem. **85**, 71 (2013).

[5] E. Capelli, O. Beneš, M. Beilmann, and R. J. M. Konings, *Thermodynamic investigation of the LiF-ThF_4 system,* J. Chem. Thermodyn. **58**, 110 (2013).

[6] O. Beneš, R. J. M. Konings, S. Wurzer, M. Sierig, and A. Dockendorf, *A DSC study of the $NaNO_3$–KNO_3 system using an innovative encapsulation technique,* Thermochim. Acta **509**, 62 (2010).

[7] J.-P. Hiernaut, J.-Y. Colle, R. Pflieger-Cuvellier, J. Jonnet, J. Somers, and C. Ronchi, *A Knudsen cell-mass spectrometer facility to investigate oxidation and vaporisation processes in nuclear fuel,* J. Nucl. Mat. **344**, 246 (2005).

[8] D. J. Santeler, *New concepts in molecular gas flow,* J. Vac. Sci. Technol. A **4**, 338 (1986).

[9] R. Hultgren, R. L. Orr, P. D. Anderson, and K. K. Kelley, *Selected value of thermodynamic properties of metals and alloys,* (John Wiley and Sons, Inc., 1963).

[10] R. T. Grimley, *The characterization of high temperature vapors,* (Ed. John Wiley and Sons, 1967) Chap. 8.

[11] M. Yamawaki, M. Hirai, M. Yasumoto, and M. Kanno, *Mass spectrometric study of vaporization of lithium fluoride,* J. Nucl. Sci. Technol. **19**, 563 (1982).

[12] J. B. Mann, *Recent developments in mass spectrometry,* in *Proc. Int. Conf on Mass Spectrometry*, edited by K. Ogata and T. Hayakwa (University Park Press, Baltimore, Tokyo and New York, 1970) pp. 814–819.

[13] J. B. Mann, *Ionization cross sections of the elements calculated from mean square radii of atomic orbitals,* J. Chem. Phys. **46**, 1646 (1967).

[14] D. W. Bonnell and J. W. Hastie, *Program SIGMA, a Fortran code for computing atomic ionization cross sections,* (NIST, Gaithersburg, MD,unpublished work, 1990-1997).

[15] J. W. Otvos and D. P. Stevenson, *Cross-sections of molecules for ionization by electrons,* J. Am. Chem. Soc. **78**, 546 (1956).

[16] H. Deutsch, C. Cornelissen, L. Cespiva, V. Bonacic-Koutecky, and D. Margreiter, *Total electron impact ionization cross section of free molecular radicals: the failure of the additivity rule revisited,* Int. J. Mass Spectrom. Ion Processes **129**, 43 (1993).

[17] H. Deutsch, K. Becker, and T. D. Märk, *A modified additivity rule for the calculation of electron impact ionization cross-section of molecules AB_n,* Int. J. Mass Spectrom. Ion Processes **167**, 503 (1997).

[18] J. P. Desclaux, *Relativistic Dirac-Fock expectation values for atoms with Z=1 to Z=120,* At. Nucl. Data Tables **12**, 311 (1973).

[19] M. W. Chase Jr.(ed.), *NIST-JANAF Thermochemical Tables Fourth Edition,* J. Phys. Chem. Ref. Data, Monograph **9**, (1998).

[20] R. J. M. Konings, J. P. M. van der Meer, and E. Walle, *Chemical aspects of Molten Salt Reactor Fuel*, Tech. Rep. (2005) ITU-TN 2005/25.

[21] D. D. Wagman, R. H. Schumm, and V. B. Parker, *A computer assisted evaluation of the thermochemical data of the compounds of thorium,* (NBSIR-77-1300, 1977).

[22] E. Capelli, O. Beneš, and R. J. M. Konings, *Thermodynamic assessment of the LiF-NaF-BeF_2-ThF_4-UF_4 system,* J. Nucl. Mater. **449**, 111 (2014).

[23] M. Eisenstadt, G. M. Rothberg, and P. Kusch, *Molecular composition of alkali fluoride vapors,* J. Chem. Phys. **29**, 797 (1958).

[24] R. Scheffee and J. Margrave, *Vapor pressure equations for species over solid and liquid LiF,* J. Chem. Phys. **31**, 1682 (1959).

[25] R. F. Porter and R. C. Schoonmaker, *Mass spectrometric study of the vaporization of LiF, NaF and LiF-NaF mixtures,* J. Chem. Phys. **29**, 1070 (1958).

[26] R. Grimley, J. Forsman, and Q. Grindstaff, *A mass spectrometric study of the fragmentation of the lithium fluoride vapor system,* J. Phys. Chem. **82**, 632 (1978).

[27] D. W. Bonnell, J. W. Hastie, and K. F. Zmbov, *Transpiration mass spectrometry of liquid LiF - vaporization termochemistry and electron-impact fragmentation,* High Temp.-High Press. **20**, 251 (1988).

[28] J. Berkowitz, H. A. Tasman, and W. A. Chupka, *Double oven experiments with lithium halide vapors,* J. Chem. Phys. **36**, 2170 (1962).

[29] D. L. Hildenbrand, W. F. Hall, F. Ju, and N. D. Potter, *Vapor pressure and vapor thermodynamic properties of some lithium and magnesium halides,* J. Chem. Phys. **40**, 2882 (1964).

[30] M. V. Veljkovic, O. M. Neskovic, M. B. Miletic, and K. F. Zmbov, *Mass spectrometric study of ionization and fragmentation of lithium fluoride vapor by electron impact,* J. Serb. Chem. Soc. **58**, 101 (1993).

[31] K. Zmbov, *Heats of formation of gaseous ThF_3 and ThF_2 from mass spectrometric studies,* J. Inorg. Nucl. Chem. **32**, 1378 (1970).

[32] K. H. Lau, R. D. Brittain, and D. L. Hildenbrand, *High temperature thermodynamic studies of some gaseous thorium fluorides,* J. Chem. Phys. **90**, 1158 (1989).

[33] C. W. Bale and et al., *Factsage Software,* (v. 6.2).

[34] A. Snelson, *Heats of vaporization of the lithium fluoride vapor species by the matrix isolation technique,* J. Chem. Phys. **73**, 1919 (1969).

[35] V. P. Glushko, L. V. Gurvich, G. A. Bergman, I. V. Veyts, V. A. Medvedev, G. A. Khachkuruzov, and V. S. Yungman, Termodinamicheskie Svoistva Individual'nykh Veshchestv. Tom IV, Nauka, Moskva (1982).

[36] A. J. Darnell and F. J. Keneshea, *Vapor pressure of thorium tetrafluoride,* J. Phys. Chem. **62**, 1143 (1958).

[37] K. Nagarajan, M. Bhupathy, R. Prasad, Z. Singh, V. Venugopal, and D. D. Sood, *Vaporization thermodynamics of thorium tetrafluoride,* Termochim. Acta **36**, 85 (1980).

[38] M. H. Rand, J. Fuger, I. Grenthe, V. Neck, and D. Rai, *Chemical thermodynamics of thorium,* (OECD Nuclear Energy Agency, Paris, 2008).

[39] K. Hilpert, *Chemistry of inorganics vapors, in: Structure and bonding - Noble gas and high temperature chemistry,* (Springer, Berlin) pp. 97–195.

[40] J. Berkowitz and W. A. Chupka, *Composition of vapors in equilibrium with salts at high temperatures,* Trans. NY Acad. Sci. **79**, 1073 (1960).

5

THERMODYNAMIC ASSESSMENT OF THE LiF-ThF_4-PuF_3-UF_4 SYSTEM

Elisa CAPELLI, Ondřej BENEŠ, Rudy J.M. KONINGS

The LiF-ThF_4-PuF_3-UF_4 system is the reference salt mixture considered for the Molten Salt Fast Reactor (MSFR) concept started with PuF_3. In order to obtain the complete thermodynamic description of this quaternary system, two binary systems (ThF_4-PuF_3 and UF_4-PuF_3) and two ternary systems (LiF-ThF_4-PuF_3 and LiF-UF_4-PuF_3) have been assessed for the first time. The similarities between CeF_3/PuF_3 and ThF_4/UF_4 compounds have been taken into account for the presented optimization as well as in the experimental measurements performed, which have confirmed the temperatures predicted by the model. Moreover, the experimental results and the thermodynamic database developed have been used to identify potential compositions for the MSFR fuel and to evaluate the influence of partial substitution of ThF_4 by UF_4 in the salt.

Parts of this chapter have been published in Journal of Nuclear Materials **462**, 43 (2015) [1].

5.1. INTRODUCTION

Mixtures of fluoride salts, such as the studied LiF-ThF_4-PuF_3-UF_4 system, are currently considered as fuel for the Molten Salt Fast Reactor (MSFR) [2]. This reactor design, which is a liquid fuelled fast (epi-thermal) spectrum reactor, can be well adapted to the thorium fuel cycle (^{232}Th/^{233}U) which offers several advantages and meets the Generation IV goals. Since ^{232}Th is not fissile, an initial load of fissile material has to be added to the fuel for the reactor start-up and the possibility of starting molten salt reactors with plutonium trifluoride PuF_3 has been demonstrated in early studies at Oak Ridge National Laboratories [3, 4] and more recently by Merle-Lucotte *et. al* [5]. The advantage of this design is the possibility to burn plutonium and minor actinides produced in the LWRs (Light Water Reactor) and produce ^{233}U needed to supply the fissile material for the ^{232}Th/^{233}U cycle. In the proposed salt composition, the LiF salt is used as solvent for both fertile (ThF_4) and fissile (PuF_3) material with relative concentrations given by neutronic and physico-chemical requirements. Moreover, UF_4 must be added to control the redox potential of the fuel via the UF_4/UF_3 ratio.

In this work, we present the thermodynamic assessment of the LiF-ThF_4-PuF_3-UF_4 system. The binary and ternary phase diagrams containing PuF_3 have been assessed for the first time based on the similarities of the proxy compounds (CeF_3/PuF_3 and ThF_4/UF_4, respectively) and on the experimental data available in the literature. All thermodynamic assessments were done according to the Calphad method using the two sublattice model for the description of the solid solutions and the modified quasi-chemical model for the description of the liquid solution. In order to validate the model developed, some selected LiF-CeF_3-ThF_4 ternary compositions have been synthesized and analysed using the Differential Scanning Calorimeter (DSC). The obtained equilibrium data have been used to optimize ternary parameters in the model so that a good agreement with the experiment has been achieved. As last step, the thermodynamic database developed and the experimental results have been used to optimize the MSFR fuel composition. Based on different criteria, several potential compositions have been identified and the influence of ThF_4 substitution with UF_4 have been investigated. In fact, this action may be useful for proliferation issues as well as for neutronic considerations.

5.2. THERMODYNAMIC MODELING

In this work, we performed the thermodynamic assessment of the LiF-ThF_4-PuF_3-UF_4 quaternary system.The binary systems ThF_4-PuF_3 and UF_4-PuF_3 and the ternary systems LiF-ThF_4-PuF_3 and LiF-UF_4-PuF_3 have been assessed for the first time while the remaining sub-systems have been taken from previous works [6, 7]. During the optimization, due to the lack of experimental data, the two following assumptions have been taken into account:

1. CeF_3 is considered as proxy compound to PuF_3.
2. ThF_4 is considered as proxy compound to UF_4.

Both assumptions are based on strong similarity of the properties of the paired compounds as experimentally evidenced for both cases and discussed in more details in our previous work [7]. It must be mentioned here that the analogy between UF_4 and ThF_4 compounds is valid only to a certain extent. In fact, there are some differences in the chemical behaviour of the two compounds, such as the possible oxidation state of uranium in the fluoride media compared to thorium which can only be tetravalent and the stoichiometry of the intermediate compounds formed in the binary systems LiF-ThF_4 and LiF-UF_4. However, the general shape of the liquidus lines for the LiF-ThF_4 and LiF-UF_4 systems are similar and the liquidus temperatures are almost identical for UF_4 content less than 23 mol%. This is particularly important for our application where the liquidus lines are of primary importance and the UF_4 content is kept small. As consequence of the assumptions made, the binary systems ThF_4-PuF_3 and UF_4-PuF_3 and the ternary systems LiF-ThF_4-PuF_3 and LiF-UF_4-PuF_3 have been assessed using the same excess Gibbs parameters as obtained for the Th- and Ce-containing systems presented in our previous paper [7].

All thermodynamic assessments performed in this study have been done according to the Calphad method using the FactSage software [8], as described throughout the next sections.

5.2.1. COMPOUNDS

The first step for a thermodynamic assessment is the definition of the Gibbs energy of pure compounds, which is given by the following relation:

$$G(T) = \Delta_f H^0(298.15) - S^0(298.15)\,T + \int_{298}^{T} C_p(T)\mathrm{d}T - T\int_{298}^{T}\left(\frac{C_p(T)}{T}\right)\mathrm{d}T \quad , \tag{5.1}$$

where $\Delta_f H^0(298)$ and $S^0(298)$ are respectively the standard enthalpy of formation and standard absolute entropy, both referring to a temperature of 298.15 K and $C_p(T)$ is the temperature function of the heat capacity at constant pressure. The thermodynamic data for all compounds used in this work are reported in Table 5.1. The data of four intermediate compounds $PuThF_7$, $PuTh_2F_{11}$, $PuUF_7$, PuU_2F_{11} have been optimized while the data of the LiF, UF_4 and PuF_3 end-members and LiF-ThF_4 and LiF-UF_4 intermediate compounds have been taken from literature [9, 10] and in case of ThF_4 from our previous work [7] in which the heat capacity of ThF_4 was revised.

As observed experimentally by Gilpatrick *et al.* [11], two intermediate compounds ($CeThF_7$, $CeTh_2F_{11}$) are stable in the CeF_3-ThF_4 binary system. Therefore, in absence of any other experimental data the most straightforward assumption was made and compounds with similar stoichiometry were supposed to be present also in the ThF_4-PuF_3 and UF_4-PuF_3 systems. Estimation of their thermodynamic properties ($\Delta_f H^0(298)$, $S^0(298)$, $C_p(T)$) were made based on the weighted average from the properties of their end-members and adding a contribution related to the compounds formation reaction. The enthalpy and entropy change at 298.15 K for these reactions (MF_4+PuF_3 = $MPuF_7$ and 2MF_4+PuF_3 = M_2PuF_{11} with M=Th, U) were assumed to be identical to the same quantities for the reactions ThF_4+CeF_3 = $ThCeF_7$ and 2ThF_4+CeF_3 = Th_2CeF_{11}. No change in the $C_p(T)$ function was considered.

Table 5.1: The $\Delta_f H^0(298.15)$ (kJ · mol^{-1}), $S^0(298.15)$ (J · K^{-1} · mol^{-1}) and C_p (J · K^{-1} · mol^{-1}) data of pure compounds used in this study.

Compound	$\Delta_f H^0(298.15)$	$S^0(298.15)$	$C_p = a + b\,T + c\,T^2 + d\,T^{-2}$			
			a	b T	c T^2	d T^{-2}
LiF (cr)	-616.931	35.66	43.309	$1.6312\cdot10^{-2}$	$5.0470\cdot10^{-7}$	$-5.691\cdot10^{5}$
LiF (l)	-598.654	42.962	64.183	-	-	-
ThF_4 (cr)	-2097.900	142.05	122.173	$8.3700\cdot10^{-3}$	-	$-1.255\cdot10^{6}$
ThF_4 (l)	-2103.654	101.237	170.0	-	-	-
UF_4 (cr)	-1914.200	151.70	114.519	$2.0555\cdot10^{-2}$	-	$-4.131\cdot10^{5}$
UF_4 (l)	-1914.658	115.400	174.74	-	-	-
PuF_3 (cr)	-1586.694	126.11	104.08	$7.070\cdot10^{-4}$	-	$-1.036\cdot10^{6}$
PuF_3 (l)	-1568.813	109.33	130.00	-	-	-
$LiThF_5$(cr)	-2719.490	181.89	165.482	$2.468\cdot10^{-2}$	$5.047\cdot10^{-7}$	$-1.824\cdot10^{6}$
Li_3ThF_7(cr)	-3960.259	236.1	282.100	$5.730\cdot10^{-2}$	$1.514\cdot10^{-6}$	$-2.962\cdot10^{6}$
$LiTh_2F_9$(cr)	-4822.329	324.29	287.655	$3.305\cdot10^{-2}$	$5.047\cdot10^{-7}$	$-3.079\cdot10^{6}$
$LiTh_4F_{17}$(cr)	-9021.140	609.0	532.001	$4.979\cdot10^{-2}$	$5.047\cdot10^{-7}$	$-5.589\cdot10^{6}$
Li_4UF_8 (cr)	-4347.620	357.55	287.755	$8.5804\cdot10^{-2}$	$2.0188\cdot10^{-6}$	$-2.690\cdot10^{6}$
$Li_7U_6F_{31}$ (cr)	-15826.900	1230.82	990.279	$2.3751\cdot10^{-1}$	$3.5329\cdot10^{-6}$	$-6.463\cdot10^{6}$
LiU_4F_{17} (cr)	-8293.761	644.70	501.387	$9.8532\cdot10^{-2}$	$5.0470\cdot10^{-7}$	$-2.222\cdot10^{6}$
Th_2PuF_{11} (cr)	-5737.637	454.41	348.424	$1.7447\cdot10^{-2}$	-	$-3.546\cdot10^{6}$
U_2PuF_{11} (cr)	-5370.237	473.71	333.117	$4.1817\cdot10^{-2}$	-	$-1.862\cdot10^{6}$

5

5.2.2. SOLID SOLUTION

The total Gibbs energy of a solution is generally described by three terms: the sum of the standard Gibbs energy of the constituents, an ideal mixing term and an excess term. The latter term is usually unknown and it has been optimized in this work. In case of solid solution, the sublattice model [12] was used considering the cationic species involved (Pu^{3+}, Th^{4+} or U^{4+}) on the first sublattice and the anionic species (F^-) on the second sublattice.Using this model, the equivalent cationic (y_A, y_B,..) and anionic fraction (y_X,y_Y,..) are defined as follows:

$$y_A = q_A n_A/(q_A n_A + q_B n_B + ...) \tag{5.2}$$

$$y_X = q_X n_X/(q_X n_X + q_Y n_Y + ...) \tag{5.3}$$

where n_i are the number of moles of ion i in solution and q_i are the absolute ionic charges. In a binary system with a common anion A,B/F, the equivalent anionic fraction y_{F^-} is equal to one and the excess Gibbs energy is espressed as a polynomial in the equivalent cationic fractions y_A and y_B:

$$\Delta G^{xs} = \sum_{i\geqq 1}\sum_{j\geqq 1} y_A^i \cdot y_B^j \cdot L_{i,j} \tag{5.4}$$

where $L_{i,j}$ is the parameter to be optimized.

In case of both the ThF_4-PuF_3 and UF_4-PuF_3 systems, the formation of a solid solution in the PuF_3-rich corner has been considered based on the experimentally confirmed

solid solution in the ThF_4-CeF_3 phase diagram [11]. The same parameters as optimized for the (Ce,Th)F_x solid solution in our previous study [7] were also used for the description of the (Pu,Th)F_x and (Pu,U)F_x solid solutions, thus:

$$\Delta G^{xs} = y_{Pu^{3+}} \cdot y^3_{Th^{4+}} \cdot 30000 \ \mathrm{J \cdot mol^{-1}} \tag{5.5}$$

$$\Delta G^{xs} = y_{Pu^{3+}} \cdot y^3_{U^{4+}} \cdot 30000 \ \mathrm{J \cdot mol^{-1}} \tag{5.6}$$

where the y terms are the site fractions of the given species. The ThF_4-UF_4 system forms a continuous solid solution [13, 14] as described by the following relation:

$$\Delta G^{xs} = y_{U^{4+}} \cdot y_{Th^{4+}} \cdot 400 \ \mathrm{J \cdot mol^{-1}} \tag{5.7}$$

In addition, the formation of solid solutions within the LiF-ThF_4 intermediate compounds and LiF-UF_4 intermediate compounds is well-established and the data for the Gibbs energy description were taken from our previous work (see Table 2 in [6]).

5.2.3. LIQUID SOLUTION

In case of the liquid solution, the description of the excess Gibbs parameter is given by the modified quasi-chemical model proposed by Pelton *et al.* [15]. This model is suitable for the description of ionic liquids as the composition of maximum short range ordering can be changed by varying the ratio between two parameters: the cation-cation coordination numbers $Z^A_{AB/FF}$ and $Z^B_{AB/FF}$ (in the present case with only one type of anion) which are listed in Table 7.3. Moreover, the same model has been used in previous works performed at Institute for Transuranium Elements (ITU) thus it allows an extension of the thermodynamic database developed.

The short range ordering is defined by the quadruplet approximation and the model treats also the second-nearest neighbour interactions, cation-cation and anion-anion. Let A and B be two generic cations and F the fluorine anion, the formation of the generic second-nearest neighbour pair (A-F-B) is given by the following reaction:

$$(A-F-A)+(B-F-B) = 2(A-F-B) \qquad \Delta g_{AB/F} \tag{5.8}$$

where $\Delta g_{AB/F}$ is the Gibbs energy change related to the pair formation and it is an empirical parameter of the model, which may be composition dependent. It can be expanded in polynomial form such as:

$$\Delta g_{AB/F} = \Delta g^0_{AB/F} + \sum_{i \geqq 1} g^{i0}_{AB/F} \chi^i_{AB/F} + \sum_{j \geqq 1} g^{0j}_{AB/F} \chi^j_{BA/F} \tag{5.9}$$

where $\Delta g^0_{AB/F}$ and $g^{ij}_{AB/F}$ are composition independent coefficients while the dependence of the parameter on composition is given by the $\chi_{AB/F}$ terms, defined as function of the cation-cation pair fractions X_{AA}, X_{BB}, X_{AB}.

In general, for a molten fluoride salt solution the charge-neutrality condition for the ABFF quadruplets must be fulfilled and it is done by the definition of the cation-cation coordination numbers respecting the absolute cationic and anionic charges (q_A, q_B,..):

$$\frac{q_A}{Z^A_{AB/FF}} + \frac{q_B}{Z^B_{AB/FF}} = \frac{q_F}{Z^F_{AB/FF}} + \frac{q_F}{Z^F_{AB/FF}}. \tag{5.10}$$

Table 5.2: Cation-cation coordination numbers of the liquid solution.

A	B	$Z^A_{AB/FF}$	$Z^B_{AB/FF}$
Li^+	Li^+	6	6
Pu^{3+}	Pu^{3+}	6	6
Th^{4+}	Th^{4+}	6	6
U^{4+}	U^{4+}	6	6
Li^+	Pu^{3+}	2	6
Li^+	Th^{4+}	2	6
Li^+	U^{4+}	2	6
Pu^{3+}	Th^{4+}	6	3
Pu^{3+}	U^{4+}	6	3
Th^{4+}	U^{4+}	6	6

Using the same approach adopted for the solid solution, the liquid solution for the ThF$_4$-PuF$_3$ and UF$_4$-PuF$_3$ systems have been described using the same parameters assessed for the ThF$_4$-CeF$_3$ system [7], which are given below:

$$\Delta g_{PuU/FF} = \Delta g_{PuTh/FF} = +335 - 6.28T + 2093\chi_{Pu(U,Th)/F} \quad \mathrm{J\cdot mol^{-1}} \tag{5.11}$$

The excess Gibbs parameters for the remaining binary systems have been taken from our previous works [6, 16] and for completeness they are listed below. No excess parameters were considered in case of the ThF$_4$-UF$_4$ system. That is, the ThF$_4$-UF$_4$ liquid was assumed to be ideal (*i.e.*$\Delta g_{ThU/FF} = 0$).

$$\Delta g_{LiTh/FF} = -10883 + \chi_{LiTh/F}(-6697 + 2.93T) + \chi_{ThLi/F}(-20930 + 19.25T) \quad \mathrm{J\cdot mol^{-1}} \tag{5.12}$$

$$\Delta g_{LiU/FF} = -16115 + \chi_{LiU}\,(-711.6 - 1.256T) + \chi_{ULi}\,(-1172 - 8.371T) \quad \mathrm{J\cdot mol^{-1}} \tag{5.13}$$

$$\Delta g_{LiPu/FF} = -2930 - 3348.6\,\chi_{LiPu} \quad \mathrm{J\cdot mol^{-1}} \tag{5.14}$$

Using the data of the binary phase diagrams, all the ternary phase diagrams have been extrapolated using the Kohler or Kohler/Toop interpolation methods depending on the symmetric or asymmetric nature of the system. In fact, the alkali fluoride LiF has a very different chemical behaviour and higher ionic nature compared to the all the other compounds which are actinide fluorides, thus it was considered as asymmetric component. Some ternary parameters ($\Delta g^{ijk}_{AB(C)}$) have to be introduced to optimize the phase diagram according to the experimental data available [17, 18] and they are listed below.

$$\Delta g^{001}_{LiTh(Pu)/FF} = -7953 \ \mathrm{J\cdot mol^{-1}} \tag{5.15}$$

$$\Delta g^{001}_{LiU(Pu)/FF} = -6698 \ \mathrm{J\cdot mol^{-1}} \tag{5.16}$$

$$\Delta g^{001}_{PuTh(Li)/FF} = +20930 \ \mathrm{J\cdot mol^{-1}} \tag{5.17}$$

$$\Delta g^{001}_{PuU(Li)/FF} = +16744 \ \mathrm{J\cdot mol^{-1}} \tag{5.18}$$

Since the optimization was performed separately on the two ternary systems (LiF-ThF_4-PuF_3 and LiF-UF_4-PuF_3), the parameters obtained for the proxy systems Th- and U- containing are different. However, the values have the same order of magnitude in agreement with the assumptions made.

5.3. EXPERIMENT

To confirm the thermodynamic assessment developed, some selected ternary compositions have been prepared and analysed in this study. The samples were synthesized using the CeF_3, LiF and ThF_4 pure components. In fact, it seems to be adequate as first step to carry out most of the experiment using ThF_4 as proxy compound to UF_4 and CeF_3 as proxy compound to PuF_3. Once possible, few measurements with PuF_3 and UF_4 will be necessary to confirm the conclusions made.

The samples analysed in this study were prepared by mixing stoichiometric quantities of the LiF and CeF_3, both obtained from AlfaAesar, and ThF_4 obtained from Rhodia (France). Since all the fluorides salts have tendency to absorb water molecules, LiF and CeF_3 compounds were subjected, prior the mixing, to a drying process at 623 K for 3 hours under Argon atmosphere. In case of ThF_4, there is an additional tendency to oxidize to form oxyfluorides impurities that can dissolve in the salt. These impurities have been converted into fluorides using a fluorinating agent, NH_4HF_2, using the procedure described in our previous work [19]. Afterwards, the purity of the salt was checked for its melting point using DSC. The powder prepared by mixing the pure compounds was filled into a specific crucible [14] designed for the DSC instrument employed in our laboratories (SETARAM MD-HTC96), which serves as barrier for the instrument detector against the corrosive fluoride vapours. It is important to notice that the whole preparation is made inside an Argon glove box to avoid possible deterioration of the samples due to oxygen and water molecules.

The samples were analysed using DSC for the experimental determination of the transition temperatures. The instrument consists of two compartments, resp. the reference and the sample compartment, that are subjected to the same controlled temperature program. For the measurements, a standard program consisting of four heating cycles up to 1573 K has been selected. The heating ramp was performed with constant heating rate of 10 K/min, while the cooling ramp was performed at different cooling rates for each cycle (5 K/min, 7 K/min, 10 K/min and 15 K/min) in order to correct for the supercooling effect, as explained below. The instrument operates under Argon flow to avoid the oxidation of the crucible at high temperature. During the experiments, a series of thermocouples placed around the compartments detects the temperature and the heat flow signal. When the salt undergo a transition, the event is registered by the instrument as a peak, giving information on the phase transitions and their relative temperatures.

In order to validate the developed thermodynamic database, seven selected compositions of the LiF-ThF_4-CeF_3 system were prepared and measured using DSC for the identification of the melting behaviour. The exact compositions and the measured temperatures are listed in Table 5.3, where T_{meas} is the average value of the four consecutive

heating cycles and where the maximum deviation observed was not larger than ± 10 K. For all the measured compositions, three phase transitions between the room temperature and 1523 K were identified, which is in agreement with the calculation. They represent respectively the ternary eutectic (Equilib. A), the solid solution stability limit (Equilib. B) and the liquidus point (Equilib. C). While in case of the first two transitions (A and B) the temperatures were identified as the onset points of the peaks during the heating process, the liquidus transition (C) was sometimes difficult to identify as it tends to form a broad shoulder in the heat flow signal. A more precise determination can be obtained from the cooling curves, which show a much sharper peak. However, during the cooling process the temperatures were not deduced directly as the onset temperatures of the peak due to supercooling event. The liquidus temperature was obtained by extrapolation to zero cooling rate by a straight line using the points measured at different rates.

The LiF-ThF_4-CeF_3 samples were prepared focusing on a very narrow range of compositions which is believed to be the most important for the MSFR fuel. The concentration ratio of LiF/ThF_4 has been set to a value suggested by preliminary version of the ternary phase diagram and close to the minimum temperature in the LiF-ThF_4 pseudo binary phase diagram ($X_{PuF_3} \sim 3\%$). The salt mixtures were then prepared by varying only the concentration of CeF_3 (proxy to PuF_3) in the mixture in order to investigate the influence of trifluoride salts concentration on the liquidus point and identify the composition of the minimum value. The lowest liquidus point was measured at 867.0 K for the LiF-ThF_4-CeF_3 (77.7-19.0-3.3) composition as reported in Table 5.3.

5.4. RESULTS

5.4.1. BINARY SYSTEMS ThF_4-PuF_3 AND UF_4-PuF_3

Based on the thermodynamic data described in the Section 7.3, the ThF_4-PuF_3 and UF_4-PuF_3 phase diagrams have been calculated and they are shown in Figures 5.1 and 5.2, respectively. As discussed above, no experimental data have been found in literature

Table 5.3: Phase equilibria in the LiF-ThF_4-CeF_3 system measured for the selected ternary compositions and the calculated transition temperatures for LiF-ThF_4-PuF_3 system (values in italic).

Composition			Equilibrium A		Equilibrium B		Equilibrium C	
x_{LiF}	x_{ThF_4}	x_{CeF_3/PuF_3}	T_{meas}	T_{calc}	T_{meas}	T_{calc}	T_{meas}	T_{calc}
0.789	0.192	0.019	818	*820*	828	*823*	885	*874*
0.778	0.190	0.032	825	*820*	832	*831*	889	*859*
0.777	0.190	0.033	824	*820*	830	*832*	867	*857*
0.777	0.189	0.034	819	*820*	831	*833*	872	*856*
0.776	0.189	0.035	822	*820*	831	*835*	870	*855*
0.775	0.189	0.036	824	*820*	833	*837*	884	*854*
0.767	0.186	0.047	821	*820*	829	*848*	874	*876*

for these two systems and thus no direct optimization was possible. Therefore, the optimization of the unknown parameters was done based on the proxy system ThF_4-CeF_3 [7, 11]. The main difference observed between the ThF_4-CeF_3 phase diagram and the assessed ThF_4-PuF_3 and UF_4-PuF_3 phase diagrams is the absence in the latter two systems of the intermediate compounds $PuThF_7$ and $PuUF_7$, which are calculated to be unstable with their thermodynamic properties estimated from the one of $CeThF_7$ and $CeUF_7$. In order to reduce this discrepancy, one of the possibilities would be to force the stability of the compounds by varying their thermodynamic properties. However, since there is no experimental evidence for the compounds stability and no indications on their decomposition temperatures, it is not obvious how to optimize the thermodynamic properties and further optimization was not undertaken.

Although there are some differences on the phase fields in the solid state, all the three phase diagrams ThF_4-CeF_3, ThF_4-PuF_3 and UF_4-PuF_3 show a very similar trend of the liquidus line. We must note here that the description of the liquidus lines are of major concern for the safety of the molten salt fuel as they determine the stability limit of the liquid phase at which the molten salt mixture must be maintained. The comparison between the liquidus line of the three systems and the experimental data for ThF_4-CeF_3 system is shown in Figure 5.3. Realising the fact that ThF_4 and UF_4 have slightly different melting points, which explains the discrepancy in the right side of the phase diagram, all the data are in very good agreement.

5.4.2. TERNARY SYSTEMS LIF-ThF_4-PuF_3 AND LIF-UF_4-PuF_3

Two ternary systems have been assessed in this work for the first time: LiF-ThF_4-PuF_3 and LiF-UF_4-PuF_3. Based on the thermodynamic description of all the sub-binary systems, the ternary phase diagrams have been extrapolated using the Kohler/Toop formalism and assuming LiF as asymmetric compound. No evidences have been found in literature on the existence of ternary compounds, hence none were considered in this study. However, some ternary excess Gibbs parameters have to be considered in order to reproduce at best the two sets of experimental data, measured by Barton *et al.* [17] and Ignatiev *et al.* [18]. The first work describes the solubility of CeF_3 in four LiF-ThF_4 compositions (T=873 K and T=1073 K) while Ignatiev *et al.* have measured the solubility of PuF_3 in two LiF-ThF_4 solvent compositions as function of temperature. The agreement obtained between the experimental data and the calculations is shown in Figure 5.4 and Figure 5.5 respectively, where the solubility of PuF_3 in LiF-ThF_4 solvent is represented by a solid line and the solubility of PuF_3 in LiF-UF_4 solvent is represented by a dashed line.

The liquidus projections of the LiF-ThF_4-PuF_3 and LiF-UF_4-PuF_3 ternary phase diagrams are shown in Figures 5.6 and 5.7 respectively, showing a very similar shape. In case of the LiF-ThF_4-PuF_3 system, seven invariant points have been found (Table 5.4) while in case of LiF-UF_4-PuF_3 five invariants points were identified (Table 5.5).

To validate the database developed, the experimental results have been compared with the calculated equilibrium temperature and a good agreement has been found (Table 5.3), showing a higher liquidus temperatures in the experiments. In Figure 5.8, the experimental points obtained for five compositions (X_{CeF_3} = 3.2, 3.3, 3.4, 3.5 and 3.6 mol%)

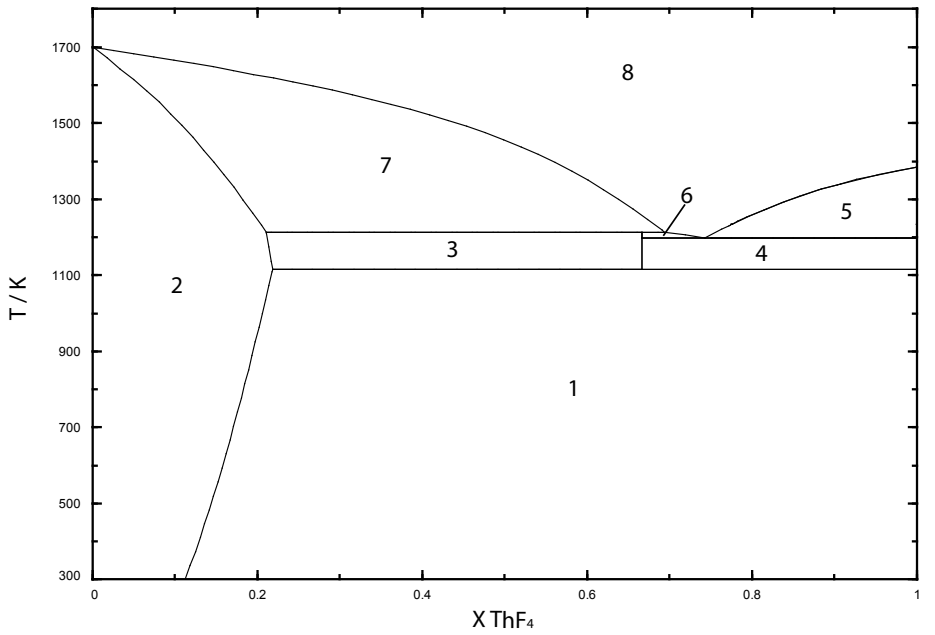

Figure 5.1: The ThF$_4$-PuF$_3$ calculated phase diagram assessed in this study. Phase fields: (1) $(Pu_{1-x}Th_x)F_{3+x}$ (ss) + ThF$_4$ (2) $(Pu_{1-x}Th_x)F_{3+x}$ (ss) (3) $(Pu_{1-x}Th_x)F_{3+x}$ (ss) + $PuTh_2F_{11}$ (4) $PuTh_2F_{11}$ + ThF$_4$ (5) ThF$_4$ + liq. (6) $PuTh_2F_{11}$ + liq. (7) $(Pu_{1-x}Th_x)F_{3+x}$ (ss) + liq. (8) Liquid

Table 5.4: Invariant equilibria and saddle points found in the LiF-ThF$_4$-PuF$_3$ system.

x_{LiF}	x_{ThF_4}	x_{PuF_3}	T / K	Type of equilibria	Crystal phases in equilibrium
0.170	0.621	0.209	1115	Quasi-Peritectic	ThF$_4$, (Th,Pu)F$_x$ (s.s.), $PuTh_2F_{11}$
0.249	0.577	0.174	1089	Quasi-Peritectic	ThF$_4$, (Th,Pu)F$_x$ (s.s.), $LiTh_4F_{17}$
0.522	0.407	0.071	1011	Quasi-Peritectic	(Th,Pu)F$_x$ (s.s.), $LiTh_4F_{17}$, $LiTh_2F_9$
0.692	0.283	0.025	863	Quasi-Peritectic	(Th,Pu)F$_x$ (s.s.), $LiTh_2F_9$, $LiThF_5$
0.724	0.253	0.023	822	Eutectic	(Th,Pu)F$_x$ (s.s.), $LiThF_5$, Li_3ThF_7
0.731	0.244	0.025	822	Saddle-point	(Th,Pu)F$_x$ (s.s.), Li_3ThF_7
0.753	0.216	0.031	820	Eutectic	(Th,Pu)F$_x$ (s.s.), Li_3ThF_7, LiF

Table 5.5: Invariant equilibria found in the LiF-UF$_4$-PuF$_3$ system.

x_{LiF}	x_{UF_4}	x_{PuF_3}	T / K	Type of equilibria	Crystal phases in equilibrium
0.092	0.686	0.221	1115	Quasi-Peritectic	UF$_4$, (U,Pu)F$_x$ (s.s.), PuU_2F_{11}
0.332	0.568	0.101	1018	Quasi-Peritectic	UF$_4$, (U,Pu)F$_x$ (s.s.), LiU_4F_{17}
0.580	0.400	0.019	877	Quasi-Peritectic	(U,Pu)F$_x$ (s.s.), LiU_4F_{17}, $Li_7U_6F_{31}$
0.741	0.246	0.013	765	Quasi-Peritectic	(U,Pu)F$_x$ (s.s.), $Li_7U_6F_{17}$, Li_4UF_8
0.733	0.257	0.010	757	Eutectic	(U,Pu)F$_x$ (s.s.), Li_4UF_8, LiF

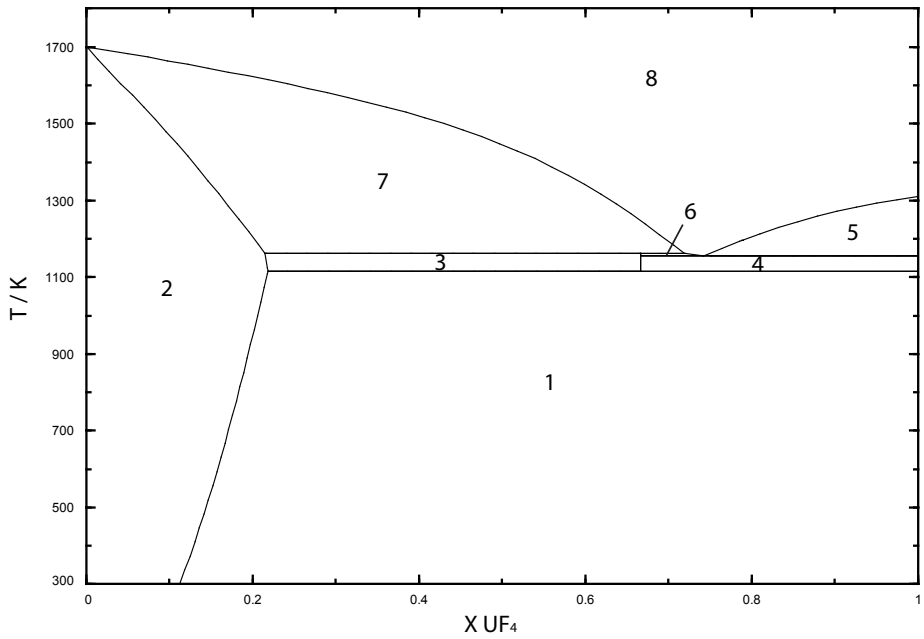

Figure 5.2: The UF_4-PuF_3 calculated phase diagram assessed in this study. Phase fields: (1) $(Pu_{1-x}U_x)F_{3+x}$ (ss) + UF_4 (2) $(Pu_{1-x}U_x)F_{3+x}$ (ss) (3) $(Pu_{1-x}U_x)F_{3+x}$ (ss) + PuU_2F_{11} (4) PuU_2F_{11} + UF_4 (5) UF_4 + liq. (6) PuU_2F_{11} + liq. (7) $(Pu_{1-x}U_x)F_{3+x}$ (ss) + liq. (8) Liquid

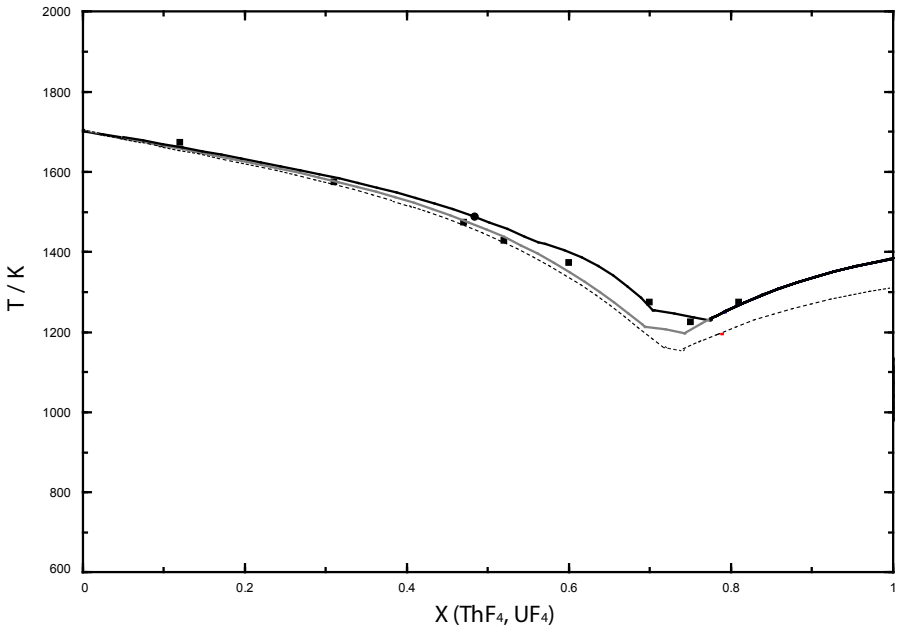

Figure 5.3: Comparison between the calculated liquidus lines for the ThF_4-CeF_3 system (black solid line), ThF_4-PuF_3 system (grey solid line) and UF_4-PuF_3 system (dashed line). (■) Data by Gilpatrick *et al.* [11] and (•) Data by Beneš *et al.* [7], both for ThF_4-CeF_3 system.

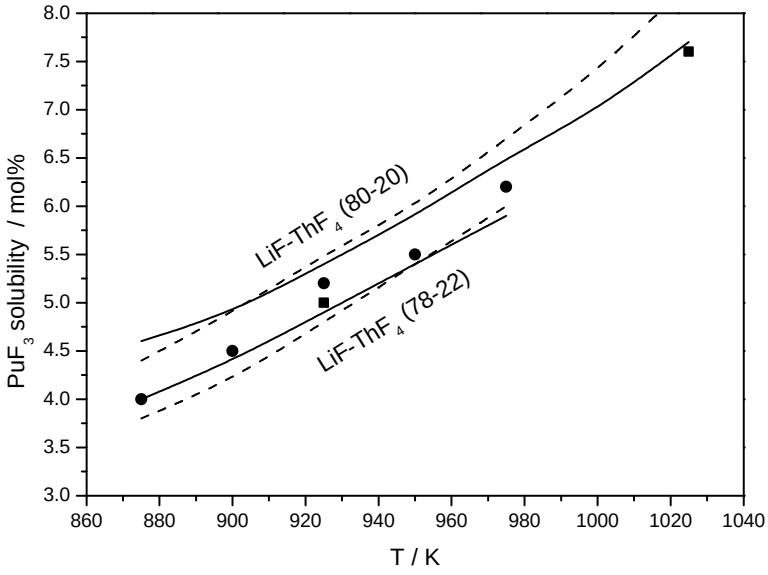

Figure 5.4: Calculated solubility of PuF_3 in LiF-ThF_4 mixtures (solid line) and LiF-UF_4 mixtures (dashed line) as a function of temperature. (■) and (•) Experimental data on PuF_3 solubility in LiF-ThF_4 (80-20) solvent and LiF-ThF_4 (78-22) solvent, respectively [18].

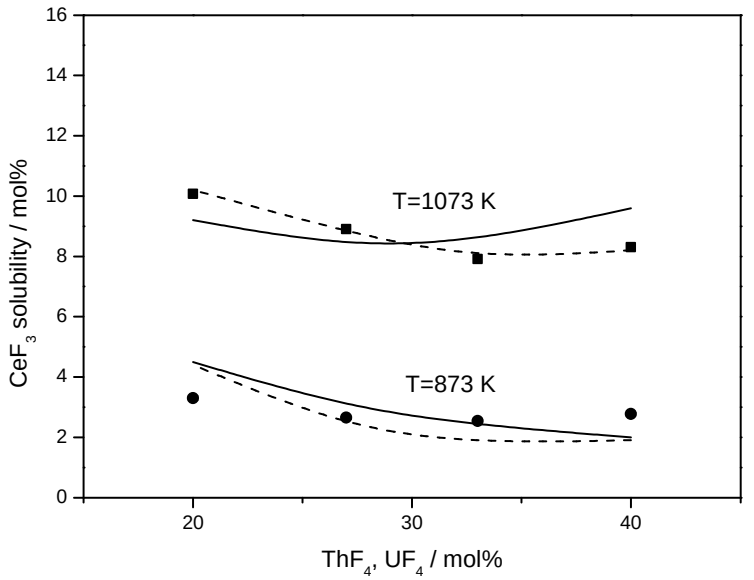

Figure 5.5: Calculated solubility of PuF_3 in the LiF-ThF_4 solvent (solid line) and in the LiF-UF_4 solvent (dashed line) as function of ThF_4/UF_4 composition for T=873 K and T=1073 K (■) and (•) Experimental data on CeF_3 solubility in different LiF-ThF_4 mixtures at T=1073 K and T=873 K, respectively [17].

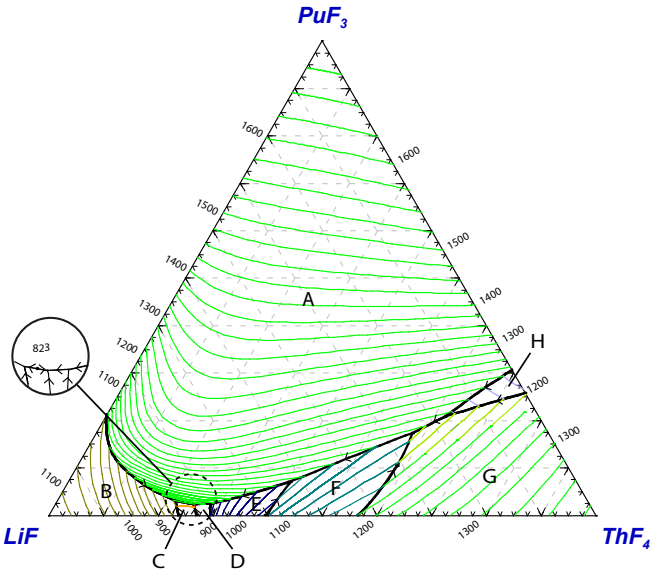

Figure 5.6: The liquidus projection of the LiF-ThF_4-PuF_3 system assessed in this study. Primary cristallization phase fields: (A) (Pu,Th)F_x (ss); (B) LiF; (C) Li_3ThF_7; (D) $LiThF_5$; (E) $LiTh_2F_9$; (F) $LiTh_4F_{17}$; (G) ThF_4; (H) $PuTh_2F_{11}$.

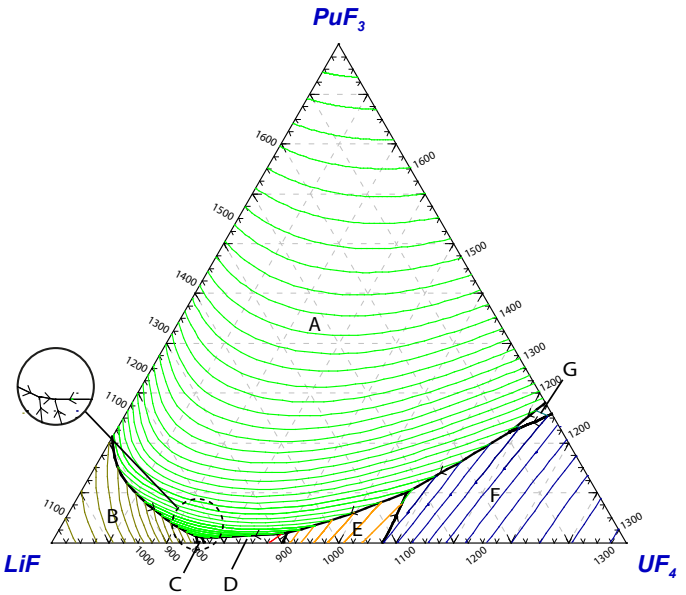

Figure 5.7: The liquidus projection of the LiF-UF$_4$-PuF$_3$ system assessed in this study. Primary cristallization phase fields: (A) (Pu,U)F$_x$ (ss); (B) LiF; (C) Li$_4$UF$_8$; (D) Li$_7$U$_6$F$_{31}$; (E) LiU$_4$F$_{17}$; (F) UF$_4$; (G) PuU$_2$F$_{11}$.

have been compared with the calculated pseudo-binary LiF-ThF_4 phase diagram having fixed composition of PuF_3. Considering the temperature range of the whole binary phase diagram the comparison between the calculation and the experiment reveals fairly good agreement for all measured compositions. In some cases the temperature shifts between the calculation and the experiment for the Equilibrium C are larger than the instrument uncertainty. This may be related to the composition uncertainty (u(x) = ± 0.001) that has larger impact on steep transition lines and to the determination of the peak onset/offset in the DSC signal (for the liquidus transition only the cooling curve can be used). The model represents the best compromise of all the experimental data measured (Equilibrium A, B and C) and available in literature (solubility data on CeF_3 and PuF_3).

5.5. FUEL OPTIMIZATION

The main result of the thermodynamic modeling described in this work is the complete description of the LiF-ThF_4-PuF_3-UF_4 system. That implies that the thermodynamic properties of each composition can be calculated from the model. Moreover, it also means that an optimization process may be performed by setting the proper criteria in order to find the most suitable composition, as described in this section. In case of the MSFR fuel, one of the main criteria considered is the melting temperature of the salt. A low melting point decreases the risk of salt freezing and reduces the problems related with the corrosion of structural materials because it allows lowering operating temperature of the reactor.

As mentioned in the introduction, reactors operating with the $^{232}Th/^{233}U$ cycle have to be started with an initial load of fissile material. An interesting solution is the use of plutonium and minor actinides separated from LWR fuel as initial fissile material achieving at the same time the closure of the fuel cycle. One of the factors that determines the total amount of material that can be added to the salt is the solubility of actinide trifluorides (PuF_3, NpF_3, AmF_3, CmF_3) in the LiF-ThF_4 mixture. Considering this limitation, the initial composition considered for the MSFR fuel contains 5 mol% of PuF_3 which is dissolved in the eutectic composition ^{7}LiF-ThF_4 (78-22 mol%). In order to avoid fluoride corrosion, it is necessary to control the redox potential by setting the right UF_4/UF_3 ratio. It implies that both UF_4 and UF_3 have to be present in the salt and as demonstrated in the MSRE project [20], the ratio UF_4/UF_3 should be around 100 to inhibit the corrosion. In this work, we consider a concentration of 1 % UF_4 as the minimum concentration required for redox control and we neglect the contribution of UF_3, as the concentration is so small that will not strongly influence the melting point of the mixture. It is important to notice that the concentration of 1 % UF_4 is the minimum required but it may be larger if necessary. Adding to the previous defined salt mixture 1 mol% of UF_4, the initial composition becomes LiF-ThF_4-PuF_3-UF_4 (73.3-20.7-5.0-1.0), which has a calculated melting point equal to 944 K. Figure 5.9 shows the LiF-ThF_4 pseudo-binary phase diagram with fixed concentration of PuF_3 and UF_4 equal to 5 mol% and 1 mol%, respectively. As shown, the initial MSFR composition (solid vertical line) does not correspond to the minimum liquidus temperature on the phase diagram and can be further lowered by decreasing the amount of ThF_4. The lowest liquidus temperature is now found at 867

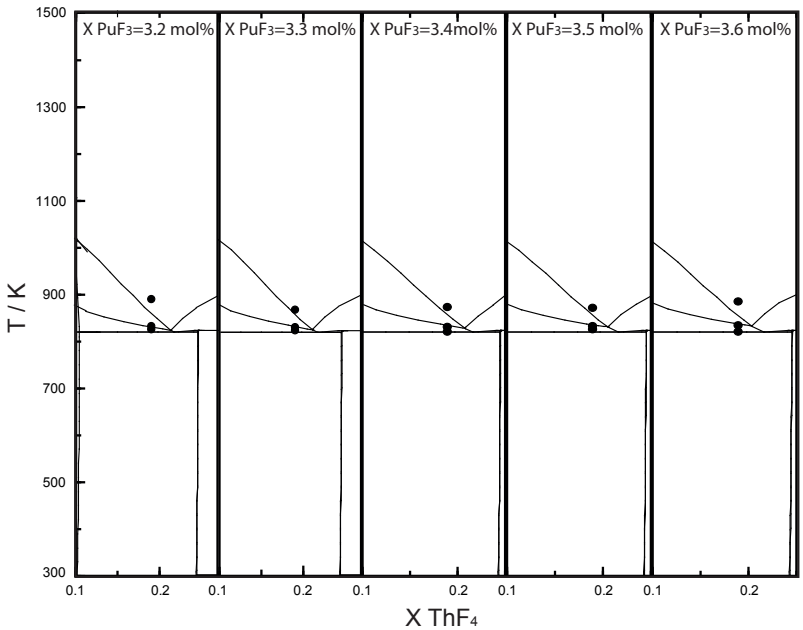

Figure 5.8: Comparison between the experimental points measured for five different LiF-ThF_4-CeF_3 compositions and the calculated pseudo binary LiF-ThF_4 phase diagram with fixed amount of PuF_3.

K for the composition LiF-ThF_4-PuF_3-UF_4 (78.0-16.0-5.0-1.0), represented in Figure 5.9 by the dashed vertical line. This salt mixture represents a promising candidate for the MSFR fuel according to its physico-chemical properties, but it is necessary to establish whether it also fullfills the reactor physics criteria.

A second fuel option may be based on a lower concentration of PuF_3, which would be compensated with a corresponding amount of $^{235}UF_4$. In fact, the total concentration of fissile material should be kept to the minimum value of 5 mol%. This fuel option, which does not maximize the waste reduction, has the advantage of offering a lower melting temperature which is significantly influenced by the total amount of PuF_3. From the calculated pseudo-ternary LiF-ThF_4-PuF_3 phase diagram with a fixed composition of 1 mol% UF_4 (Figure 5.10), the lowest eutectic is identified for the LiF-ThF_4-PuF_3-UF_4 (75.4-20.6-3.0-1.0) composition at T=819 K. The low melting point of this salt mixture, around 46 K lower than the previous one, makes this composition suitable as candidate fuel for the MSFR but the proportion of thorium/uranium in the initial fissile load should be optimised based on neutronic calculations and non-proliferation issues.

In fact, keeping the sum of ThF_4 and UF_4 constant while increasing the UF_4/ThF_4 ratio it is possible to increase the fissile concentration in the salt and mantaining the uranium enrichment to reasonable values (< 20 %) [21]. In order to evaluate the influence of the partial substitution of ThF_4 by UF_4 on the liquidus temperature, we have performed several calculations starting from the LiF-ThF_4-PuF_3-UF_4 (75.4-20.6-3.0-1.0) composition (calculated lowest liquidus point). Considering the extreme case when the total amount of (ThF_4+UF_4) is fully represented by UF_4 the composition becomes LiF-UF_4-PuF_3 (75.4-21.6-3.0) with calculated liquidus temperature of 842 K. Although this value is slightly higher compared to the minimum temperature predicted in case of only 1 mol % of UF_4 present in the mixture, a total increase of 20 K for the extreme case is considered to be acceptable. Moreover, other important properties as vapour pressure and boiling point have been calculated for the two extreme cases and are shown in Table 6.8. The vapour pressure data have been calculated for the temperature T_{oper}, which is 50 K higher than the liquidus temperature to give enough margin to be considered as a safe operation temperature of the MSFR. The main contribution to the vapour pressure is given by the following gaseous species: LiF, Li_2F_2, Li_3F_3, ThF_4, UF_4 and PuF_3. From the results, it is possible to conclude that the partial substitution of ThF_4 with UF_4 influences the physico-chemical properties of the mixture. However, considering the total amount of ThF_4 and UF_4 constant and increasing the amount of UF_4, it is possible to decrease the uranium enrichment to reasonable values keeping good physico-chemical properties.

5.6. CONCLUSIONS

In this work, the full thermodynamic description of the LiF-ThF_4-PuF_3-UF_4 system has been performed. The binary and ternary systems containing PuF_3 have been assessed for the first time based on the similarities between the proxy compounds (PuF_3/CeF_3 and ThF_4/UF_4) and the experimental data available in literature. The model developed

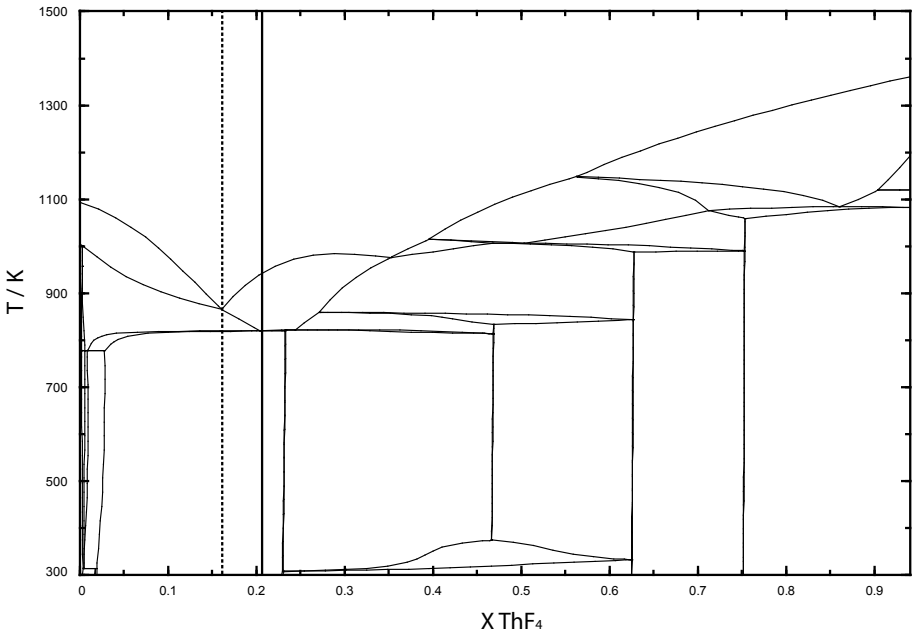

Figure 5.9: The pseudo binary LiF-ThF$_4$ phase diagram having a fixed concentration of 5 mol% PuF$_3$ and 1 mol% of UF$_4$. The solid line represent the first considered fuel composition while the dashed line represent the composition showing the lowest liquidus temperature.

Table 5.6: Influence of the partial substitution of ThF$_4$ with UF$_4$ on the most important fuel properties.

Composition	T liquidus (K)	T boiling (K)	P at T^*_{oper} (Pa)
LiF-ThF$_4$-UF$_4$-PuF$_3$ (75.4-20.6-1.0-3.0)	819 K	2033 K	$7.39 \cdot 10^{-4}$
LiF-UF$_4$-PuF$_3$ (75.4-21.6-3.0)	842 K	2002 K	$1.70 \cdot 10^{-3}$

*T$_{oper}$ is the operation temperature defined here as 50 K higher than the liquidus temperature.

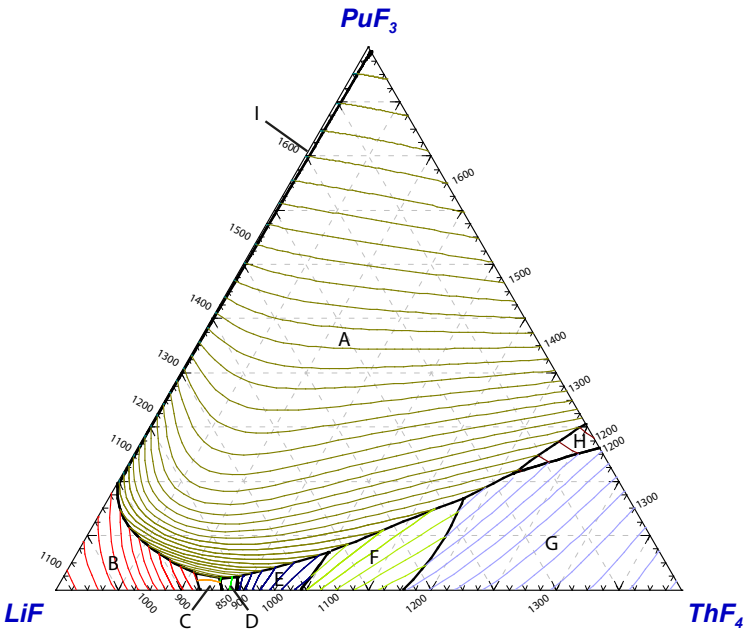

Figure 5.10: The calculated LiF-ThF_4-PuF_3 phase diagram with a fixed concentration of UF_4 set to 1 mol%. Primary phase fields: (A) (Pu,Th)F_x (s.ss); (B) LiF; (C) Li_3(Th, U)F_7; (D) Li_7(Th, U)$_6F_{31}$; (E) Li(Th,U)$_2F_9$ (F) Li(Th, U)$_4F_{17}$; (G) (Th,U)F_x (s.s.) (H) $PuTh_2F_{11}$ (I) (Pu,U)F_x (s.s.).

was able to reproduce very well the solubility measurements of CeF_3 and PuF_3 in LiF-ThF_4, giving justification for the assumptions made.

In order to verify the validity of the model developed, the DSC technique has been used to analyse selected LiF-ThF_4-CeF_3 compositions and the results have confirmed the phase equilibrium predicted. Moreover, using the thermodynamic database developed some potential compositions for the MSFR fuel have been selected based on their physico-chemical properties (mainly based on the melting point). All the considered compositions are summarized in Table 5.7 and the most important properties for these salt mixtures have been calculated.

All the proposed compositions have a concentration of 1 mol% UF_4, which is the assumed minimum required for redox control via UF_4/UF_3 ratio. However, as explained in this work the concentration of UF_4 required may be larger for neutronic reasons. Therefore the influence of partial substitution of ThF_4 with UF_4 on the different important fuel properties have been investigated and it was concluded to be small for the considered composition.

ACKNOWLEDGEMENTS

This work was supported by the EVOL project in the 7th Framework Programme of the European Commision (Grant agreement No.249696). The authors would like to thank E. Merle-Lucottte and M. Allibert of the Research Group of CNRS Grenoble for the fruitful discussion.

Table 5.7: The potential fuel composition and the related fuel properties.

Composition	T liquidus (K)	T boiling (K)	P at T_{oper} * (Pa)
LiF-ThF_4-UF_4-PuF_3 ** (73.3-20.7-1.0-5.0)	944 K	2035 K	$4.62 \cdot 10^{-2}$
LiF-ThF_4-UF_4-PuF_3 (78.0-16.0-1.0-5.0)	867 K	2035 K	$5.33 \cdot 10^{-3}$
LiF-ThF_4-UF_4-PuF_3 (75.3-20.6-1.0-3.1)	819 K	2032 K	$7.26 \cdot 10^{-4}$

*T_{oper} is the operation temperature defined here as 50 K higher than the liquidus temperature.
** Starting fuel composition defined by MSFR concept.

REFERENCES

[1] E. Capelli, O. Beneš, and R. J. M. Konings, *Thermodynamic assessment of the LiF-ThF_4–PuF_3-UF_4 system,* J. Nucl. Mater. **462**, 43 (2015).

[2] S. Delpech, E. Merle-Lucotte, D. Heuer, M. Allibert, V. Ghetta, C. Le-Brun, X. Doligez, and G. Picard, *Reactor physics and reprocessing scheme for innovative molten salt reactor system,* J. Fluor. Chem. **130**, 11 (2009).

[3] D. B. Grimes, *Molten Salt Reactor Program: Quarterly progress report,* Tech. Rep. ORNL-2551 (1958).

[4] R. E. Thoma, *Chemical Feasibility of fueling molten-salt reactors with PuF_3,* Tech. Rep. ORNL-TM-2256 (1968).

[5] E. Merle-Lucotte, D. Heuer, C. L. Brun, L. Mathieu, R. Brissot, E. Liatard, O. Meplan, and A. Nuttin, *Fast thorium molten salt reactors started with plutonium,* Proceedings of the International Congress on Advances in Nuclear Power Plants (ICAPP), Reno, USA , (2006).

[6] E. Capelli, O. Beneš, and R. J. M. Konings, *Thermodynamic assessment of the LiF-NaF-BeF_2-ThF_4-UF_4 system,* J. Nucl. Mater. **449**, 111 (2014).

[7] O. Beneš and R. J. M. Konings, *Thermodynamic assessment of the LiF–CeF_3–ThF_4–UF_4 system,* J. Nucl. Mater. **435**, 164 (2013).

[8] C. W. Bale, E. Bélisle, P. Chartrand, S. A. Decterov, G. Eriksson, K. Hack, I. H. Jung, Y. B. Kang, J. Melançon, A. D. Pelton, C. Robelin, and S. Petersen, *Factsage thermochemical software and databases - recent developments,* CALPHAD **33**, 295 (2009).

[9] M. W. Chase Jr.(ed.), *NIST-JANAF Thermochemical Tables Fourth Edition,* J. Phys. Chem. Ref. Data, Monograph **9**, (1998).

[10] R. J. M. Konings, L. R. Morss, and J. Fuger, *The chemistry of the actinide and transactinide elements,* (Springer, Dordrecht, The Netherlands, 2006) Chap. 19.

[11] L. O. Gilpatrick, C. J. Barton, and H. Insley, *Molten-Salt Reactor Program: Semiannual Progress Report,* Tech. Rep. ORNL-TM-4622 (1970).

[12] A. D. Pelton, *A database and sublattice model for molten salts,* CALPHAD **12**, 127 (1988).

[13] C. F. Weaver, R. E. Thoma, H. Insley, and H. A. Friedman, *Phase equilibria in the systems UF_4-ThF_4 and LiF-UF_4-ThF_4,* J. Am. Ceram. Soc. **43**, 213 (1960).

[14] O. Beneš, M. Beilmann, and R. J. M. Konings, *Thermodynamic assessment of the LiF–NaF–ThF_4–UF_4 system,* J. Nucl. Mater. **405**, 186 (2010).

[15] A. D. Pelton, P. Chartrand, and G. Eriksson, *The Modified Quasi-chemical Model: Part IV. Two sublattice quadruplet approximation,* Metall. Trans. **32A**, 1409 (2001).

[16] O. Beneš and R. J. M. Konings, *Actinide burner fuel: Potential compositions based on the thermodynamic evaluation of MF–PuF_3 $M = Li, Na, K, Rb, Cs$ and LaF_3–PuF_3 systems,* J. Nucl. Mater. **377**, 449 (2008).

[17] C. J. Barton, M. A. Bredig, L. O. Gilpatrick, and J. A. Fredricksen, *Solubility of cerium trifluoride in molten mixtures of lithium, beryllium and thorium fluorides,* Inorg. Chem. **9**, 307 (1970).

[18] V. Ignatiev, O. Feynberg, A. Merzlyakov, A. Surenko, A. Zagnitko, V. Subbotin, R. Fazilov, M. Gordeev, A. Panov, and A. Toropov, *Progress in development of MOSART concept with th support,* Proceedings of the International Congress on Advances in Nuclear Power Plants (ICAPP), Chicago,USA (2012).

[19] E. Capelli, O. Beneš, M. Beilmann, and R. J. M. Konings, *Thermodynamic investigation of the LiF-ThF_4 system,* J. Chem. Thermodyn. **58**, 110 (2013).

[20] E. L. Compere, S. S. Kirslis, E. G. Bohlmann, F. F. Blankenship, and W. R. Grimes, *Fission Product Behavior in the MSRE,* Tech. Rep. ORNL-4865 (1975).

[21] D. Heuer, E. Merle-Lucotte, M. Allibert, M. Brovchenko, V. Ghetta, and P. Rubiolo, *Towards the thorium fuel cycle with molten salt fast reactors,* Ann. Nucl. Energy **64**, 421 (2014).

6

THERMODYNAMIC ASSESSMENT OF THE LiF-NaF-BeF_2-ThF_4-UF_4 SYSTEM

Elisa CAPELLI, Ondřej BENEŠ, Rudy J.M. KONINGS

The present study describes the full thermodynamic assessment of the LiF-NaF-BeF_2-ThF_4-UF_4 system which is one of the key systems considered for a molten salt reactor fuel. The work is an extension of the previously assessed LiF-NaF-ThF_4-UF_4 system with addition of BeF_2 which is characterized by very low neutron capture cross section and a relatively low melting point. To extend the database the binary BeF_2-ThF_4 and BeF_2-UF_4 systems were optimized and the novel data were used for the thermodynamic assessment of BeF_2 containing ternary systems for which experimental data exist in the literature. The obtained database is used to optimize the molten salt reactor fuel composition and to assess its properties with the emphasis on the melting behaviour.

Parts of this chapter have been published in Journal of Nuclear Materials **449**, 111 (2014) [1].

6.1. INTRODUCTION

Alkali metal and alkaline earth fluoride systems and their mixtures in which actinide fluorides can be dissolved are key materials for a molten salt reactor (MSR) fuel. MSR belongs to the Generation IV nuclear reactors and as a future reactor concept meets the highest safety requirements with high reliability and efficiency. It is therefore mandatory to understand the fuel properties and to have good knowledge of any changes upon composition shifts which may occur during the fission reaction. Since MSR fuel is typically a multi-component system containing three or more initial components it is almost impossible to measure every composition to seek for its properties. Therefore the creation of a thermodynamic database is highly useful as it describes the whole system by a mathematical model that is usually based and confirmed by series of experiments. With such database one can predict some of the properties needed for the reactor safety assessment, like melting behaviour, vapour pressure, heat capacity or solubility of actinides.

A thermodynamic database describing the most relevant systems for a MSR has been developed at JRC-ITU within the past decade. Recently we have presented [2] a full thermodynamic description of the LiF-NaF-ThF_4-UF_4 system which has been assessed as part of the investigation of the fuel behaviour of the Molten Salt Fast Reactor concept (MSFR) [3]. In the present study we extend this system by addition of BeF_2 which has very low neutron capture cross section and together with ^{7}LiF is considered as the key solvent for ThF_4 and UF_4 in the molten salt thermal breeder reactor design. We first thermodynamically optimize the relevant BeF_2-containing binary sub-systems and after the assessment of the ternary systems we perform the optimization of the fuel composition with respect to its melting behaviour. Once the fuel compositions are identified the thermodynamic properties are calculated and discussed in view of the reactor safety.

6.2. THERMODYNAMIC MODELLING

To obtain the full thermodynamic description of the LiF-NaF-BeF_2-ThF_4-UF_4 system it is necessary to assess all binary sub-systems which are defined by all pair combinations of the end-members. Thermodynamic assessments of two binary BeF_2-ThF_4 and BeF_2-UF_4 phase diagrams have been performed in this study, whereas the optimized data of the remaining binary systems have been taken from our previous studies [2, 4]. We must note here that based on the performed extensive investigation of the LiF-ThF_4 system reported in our recent study [5], a new value for the heat capacity of the ThF_4 liquid phase has been evaluated and this change must be considered in all ThF_4-containing systems. Therefore, the NaF-ThF_4 phase diagram was re-assessed in this study as well. Nevertheless, since only minor changes were observed compared to [2], it is not necessary to show the phase diagram in this paper and we only report the slightly modified excess Gibbs energy values.

6.2.1. COMPOUNDS

The thermodynamic stability of any chemical specie is determined by the Gibbs energy which for compounds is defined as:

$$G(T) = \Delta_f H^0(298.15) - S^0(298)\,T + \int_{298.15}^{T} C_p(T)\mathrm{d}T - T\int_{298}^{T}\left(\frac{C_p(T)}{T}\right)\mathrm{d}T \quad , \tag{6.1}$$

where $\Delta_f H^0(298.15)$ and $S^0(298.15)$ are respectively the standard enthalpy of formation and standard absolute entropy, both referring to a temperature of 298.15 K. The $C_p(T)$ term is the temperature function of the heat capacity at constant pressure. The thermodynamic quantities of all compounds considered in the LiF-NaF-BeF_2-ThF_4-UF_4 system are reported in Table 6.1. The data are taken from our previous studies [2, 4], except the data of liquid ThF_4 which have been modified by a better estimation of the heat capacity described in [5], and the thermodynamic data of the intermediate compounds from the LiF-ThF_4 and NaF-ThF_4 systems which have been re-assessed in order to correctly reproduce the crystallization phase fields of the higher order systems. The data of the ternary compound $Na_3BeTh_{10}F_{45}$ were obtained from the optimization of the corresponding ternary system performed in this study.

Table 6.1: The $\Delta_f H^0(298.15)$ (kJ · mol^{-1}), $S^0(298.15)$ (J · K^{-1} · mol^{-1}) and C_p (J · K^{-1} · mol^{-1}) data of pure compounds used in this study.

Compound	$\Delta_f H^0(298.15)$	$S^0(298.15)$	$C_p = a + b\,T + c\,T^2 + d\,T^{-2}$			
			a	b T	c T^2	d T^{-2}
LiF (s)	-616.931	35.66	43.309	$1.6312\cdot10^{-2}$	$5.0470\cdot10^{-7}$	$-5.691\cdot10^{5}$
LiF (l)	-598.654	42.962	64.183	-	-	-
NaF (s)	-576.650	51.21	47.630	$1.4790\cdot10^{-2}$	-	$-4.643\cdot10^{5}$
NaF (l)	-557.730	52.755	72.989	-	-	-
α-BeF_2(s)	-1026.800	53.35	19.18	$1.0954\cdot10^{-1}$		
β-BeF_2(s)	-1025.560	56.11	39.46	$4.626\cdot10^{-2}$		
BeF_2(l)	-1021.657	60.49	40.98	$4.494\cdot10^{-2}$		
ThF_4 (s)	-2097.900	142.05	122.173	$8.3700\cdot10^{-3}$	-	$-1.255\cdot10^{6}$
ThF_4 (l)	-2103.654	101.237	170.0	-	-	-
UF_4 (s)	-1914.200	151.70	114.519	$2.0555\cdot10^{-2}$	-	$-4.132\cdot10^{5}$
UF_4 (l)	-1914.658	115.400	174.74	-	-	-
$LiBeF_3$(s)	-1651.488	89.24	54.39	$1.2552\cdot10^{-1}$		
Li_2BeF_4(s)	-2267.654	139.68	90.78	$1.4915\cdot10^{-1}$	$-1.8416\cdot10^{-8}$	$1.971\cdot10^{5}$
α-$NaBeF_3$(s)	-1655.803	87.790	66.811	$1.2433\cdot10^{-1}$		$-4.643\cdot10^{5}$
β-$NaBeF_3$(s)	-1653.578	91.390	66.811	$1.2433\cdot10^{-1}$		$-4.643\cdot10^{5}$
α-Na_2BeF_4(s)	-2267.696	122.512	114.441	$1.3912\cdot10^{-1}$		$-9.286\cdot10^{5}$
β-Na_2BeF_4(s)	-2262.112	133.612	114.441	$1.3912\cdot10^{-1}$		$-9.286\cdot10^{5}$
γ-Na_2BeF_4(s)	-2254.612	146.260	114.441	$1.3912\cdot10^{-1}$		$-9.286\cdot10^{5}$
$LiNaBeF_4$(s)	-2270.641	133.224	110.12	$1.4064\cdot10^{-1}$	$5.0470\cdot10^{-7}$	$-1.033\cdot10^{6}$
$LiNa_2Be_2F_7$(s)	-3921.787	235.788	176.93	$2.6497\cdot10^{-1}$	$5.0470\cdot10^{-7}$	$-1.498\cdot10^{6}$
$LiNa_5Be_3F_{12}$(s)	-6804.371	384.772	339.00	$4.1888\cdot10^{-1}$	$5.0470\cdot10^{-7}$	$-2.891\cdot10^{6}$

Continued on next page

Table 6.1 – *Continued from previous page*

Compound	$\Delta_f H^0$(298.15)	S^0(298.15)	C_p = a + b T + c T^2 + d T^{-2}			
			a	b T	c T^2	d T^{-2}
$LiThF_5$(s)	-2719.490	181.89	165.482	$2.468{\cdot}10^{-2}$	$5.047{\cdot}10^{-7}$	$-1.824{\cdot}10^{6}$
Li_3ThF_7(s)	-3960.259	236.1	282.100	$5.730{\cdot}10^{-2}$	$1.514{\cdot}10^{-6}$	-2.962c
$LiTh_2F_9$(s)	-4822.329	324.29	287.655	$3.305{\cdot}10^{-2}$	$5.047{\cdot}10^{-7}$	$-3.079{\cdot}10^{6}$
$LiTh_4F_{17}$(s)	-9021.140	609.0	532.001	$4.979{\cdot}10^{-2}$	$5.047{\cdot}10^{-7}$	$-5.589{\cdot}10^{6}$
Li_4UF_8 (s)	-4347.620	357.55	287.755	$8.5804{\cdot}10^{-2}$	$2.0188{\cdot}10^{-6}$	$-2.690{\cdot}10^{6}$
$Li_7U_6F_{31}$ (s)	-15826.900	1230.82	990.279	$2.3751{\cdot}10^{-1}$	$3.5329{\cdot}10^{-6}$	$-6.463\cdot10^{6}$
LiU_4F_{17} (s)	-8293.761	644.70	501.387	$9.8532{\cdot}10^{-2}$	$5.0470{\cdot}10^{-7}$	$-2.222{\cdot}10^{6}$
Na_4ThF_8 (s)	-4355.195	450.4	312.693	$6.7530{\cdot}10^{-2}$	-	$-3.112{\cdot}10^{6}$
$Na_7Th_2F_{15}$ (s)	-8285.600	677.6	577.756	$1.2027{\cdot}10^{-1}$	-	$-5.760{\cdot}10^{6}$
Na_2ThF_6 (s)	-3282.870	255.9	217.433	$3.7950{\cdot}10^{-2}$	-	$-2.184{\cdot}10^{6}$
$Na_3Th_2F_{11}$ (s)	-5910.275	526.4	387.236	$6.1110{\cdot}10^{-2}$	-	$-3.903{\cdot}10^{6}$
$Na_7Th_6F_{31}$ (s)	-16653.219	1364.0	1066.448	$1.5375{\cdot}10^{-2}$	-	$-1.078{\cdot}10^{7}$
$NaThF_5$ (s)	-2693.871	199.2	169.803	$2.3160{\cdot}10^{-2}$	-	$-1.719{\cdot}10^{6}$
$NaTh_2F_9$ (s)	-4791.776	348.3	291.976	$3.1530{\cdot}10^{-2}$	-	$-2.974{\cdot}10^{6}$
α-Na_3UF_7 (s)	-3633.100	366.5	257.409	$6.4925{\cdot}10^{-2}$	-	$-1.806{\cdot}10^{6}$
β-Na_3UF_7 (s)	-3632.600	367.1	257.409	$6.4925{\cdot}10^{-2}$	-	$-1.806{\cdot}10^{6}$
Na_2UF_6 (s)	-3089.500	272.3	209.779	$5.0135{\cdot}10^{-2}$	-	$-1.342{\cdot}10^{6}$
$Na_5U_3F_{17}$ (s)	-8623.600	828.5	581.708	$1.3561{\cdot}10^{-1}$	-	$-3.561{\cdot}10^{6}$
$Na_7U_6F_{31}$ (s)	-15608.800	1363.984	1020.526	$2.2686{\cdot}10^{-1}$	-	$-5.729{\cdot}10^{6}$
NaU_2F_9 (s)	-4430.200	354.6	276.669	$5.5900{\cdot}10^{-2}$	-	$-1.291{\cdot}10^{6}$
NaU_4F_{17} (s)	-8260.600	655.57	505.708	$9.7010{\cdot}10^{-2}$	-	$-2.117{\cdot}10^{6}$
$Na_3BeTh_{10}F_{45}$ (s)	-23874510	1623	1404.077	$1.7433\cdot10^{-1}$	-	$-1.394{\cdot}10^{7}$

6.2.2. SOLID SOLUTION

The two binary systems assessed in this study (BeF_2-ThF_4 and BeF_2-UF_4) are simple eutectic systems with no experimentally confirmed solubility in the solid state. However, limited solubility in the solid state appears in the ternary field of the LiF-BeF_2-ThF_4 system [6]. It is found in the narrow region of the Li_3ThF_7 compound. For the description of the excess Gibbs parameters of this solid solution the classical polynomial formalism has been applied with chosen end-members Li_3ThF_7, BeF_2 and hypothetical $LiBeThF_7$. The binary sub-interactions that, with the successive Kohler extrapolation, describe the ternary solid solution are given by the following general equation:

$$G_m^{xs} = \sum_{i,j} X_1 \cdot X_2 \cdot L_{i,j} \quad , \tag{6.2}$$

in which X_1 and X_2 are the mole fractions of the mixed end-members and the $L_{i,j}$ term is in the form of general equation:

$$L_{i,j} = A + BT + CT\ln T + DT^2 .... \tag{6.3}$$

of which the parameters to be optimized during the thermodynamic assessment. The optimized parameters obtained in this study are given below:

$$G_m^{xs} = X_{Li_3ThF_7} \cdot X_{BeF_2} \cdot -35000 \quad \mathrm{J \cdot mol^{-1}}, \tag{6.4}$$

$$G_m^{xs} = X_{Li_3ThF_7} \cdot X_{LiBeThF_7} \cdot -38000 \quad \mathrm{J \cdot mol^{-1}}, \tag{6.5}$$

$$G_m^{xs} = X_{BeF_2} \cdot X_{LiBeThF_7} \cdot 21500 \quad \mathrm{J \cdot mol^{-1}}. \tag{6.6}$$

The Gibbs energies of the Li_3ThF_7 end-member are taken from Table 6.1, whereas BeF_2 had to be destabilized according to:

$$G(BeF_2(s.s.)) = G(\beta - BeF_2) + 10500 \quad \mathrm{J \cdot mol^{-1}}, \tag{6.7}$$

while the data for hypothetical $LiBeThF_7$ were estimated as:

$$G(LiBeThF_7(s.s.)) = G(LiF) + G(\beta - BeF_2) + G(ThF_4). \tag{6.8}$$

We must note at this point that due to the re-assessment of the LiF-ThF_4 binary system performed in our previous study [5] and with slight modification done in the presented paper for LiF-ThF_4 and NaF-ThF_4 systems new data for the containing intermediate compounds have been determined. Consequently, all solid solutions that are based on these compounds had to be re-optimized accordingly and the updated excess Gibbs energy data are given in Table 6.2.

6.2.3. LIQUID SOLUTION

The current study is performed within the frame of an extension of the fluoride salt fuel database by the BeF_2 component and therefore a compatibility of the thermodynamic models must be kept. For that reason the quasichemical model based on quadruplet approximation [7] has been used for the description of the excess Gibbs parameters of the liquid phase.

The quadruplets consist of two anions and two cations and their representation is given in Figure 6.1. Two interactions are distinguished, the first nearest neighbor (FNN) interaction between cation and anion and the second nearest neighbor (SNN) interaction between two closest ions of the same sublattice. The parameters of the modified quasichemical model are related to the Gibbs energy changes $\Delta g_{AB/F}$ for the SNN pair-exchange reaction represented below:

$$(A-F-A) + (B-F-B) = 2(A-F-B) \qquad \Delta g_{AB/F}, \tag{6.9}$$

where A and B represent the cations and F the F^- anion as the only anion considered in this study. The $\Delta g_{AB/F}$ parameter for reaction 6.9 can be expanded as a polynomial such as

$$\Delta g_{AB/F} = \Delta g^0_{AB/F} + \sum_{(i+j)\geqq 1} g^{ij}_{AB/F} \chi^i_{AB/F} \chi^j_{BA/F} \tag{6.10}$$

Table 6.2: The modified excess Gibbs energy functions of solid solutions from LiF-ThF_4 and NaF-ThF_4 systems.

Solid solution	ΔG^{xs} (J · mol^{-1})
$(Li,Na)_7Th_6F_{31}$	$\Delta G^{xs} = X_{Li_7Th_6F_{31}} \cdot X_{Na_7Th_6F_{31}} \cdot (-100000)$
	$+X_{Li_7Th_6F_{31}} \cdot X^2_{Na_7Th_6F_{31}} \cdot (-150000)$
	${}^*G^{\circ}_{Li_7Th_6F_{31\_ss}} = -17259817 + 5952.07 \cdot T - 1036.2 \cdot TlnT$
	$-0.0822 \cdot T^2 - 5.8882 \cdot 10^{-7} \cdot T^3 + 5756933 \cdot T^{-1}$
$Li(Th,U)_4F_{17}$	$\Delta G^{xs} = X_{LiTh_4F_{17}} \cdot X_{LiU_4F_{17}} \cdot (-60000)$
$Li(Th,U)_2F_9$	$\Delta G^{xs} = X_{LiTh_2F_9} \cdot X_{LiU_2F_9} \cdot (-28000)$
$Li_7(Th,U)_6F_{31}$	$\Delta G^{xs} = X_{LiThF_5} \cdot X_{Li_7U_6F_{31}} \cdot (-40000)$
$Li_3(Th,U)F_7$	$\Delta G^{xs} = X_{Li_3ThF_7} \cdot X_{Li_3UF_7} \cdot (-20000)$
$Na_7(Th,U)_2F_{15}$	$\Delta G^{xs} = X_{Na_7Th_2F_{15}} \cdot X_{Na_7U_2F_{15}} \cdot (-135000)$
$Na_2(Th,U)F_6$	$\Delta G^{xs} = X_{Na_2ThF_6} \cdot X_{Na_2UF_6} \cdot (15500)$
	$+X^2_{Na_2ThF_6} \cdot X_{Na_2UF_6} \cdot (12500)$
	$+X_{Na_2ThF_6} \cdot X^2_{Na_2UF_6} \cdot (-15000)$
$Na_7(Th,U)_6F_{31}$	$\Delta G^{xs} = X_{Na_7Th_6F_{31}} \cdot X_{Na_7U_6F_{31}} \cdot (-90000)$
$Na(Th,U)_2F_9$	$\Delta G^{xs} = X_{NaTh_2F_9} \cdot X_{NaU_2F_9} \cdot (-6000)$
$Na_3Th_2F_{11}$-$Na_5U_3F_{17}$	$\Delta G^{xs} = X_{Na_3Th_2F_{11}} \cdot X_{Na_5U_3F_{17}} \cdot (-25000)$
	$+X^2_{Na_3Th_2F_{11}} \cdot X_{Na_5U_3F_{17}} \cdot (-10000)$

*Hypothetical end-member.

where $\Delta g^0_{AB/F}$ and $g^{ij}_{AB/F}$ are composition independent coefficients (although possibly temperature dependent) obtained from the optimization of the experimental data for binary $AF-BF$ solutions. The $\chi_{AB/F}$ term is a composition variable and is defined as

$$\chi_{AB/F} = \left(\frac{X_{AA}}{X_{AA}+X_{AB}+X_{BB}}\right). \tag{6.11}$$

The excess Gibbs parameters of all binary sub-systems from the LiF-NaF-BeF_2-ThF_4-UF_4 system are reported below. While the data of BeF_2-ThF_4 and BeF_2-UF_4 binary systems are fully novel and obtained in this study, the data of the NaF-ThF_4 system have been slightly re-assessed due to the modified heat capacity data of the ThF_4 liquid phase made in our earlier study [5]. The rest of the binary data presented below are taken from our previous publications [2, 4, 5], considering no excess Gibbs energy for the liquid phase of the ThF_4-UF_4 system.

$$\Delta g_{BeTh/FF} = 9628 - 5.86T \quad \mathrm{J\cdot mol^{-1}} \tag{6.12}$$

$$\Delta g_{BeU/FF} = 502 + 3.14T + \chi_{BeU/F}(2428 + 0.419T) + \chi_{UBe/F}(800 + 2.09T) \quad \mathrm{J\cdot mol^{-1}} \tag{6.13}$$

$$\begin{aligned}\Delta g_{NaTh/FF} = &-26874 + \chi_{NaTh/F}(10046 - 12.56T)\\ &+ \chi_{ThNa/F}(-30106 + 16.74T) \quad \mathrm{J\cdot mol^{-1}}\end{aligned} \tag{6.14}$$

$$\begin{aligned}\Delta g_{LiTh/FF} = &-10883 + \chi_{LiTh/F}(-6697 + 2.93T)\\ &+ \chi_{ThLi/F}(-20930 + 19.25T) \quad \mathrm{J\cdot mol^{-1}}\end{aligned} \tag{6.15}$$

$$\Delta g_{LiNa/FF} = -2307.47 + 0.4281T \quad \mathrm{J\cdot mol^{-1}} \tag{6.16}$$

$$\begin{aligned}\Delta g_{LiBe/FF} = &-8200.6 - 6.276T + (12552 - 17.154T)\,\chi_{BeLi}\\ &+ (18158.6 - 7.531T)\,\chi^2_{BeLi} + 1.674T\,\chi_{LiBe} \quad \mathrm{J\cdot mol^{-1}}\end{aligned} \tag{6.17}$$

$$\begin{aligned}\Delta g_{NaBe/FF} = &-29288 + (-10460 + 9.456T)\,\chi_{NaBe}\\ &+ (33472 - 29.832T)\,\chi^2_{BeNa} \quad \mathrm{J\cdot mol^{-1}}\end{aligned} \tag{6.18}$$

$$\Delta g_{LiU/FF} = -16108 + (-711.3 - 1.255T)\,\chi_{LiU} + (-1172 - 8.368T)\,\chi_{ULi} \quad \mathrm{J\cdot mol^{-1}} \tag{6.19}$$

$$\begin{aligned}\Delta g_{NaU/FF} = &-25104 + 4.184T + (-7615 - 4.184T)\,\chi_{NaU}\\ &+ (-14393 + 6.276T)\,\chi_{UNa} \quad \mathrm{J\cdot mol^{-1}}\end{aligned} \tag{6.20}$$

The strength of this model is to freely choose the composition of maximum short range ordering which makes it very useful for phase diagram optimization as at this composition the solution tends to have the lowest excess Gibbs energy. Such composition in a binary system is defined by the selection of cation-cation coordination numbers $Z^A_{AB/FF}$ and $Z^B_{AB/FF}$. $Z^A_{AB/FF}$ and $Z^B_{AB/FF}$ values that have been used for the assessment of BeF_2-ThF_4 and BeF_2-UF_4 binary systems are reported in Table 6.3 and because these coordination numbers correspond exactly to one composition they are composition independent.

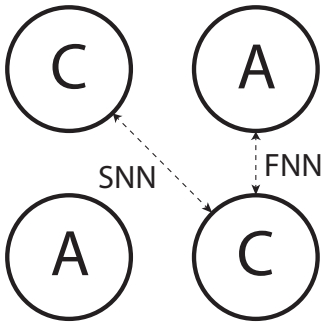

Figure 6.1: A schematic representation of FNN and SNN within the quadruplet approximation.

Table 6.3: Cation-Cation coordination numbers of the liquid solution.

A	B	Z^A_{AB}	Z^B_{AB}
Be^{2+}	Be^{2+}	4.8	4.8
Th^{4+}	Th^{4+}	6	6
U^{4+}	U^{4+}	6	6
Be^{2+}	Th^{4+}	3	6
Be^{2+}	U^{4+}	3	6

The electro-neutrality of the system is kept by the definition of the anion-anion coordination numbers which are calculated according to the following equation after the selection of the cation-cation coordination numbers.

$$\frac{q_A}{Z^A_{AB/FF}} + \frac{q_B}{Z^B_{AB/FF}} = \frac{q_F}{Z^F_{AB/FF}} + \frac{q_F}{Z^F_{AB/FF}} \tag{6.21}$$

The q_A, q_B and q_F terms in the above given formula are the absolute charges of various ions.

For the modelling of higher order systems Kohler and Toop extrapolations have been employed depending whether the system was treated as symmetric or asymmetric, respectively. Thus two groups of compounds are considered; the first one containing monovalent, highly ionic fluorides LiF and NaF, while the other group contained BeF_2, ThF_4 and UF_4 with cationic valencies higher than one. With such distinction better extrapolations were achieved compared to the symmetric approximation. Nevertheless, in some of the systems ternary excess Gibbs parameters had to be considered to optimize the invariant equilibria according to experimental data. The values for the ternary

parameters for given systems are listed below:

$$\Delta g_{UTh(Be)/FF} = 1256\ \mathrm{J\cdot mol^{-1}} \tag{6.22}$$

$$\Delta g_{BeNa(Th)/FF} = -6279\ \mathrm{J\cdot mol^{-1}} \tag{6.23}$$

$$\Delta g_{BeTh(Na)/FF} = -20930\ \mathrm{J\cdot mol^{-1}} \tag{6.24}$$

$$\Delta g_{LiBe(U)/FF} = 2093\ \mathrm{J\cdot mol^{-1}} \tag{6.25}$$

$$\Delta g_{BeNa(U)/FF} = -2093\ \mathrm{J\cdot mol^{-1}} \tag{6.26}$$

$$\Delta g_{BeU(Na)/FF} = -18836\ \mathrm{J\cdot mol^{-1}} \tag{6.27}$$

$$\Delta g_{BeTh(Li)/FF} = -10465\ \mathrm{J\cdot mol^{-1}} \tag{6.28}$$

6.3. RESULTS

In this section the optimized BeF_2-ThF_4 and BeF_2-UF_4 binary systems are described together with BeF_2 and actinide fluoride (ThF_4 and/or UF_4) containing ternary phase diagrams. These systems have been assessed based on available experimental data, as discussed throughout the next sections.

6.3.1. BeF_2-ThF_4 AND BeF_2-UF_4 PHASE DIAGRAMS

The BeF_2-ThF_4 phase diagram has been already thermodynamically assessed in the study by van der Meer *et al.* [8], but since a different thermodynamic model for the description of the liquid phase has been used in the present study, this system had to be re-assessed for compatibility with the rest of the database. BeF_2-ThF_4 is a simple eutectic system and the optimization was performed based on the experimental data by Thoma *et al.* [9] who used three different techniques to determine the solid-liquid equilibria. Their results, obtained by thermal analysis, thermal gradient quenching technique and by extrapolation from the NaF-BeF_2-ThF_4 system are superimposed with our calculated phase diagram in Figure 6.2 and a very good agreement is evident. The calculated eutectic point corresponds to T=799 K and X(ThF_4) = 0.021, which is nearly identical to the values experimentally determined (T_{exp} = 800±3 K, X_{exp}(ThF_4) = 0.02 [9]).

For the reasons explained in the previous paragraph, we have performed the optimization of the BeF_2-UF_4 system using the quasi-chemical model with quadruplet approximation for the description of the liquid phase. The thermodynamic assessment of the phase diagram has been based on the experimental data measured by Jones *et al.* [10], who used thermal analysis to obtain the solidus and liquidus equilibria. Similar to the BeF_2-ThF_4 system BeF_2-UF_4 is a simple eutectic system with experimentally determined eutectic at T_{exp} = 808±2 K and X_{exp}(ThF_4) = 0.005. The calculated phase diagram, shown in Figure 6.3, reveals eutectic at T=808 K and X(ThF_4) = 0.013 which is in very good agreement with the experiments.

Both binary phase diagrams are described as simple eutectic systems with the eutectic found in both cases at BeF_2 rich region. However, when comparing the two liquidus shapes, it is evident that in case of the BeF_2-UF_4 system the increase of the liquidus equilibrium is significantly steeper than in case of BeF_2-ThF_4. This also indicates that the

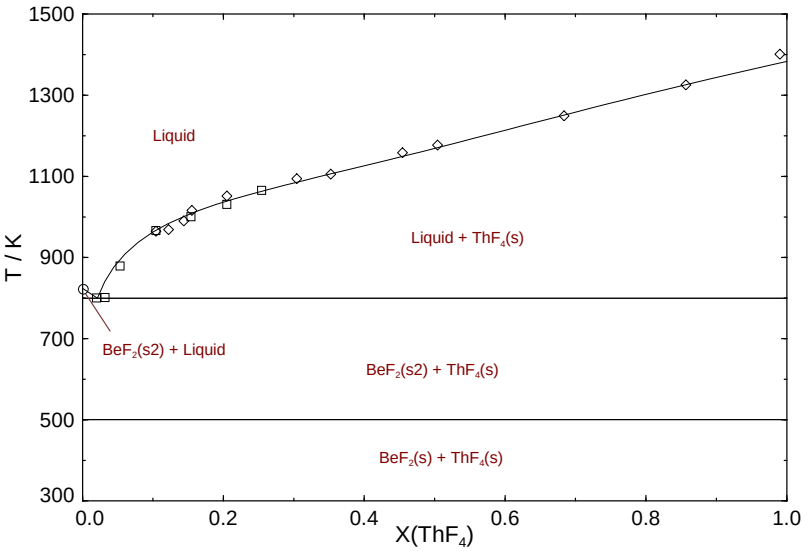

Figure 6.2: The BeF_2-ThF_4 phase diagram optimized in this study. The experimental data are taken from Thoma *et al.* [9]: ◇ - obtained by thermal analysis; ○ - obtained by thermal gradient quenching technique; □ - obtained by extrapolation from the NaF-BeF_2-ThF_4 system.

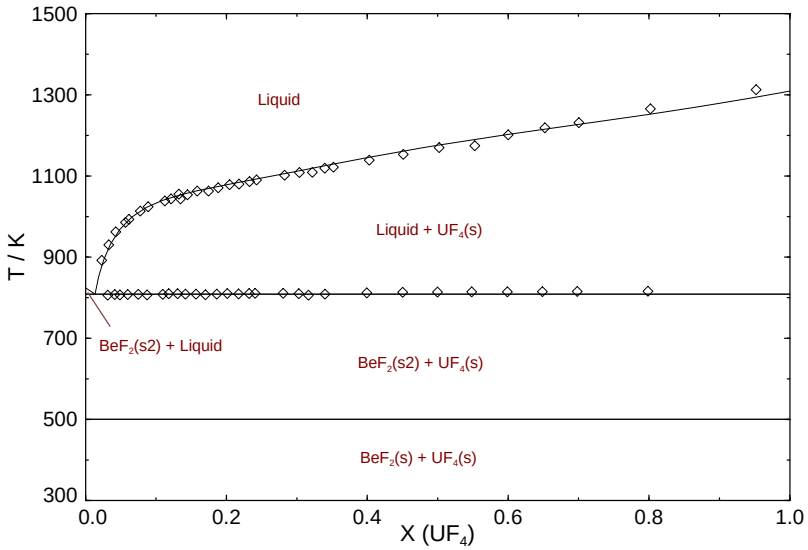

Figure 6.3: The BeF_2-UF_4 phase diagram optimized in this study. ◊ - Experimental data are taken from Jones *et al.* [10].

solubility of UF_4 in molten BeF_2 is somewhat lower than solubility of ThF_4. To interpret this observation we have compared the calculated entropy of mixing of (Be,Th)F_x and (Be,U)F_x liquid solutions and as shown in Figure 6.4 the entropy values of the former solution are much higher than in the case of (Be,U)F_x. One of the explanations could be due to the short range ordering which is reflected by configurational entropy which decreases with increasing degree of system ordering.

6.3.2. LiF-BeF_2-ThF_4 PHASE DIAGRAM

The optimization of the LiF-BeF_2-ThF_4 system has been based on the equilibrium data measured by Thoma *et al.* [9] The calculated liquidus projection of the LiF-BeF_2-ThF_4 system is shown in Figure 6.5 indicating six invariant equilibria and one saddle point. All calculated equilibria are reported in Table 6.4 and are in a good agreement with the experiment. The lowest eutectic has been determined at T=632.2 K and the LiF-BeF_2-ThF_4 (47.5-50.7-1.8) composition. A ternary solid solution of limited solubility found in the region of the Li_3ThF_7 compound [6] was considered during the assessment of the ternary system. It forms the primary crystallization phase indicated by the 'E'-region in Figure 6.5. Furthermore, a miscibility gap originating from the LiF-BeF_2 system extends into ternary field with the maximal extend indicated by the 'I'-region in the figure.

The calculated phase diagram is in fair agreement with the one assessed by van der Meer *et al.* [8] using a classical polynomial formalism for the description of the excess Gibbs parameters of the liquid phase. Only a slight discrepancy is found on the groove separating the ThF_4 and $LiTh_4F_{17}$ primary crystallization fields which is in the case of the work of van der Meer *et al.* somewhat more shifted towards the BeF_2 corner.

6.3.3. LiF-BeF_2-UF_4 PHASE DIAGRAM

The assessment of the LiF-BeF_2-UF_4 ternary system was based on experimentally determined equilibrium points reported by Jones *et al.* [10] and Weaver *et al.* [11] and considering the vapour pressure data measured by Smith *et al.* [12]. As confirmed by Jones *et al.* [10] and Thoma [13] no ternary compounds are found within the LiF-BeF_2-UF_4 system and no ternary solid solutions has been reported as well. The liquidus projection of

Table 6.4: Invariant equilibria and saddle points found in the LiF-BeF_2-ThF_4 system.

x_{LiF}	x_{BeF_2}	x_{ThF_4}	T / K	Type of equilibria	Crystal phases in equilibrium
0.690	0.089	0.221	838.3	Quasi-Peritectic	$LiTh_2F_9$, Li_3ThF_7 *s.s.*, $LiThF_5$
0.080	0.887	0.033	754.8	Quasi-Peritectic	ThF_4, β-BeF_2, $LiTh_4F_{17}$
0.674	0.295	0.031	719.3	Eutectic	LiF, Li_2BeF_4, Li_3ThF_7 *s.s.*
0.555	0.420	0.025	679.0	Quasi-Peritectic	Li_2BeF_4, $LiTh_2F_9$, Li_3ThF_7 *s.s.*
0.456	0.522	0.022	650.6	Quasi-Peritectic	β-BeF_2, $LiTh_2F_9$, $LiTh_4F_{17}$
0.667	0.303	0.030	719.6	Saddle point	Li_3ThF_7 *s.s.*, Li_2BeF_4
0.475	0.507	0.018	632.2	Eutectic	β-BeF_2, Li_2BeF_4, $LiTh_2F_9$

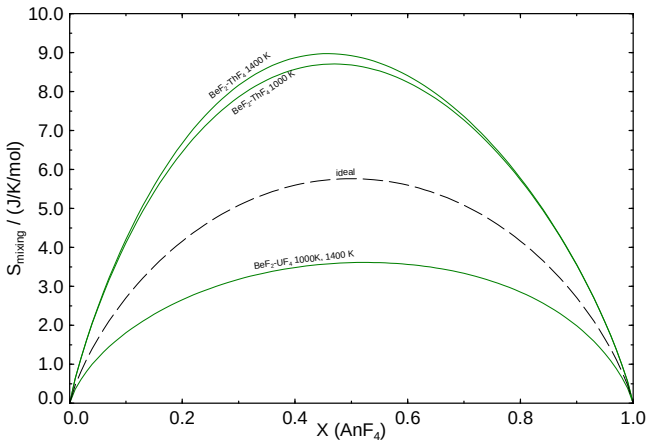

Figure 6.4: The calculated entropy of mixing for BeF_2-AnF_4 systems, where An = Th, U for selected temperatures T =1000 K and 1400 K. The dashed line represents an ideal configurational entropy.

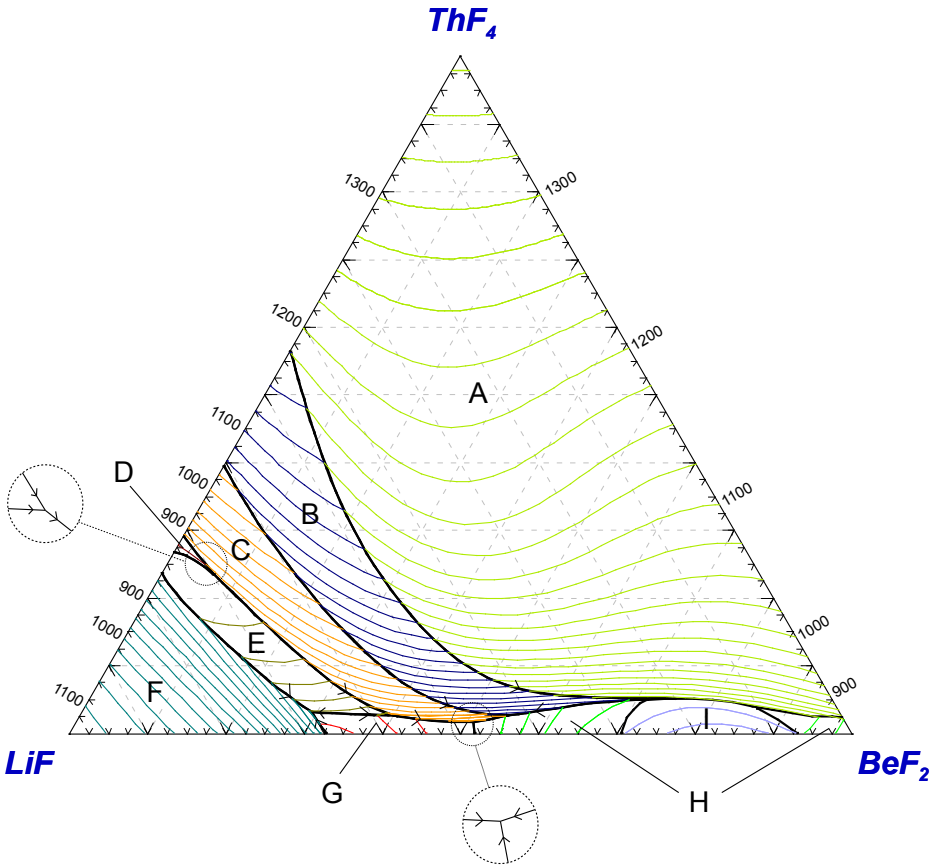

Figure 6.5: The liquidus projection of the assessed LiF-BeF_2-ThF_4 system. Primary crystallization fields: A - ThF_4; B - $LiTh_4F_{17}$; C - $LiTh_2F_9$; D - $LiThF_5$; E - Li_3ThF_7 *s.s.*; F - LiF; G - Li_2BeF_4; H - β-BeF_2; I - Liquid (miscibility gap).

the assessed phase diagram calculated in this study is given in Figure 6.6 indicating five invariant equilibria (2 eutectics and 3 quasi-peritectics) and one saddle point. These points agree very well with the experimentally determined phase diagram [11] (maximum discrepancy 10 K) and their exact calculated compositions, temperatures and solid phases in equilibrium are reported in Table 6.5. The calculated phase diagram agrees well with the previously assessed LiF-BeF_2-UF_4 phase diagram published by van der Meer *et al.* [8].

Furthermore, we have compared the apparent partial vapour pressures of LiF, BeF_2 and UF_4 gaseous species determined from our thermodynamic assessment with experimentally determined data measured by Smith *et al.* [12]. The comparison indicates good agreement for all three measured compositions. An example is given in Figure 6.7 showing a comparison between our calculation (line) with the experimental data (symbols) for the LiF-BeF_2-UF_4 (86.4-9.6-4.0 at%) composition. Note that the calculated vapour pressure for a given species shown in the presented figures is equal to the total vapour pressure of all vapour species bearing the same cation. E.g. the vapour pressure of LiF is determined as the equivalent sum of one unit of LiF(g), two units of Li_2F_2(g), three units of Li_3F_3(g) and one unit of $LiBeF_3$(g) species. This was necessary to do in order to make a correct comparison with the experimentally observed vapour pressures which were not determined directly in the gas phase, but from the deposits of the evaporated material.

6.3.4. NAF-BEF_2-THF_4 PHASE DIAGRAM

The optimization of the NaF-BeF_2-ThF_4 phase diagram was based on the experimental data by Thoma *et al.* [14] and the X-ray diffraction studies performed by Brunton [15] who established a correct stoichiometry of the $Na_3BeTh_{10}F_{45}$ ternary compound based on the single crystal data. The liquidus projection of the assessed NaF-BeF_2-ThF_4 phase diagram is given in Figure 6.8 with indicated primary crystallization fields. It consists of 16 invariant equilibria with the lowest calculated eutectic at 613 K and the NaF-BeF_2-ThF_4 (40.3-58.0-1.7) composition. All invariant equilibria, their temperatures and compositions, and corresponding phases in equilibrium are reported in Table 6.6. Two saddle points are found in the ternary phase diagram and their description is given in the table as well. The stability limit of the $Na_3BeTh_{10}F_{45}$ ternary compound was found at 1059 K, at which it decomposes to the (Na,Th)F_x solid solution (rich on ThF_4) and the

Table 6.5: Invariant equilibria and saddle points found in the LiF-BeF_2-UF_4 system.

x_{LiF}	x_{BeF_2}	x_{UF_4}	T / K	Type of equilibria	Crystal phases in equilibrium
0.0193	0.0294	0.9513	781.3	Quasi-Peritectic	BeF_2, U_4LiF_{17}, UF_4
0.2255	0.7281	0.0464	742.9	Quasi-Peritectic	LiF, $U_6Li_7F_{31}$, ULi_4F_8
0.0835	0.6868	0.2298	708.1	Eutectic	LiF, $U_6Li_7F_{31}$, Li_2BeF_4
0.0161	0.5311	0.4529	663.7	Quasi-Peritectic	U_4LiF_{17}, $U_6Li_7F_{31}$, Li_2BeF_4
0.0112	0.479	0.5099	633.9	Eutectic	BeF_2, U_4LiF_{17}, Li_2BeF_4
0.0499	0.6527	0.2974	713.4	Saddle point	$U_6Li_7F_{31}$, Li_2BeF_4

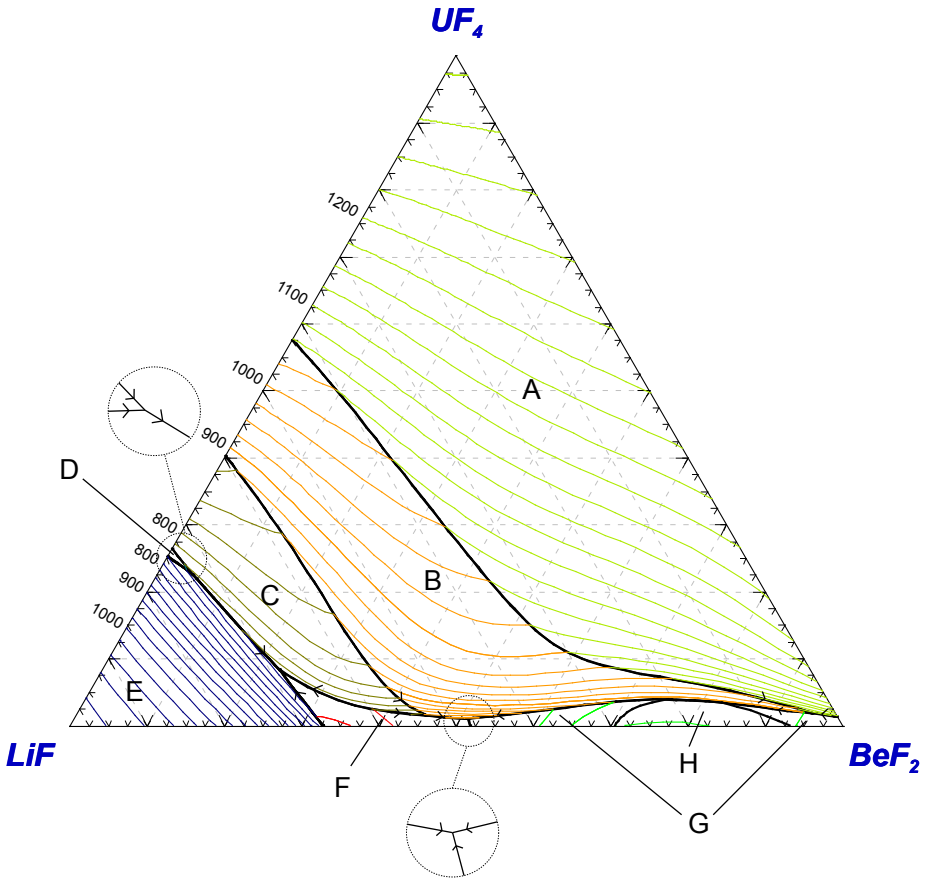

Figure 6.6: The liquidus projection of the assessed LiF-BeF_2-UF_4 system. Primary crystallization fields: A - UF_4; B - LiU_4F_{17}; C - $Li_7U_6F_{31}$; D - Li_4UF_8; E - LiF; F - Li_2BeF_4; G - β-BeF_2; H - Liquid (miscibility gap).

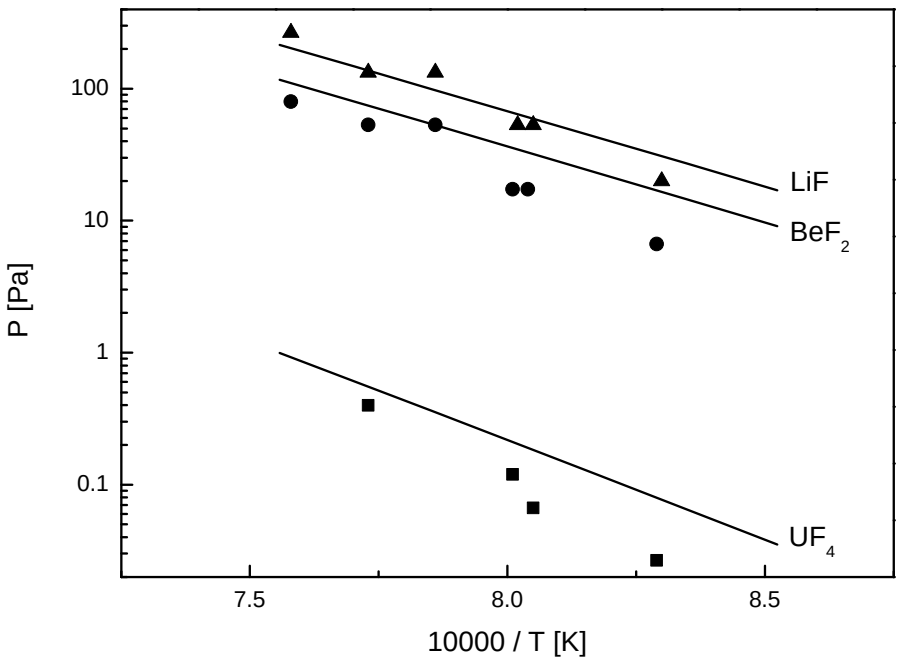

Figure 6.7: Apparent partial vapour pressure above the LiF-BeF_2-UF_4 (86.4-9.6-4.0 at%) melt.
Symbols represent experimental data determined by Smith *et al.* [12]: ▲ - apparent pressure of LiF; • - apparent pressure of BeF_2; ■ - apparent pressure of UF_4. Lines represent the calculation based on the thermodynamic assessment.

liquid. A miscibility gap found in the NaF-BeF_2 binary system extends into ternary field in the BeF_2-rich region and its maximal range is highlighted by N-region in Figure 6.8.

Table 6.6: Invariant equilibria and saddle points found in the NaF-BeF_2-ThF_4 system.

x_{ThF_4}	x_{NaF}	x_{BeF_2}	T / K	Type of equilibria	Crystal phases in equilibrium
0.272	0.4979	0.2301	1011.97	Peritectic	$Th_{10}Na_3BeF_{45}$, Th_2NaF_9, ThF_4
0.3785	0.6055	0.016	954.68	Quasi-Peritectic	$Th_2Na_3F_{11}$,$Th_6Na_7F_{31}$,$ThNa_2F_6$
0.2362	0.6042	0.1596	892.79	Peritectic	$Th_6Na_7F_{31}$, Th_2NaF_9, $ThNaF_5$
0.2237	0.7677	0.0086	884.27	Peritectic	$Th_2Na_7F_{15}$, $ThNa_2F_6$, $ThNa_4F_8$
0.2261	0.6151	0.1588	883.2	Quasi-Peritectic	$Th_6Na_7F_{31}$, $ThNa_2F_6$, $ThNaF_5$
0.2179	0.7694	0.0127	882.98	Quasi-Peritectic	$Th_2Na_7F_{15}$, NaF, $ThNa_4F_8$
0.1577	0.7493	0.093	829.22	Quasi-Peritectic	$Th_2Na_7F_{15}$, NaF, $ThNa_2F_6$
0.0866	0.6137	0.2997	750.31	Quasi-Peritectic	$ThNa_2F_6$, $ThNaF_5$, Na_2BeF_4
0.1035	0.7195	0.177	741.87	Eutectic	$ThNa_2F_6$, NaF, Na_2BeF_4
0.0705	0.5988	0.3307	737.34	Quasi-Peritectic	Na_2BeF_4, $NaThF_5$, Th_2NaF_9
0.0603	0.5928	0.3469	730.76	Quasi-Peritectic	Na_2BeF_4, $Th_{10}Na_3BeF_{45}$, Th_2NaF_9
0.0303	0.3518	0.618	674.52	Quasi-Peritectic	BeF_2, $Th_{10}Na_3BeF_{45}$, ThF_4
0.0171	0.4132	0.5697	618	Quasi-Peritectic	β-$NaBeF_3$, α-$NaBeF_3$, $Th_{10}Na_3BeF_{45}$
0.0079	0.5524	0.4398	618	Quasi-Peritectic	β-$NaBeF_3$, α-$NaBeF_3$, $Th_{10}Na_3BeF_{45}$
0.0076	0.5553	0.4371	615.01	Eutectic	Na_2BeF_4, $Th_{10}Na_3BeF_{45}$, α-$NaBeF_3$
0.0172	0.4026	0.5803	612.96	Eutectic	BeF_2, $Th_{10}Na_3BeF_{45}$, α-$NaBeF_3$
0.0916	0.6668	0.2416	785	Saddle point	Na_2ThF_6, Na_2BeF_4
0.013	0.4955	0.4915	644.5	Saddle point	β-$NaBeF_3$, $Na_3BeTh_{10}F_{45}$

6.3.5. NaF-BeF_2-UF_4 PHASE DIAGRAM

The assessment of the NaF-BeF_2-UF_4 system has been based on the experimental data published by Eichelberger *et al.* [16] who used thermal analysis, polarized light microscopy and high temperature X-ray diffraction with X-ray diffraction studies of the quenched samples. No ternary compounds and ternary solid solutions were observed in the system. The assessed phase diagram is given in Figure 6.9 indicating 15 invariant equilibria and 3 saddle points. The exact compositions and temperatures of each of the equilibria are given in Table 6.6 and generally a good agreement between our calculation and the data by Eichelberger *et al.* [16] has been achieved. The lowest eutectic found in the system was determined at 613 K and the NaF-BeF_2-UF_4 (55.3-43.1-1.6) composition which is in excellent agreement with the measured value of 612 K and NaF-BeF_2-UF_4 (56-43.5-1.5). Slight discrepancies between the phase diagram published by Eichelberger *et al.* [16] and our assessment is related to the primary crystallization fields of the NaU_2F_9 and NaU_4F_{17} compounds (region B and J, respectively, in Figure 6.9) which are in the case of our assessment slightly shifted towards the NaF corner, whereas the phase diagram suggested by Eichelberger *et al.* indicates larger extension towards the BeF_2 side.

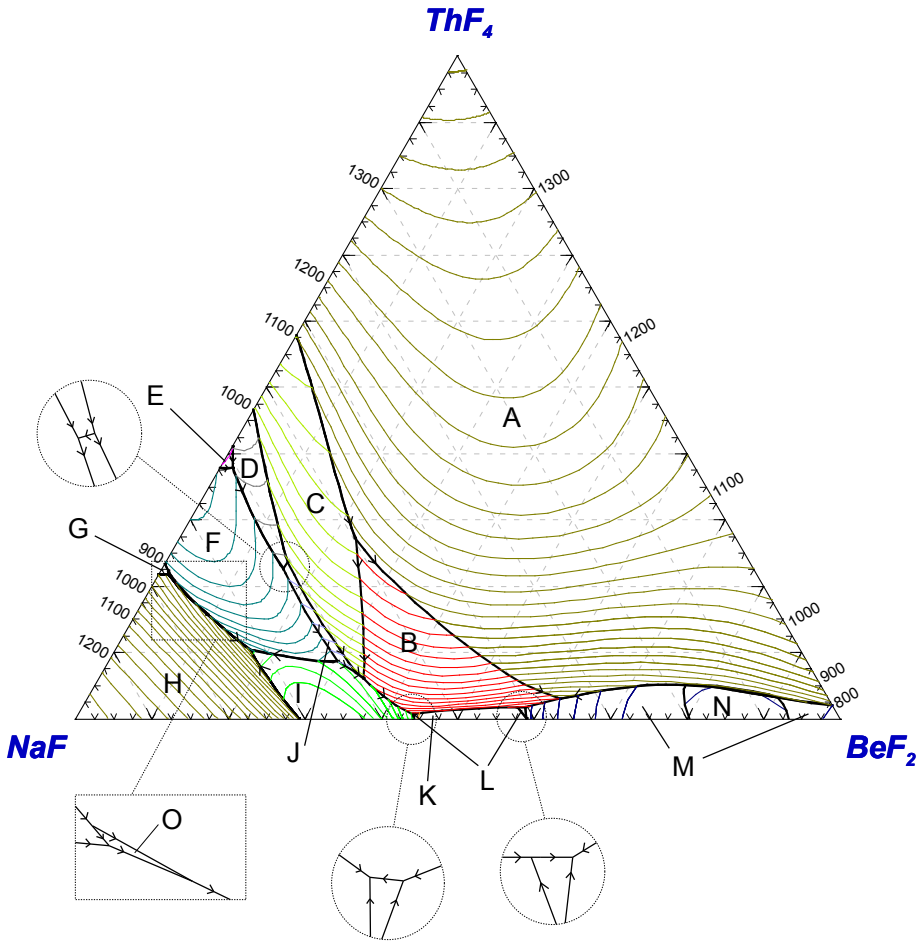

Figure 6.8: The liquidus projection of the assessed NaF-BeF_2-ThF_4 system. Primary crystallization fields: A - (Na,Th)F_4; B - $Na_3BeTh_{10}F_{45}$; C - $NaTh_2F_9$; D - $Na_7Th_6F_{31}$; E - $Na_3Th_2F_{11}$; F - Na_2ThF_6; G - Na_4ThF_8; H - NaF; I - Na_2BeF_4; J - $NaThF_5$; K - β-$NaBeF_3$; L - α-$NaBeF_3$; M - β-BeF_2; N - Liquid (miscibility gap); O - $Na_7Th_2F_{15}$.

This may be due to the fact that a miscibility gap in the NaF-BeF_2 system has been considered in the case of our assessment and this region of immiscibility slightly extends into ternary field, as indicated by the region N in Figure 6.9. However, an important fact is that the liquidus surface is very well reproduced in the whole range of the ternary system which is most important when studying the melting behaviour of the molten salt reactor fuel.

6.3.6. BeF_2-ThF_4-UF_4 PHASE DIAGRAM

The liquidus projection of the optimized BeF_2-ThF_4-UF_4 phase diagram is shown in Figure 6.10 and from the point of view of crystallization phase fields it is the simplest one from all ternary phase diagrams presented in this study. It has no invariant equilibria with the lowest melting point corresponding to the eutectic in the BeF_2-ThF_4 binary system at 799 K. The calculated phase diagram is in agreement with the phase diagram presented by Weaver *et al.* [17].

6.4. BeF_2 EFFECT ON MELTING TEMPERATURE OF THE MSR FUEL

One of the most important applications of the developed thermodynamic database is the possibility to evaluate the performance of several salt mixtures predicting the physicochemical properties and thus to optimize the fuel composition. After closing the ^{232}Th/^{233}U fuel cycle, the MSFR fuel mainly contains fertile ThF_4 and fissile UF_4 dissolved in a single component solvent (^{7}LiF). The proposed total concentration of ThF_4 and UF_4 has been set to 22.5 mol%, in agreement with the eutectic point in the binary system LiF-ThF_4. As reported by Merle-Lucotte *et al.* [18], the fraction of $^{233}UF_4$ must range between 2.4 mol% and 2.7 mol% in order to have a critical reactor with positive breeding ratio. Therefore, an average value of 2.55 mol% of UF_4 has been considered in this work as target boundary reference value for the fuel optimization, leading to LiF-ThF_4-UF_4 (77.5-19.95-2.55) composition. This composition is shown by a solid line in Figure 6.11, representing the pseudo-binary LiF-ThF_4 system with a concentration of UF_4 at 2.55 mol% calculated based on the developed thermodynamic database. The corresponding calculated liquidus temperature is T=850 K. According to this phase diagram, which is generally in a good agreement with the previously published one [2], the lowest melting temperature (T=830 K) corresponds to the LiF-ThF_4-UF_4 (76.2-21.3-2.55) composition (highlighted as dashed line in the Figure). It is thus only slightly shifted from the initial composition and can be considered as recommended fuel option for a concept containing only the three cations mentioned above. The pseudo-binary phase diagram has been calculated also for the UF_4 composition limits (2.4 mol% and 2.7 mol%) and no significant differences have been found.

Addition of further components in the fuel mixture allows to optimize the physicochemical properties of the fuel and to reduce the melting temperature. In case of reactors operating with thermal neutron spectrum, the choice is limited to atoms with a very low capture cross section, such Be and ^{7}Li, to guarantee a good breeding capacity of the

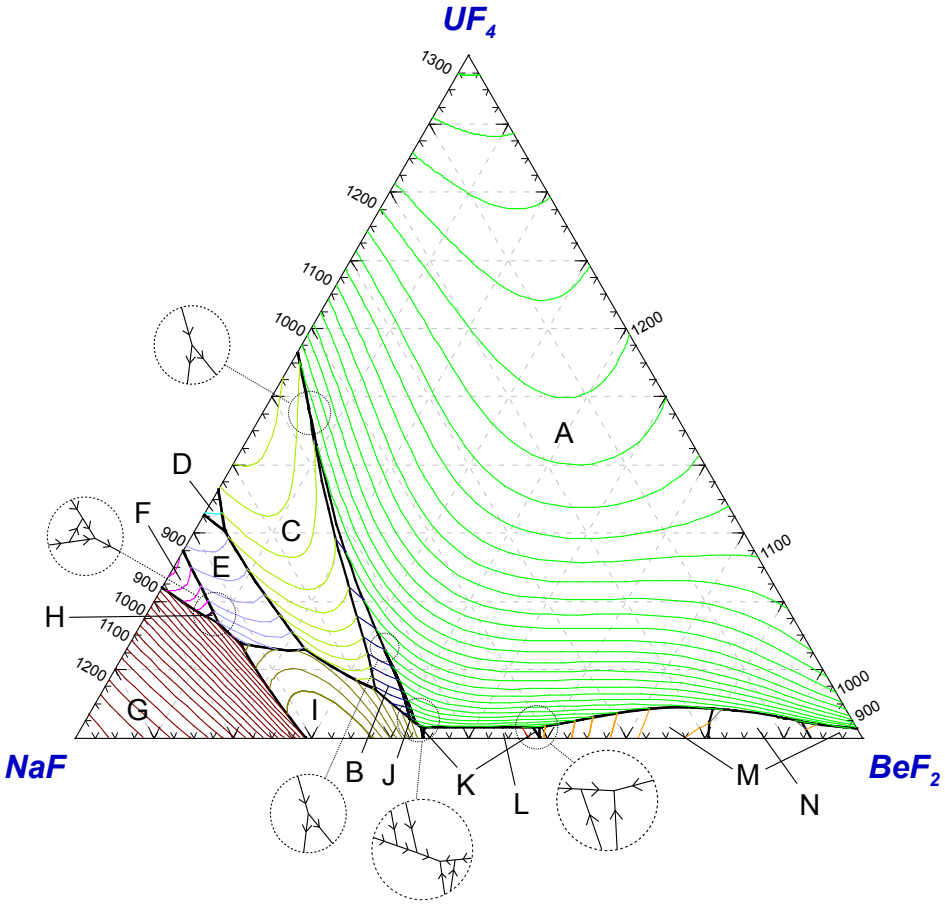

Figure 6.9: The liquidus projection of the assessed NaF-BeF_2-UF_4 system. Primary crystallization fields: A - UF_4; B - U_2NaF_9; C - $Na_7U_6F_{31}$; D - $Na_5U_3F_{17}$; E - Na_2UF_6; F - α-Na_3UF_7; G - NaF; H - β-Na_3UF_7; I - Na_2BeF_4; J - NaU_4F_{17}; K - β-$NaBeF_3$; L - α-$NaBeF_3$; M - β-BeF_2; N - Liquid (miscibility gap).

Table 6.7: Invariant equilibria and saddle points found in the NaF-BeF_2-UF_4 system.

x_{UF_4}	x_{NaF}	x_{BeF_2}	T / K	Type of equilibria	Crystal phases in equilibrium
0.4833	0.4620	0.0547	933.07	Peritectic	NaU_2F_9, UF_4, $Na_7U_6F_{31}$
0.3032	0.6587	0.0381	903.86	Quasi-peritectic	$Na_5U_3F_{17}$, $Na_7U_6F_{31}$, Na_2UF_6
0.1274	0.5426	0.3301	823.05	Peritectic	NaU_2F_9, UF_4, NaU_4F_{17}
0.1853	0.7326	0.0821	801.00	Quasi-peritectic	α-Na_3UF_7, β-Na_3UF_7, Na_2UF_6
0.1778	0.7453	0.0769	801.00	Peritectic	α-Na_3UF_7, β-Na_3UF_7, NaF
0.1285	0.6666	0.2049	777.30	Saddle point	Na_2UF_6, Na_2BeF_4
0.1188	0.6335	0.2477	771.82	Saddle point	Na_2BeF_4, $Na_7U_6F_{31}$
0.1296	0.6430	0.2274	769.25	Eutectic	Na_2UF_6, $Na_7U_6F_{31}$, Na_2BeF_4
0.1680	0.7348	0.0972	768.78	Quasi-peritectic	Na_2UF_6, β-Na_3UF_7, NaF
0.1389	0.7209	0.1402	736.46	Eutectic	Na_2UF_6, NaF, Na_2BeF_4
0.0716	0.5830	0.3454	719.51	Quasi-peritectic	NaU_2F_9, $Na_7U_6F_{31}$, Na_2BeF_4
0.0283	0.5608	0.4109	651.35	Quasi-peritectic	NaU_2F_9, NaU_4F_{17}, Na_2BeF_4
0.0162	0.4922	0.4916	645.07	Saddle point	UF_4,$NaBeF_3$
0.0224	0.5572	0.4204	634.08	Quasi-peritectic	UF_4, NaU_4F_{17}, Na_2BeF_4
0.0161	0.5483	0.4356	618.03	Quasi-peritectic	UF_4, β-$NaBeF_3$, α-$NaBeF_3$
0.0156	0.4106	0.5738	618.00	Quasi-peritectic	UF_4, β-$NaBeF_3$, α-$NaBeF_3$
0.0155	0.4019	0.5826	614.02	Eutectic	UF_4, β-$NaBeF_3$, BeF_2
0.0163	0.5532	0.4305	612.69	Eutectic	UF_4, β-$NaBeF_3$, Na_2BeF_4

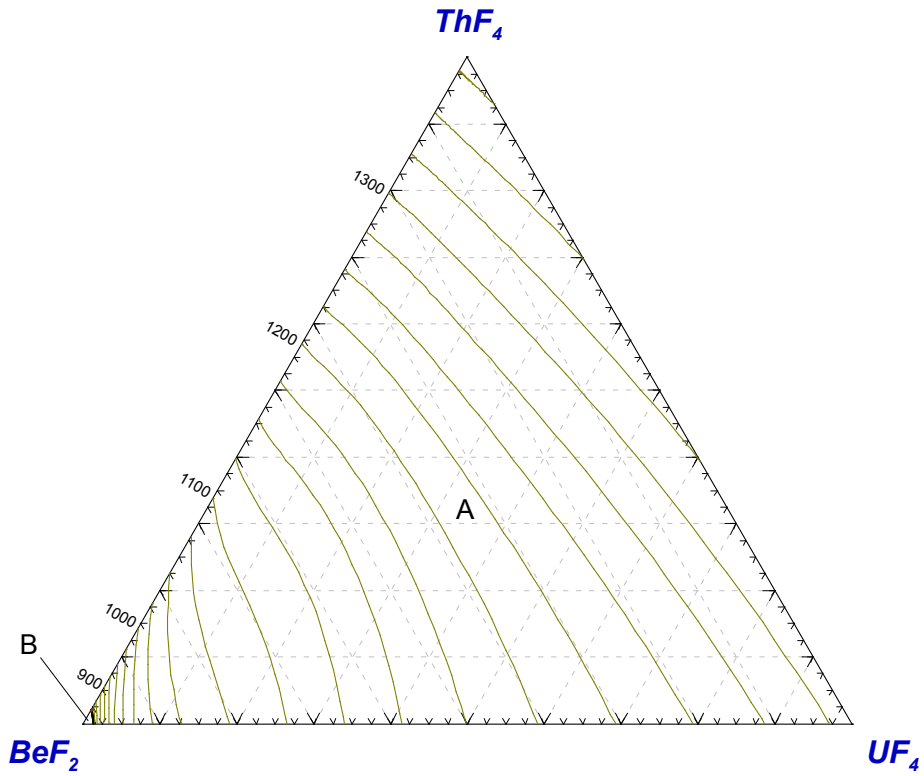

Figure 6.10: The liquidus projection of the calculated BeF_2-ThF_4-UF_4 system. Primary crystallization fields: A - $(Th,U)F_4$; B - β-BeF_2.

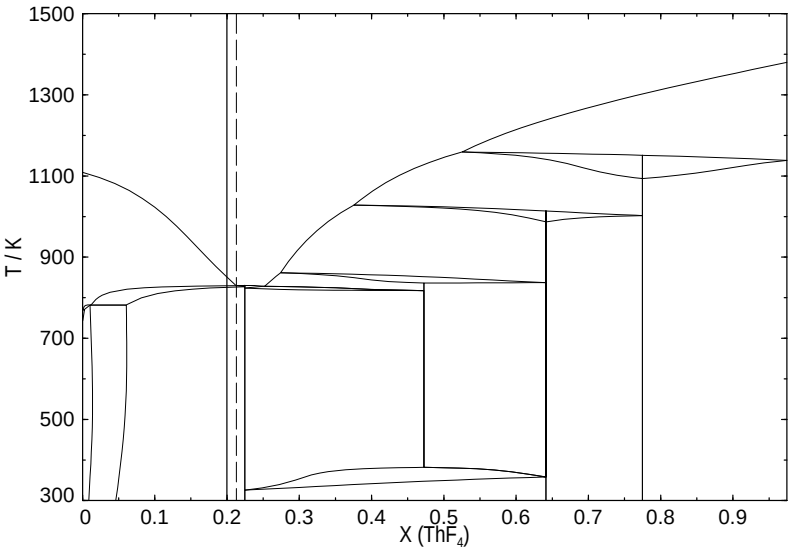

Figure 6.11: The calculated LiF-ThF_4 pseudo-binary phase diagram with fixed concentration of UF_4 set to 2.55 mol%. The solid line represents the initial MSFR composition and the dashed line the optimized composition.

reactor. For this reason the influence of BeF_2 on the melting behaviour of the fuel has been investigated in this work. However, it must be considered that the presence of BeF_2 implies different problems due to its high chemical toxicity and it may complicate the reprocessing chemistry. Furthermore, high concentration of BeF_2 also increases viscosity of the salt.

In the first step the concentrations of ThF_4 and UF_4 have been fixed to the values of 19.95 and 2.55 mol% respectively, as defined in the MSFR concept [18]. With such concentrations of ThF_4 and UF_4, the calculated LiF-BeF_2 pseudo-binary phase diagram (Figure 6.12) indicates the lowest melting temperature at T=825 K and the LiF-BeF_2-ThF_4-UF_4 (75.7-1.8-19.95-2.55) composition. Comparing this melting temperature with the one obtained without BeF_2, a reduction of only 5 K is observed, which is a small decrease to justify the addition of a new component.

In the second step we considered a variable concentration of ThF_4. The melting behaviour of such mixture is described by the pseudo-ternary phase diagram given in Figure 6.13. It shows that for a significant decrease of the melting temperature, the concentration of BeF_2 must be increased and the concentration of ThF_4 reduced.

Since the MSFR concept is a non-moderated reactor with not so tight neutron economy, atoms with higher capture cross section may also be interesting as possible solvent additive. One of the discussed candidates to reduce the melting point is NaF and the influence on the melting behaviour of the salt when adding NaF has been already studied in our previous article [2]. The recommended composition found has been revised considering the new LiF-ThF_4 assessment and the lowest melting temperature was found at T=770 K for the composition LiF-NaF-ThF_4-UF_4 (47.3-25.9-24.3-2.55). We note here that as in case of BeF_2, the introduction of NaF can give rise to some issues during the salt reprocessing, but this is still subject of further research. As well neutronic calculations must confirm if such concentration of NaF will still permit positive breeding gain.

The subsequent step is to study the behaviour of the fuel in the presence of the five components described in this work (LiF, NaF, BeF_2, ThF_4, UF_4). Constraining the concentration of ThF_4 and UF_4 to 19.95 mol% and 2.55 mol% respectively, the LiF-NaF-BeF_2 pseudo-ternary phase diagram has been calculated and the liquidus projection is given in Figure 6.14. The calculated phase diagram consist of thirteen invariant equilibria and the lowest eutectic has been found at T=753 K. The composition corresponding to this eutectic is LiF-NaF-BeF_2-ThF_4-UF_4 (41.8-31.1-4.6-19.95-2.55) and since it meets the concentration criteria of ThF_4 and UF_4 while having low concentration of BeF_2, it can be considered as alternative fuel composition.

Furthermore, it has been observed that a lower melting temperature can be achieved by decreasing the quantity of ThF_4 in the salt as highlighted in Figure 6.15, in which the lowest eutectic temperature is plotted as a function of the ThF_4 concentration. The concentration of UF_4 is kept constant (2.55 mol%) and the composition related to the pseudo-ternary eutectic is given in Figure 6.15 as well. It has been observed that the concentration of BeF_2 required to reach to lowest melting temperature rises while the one of ThF_4 decreases.To give an overview, a ThF_4 concentration decrease from 20 mol%

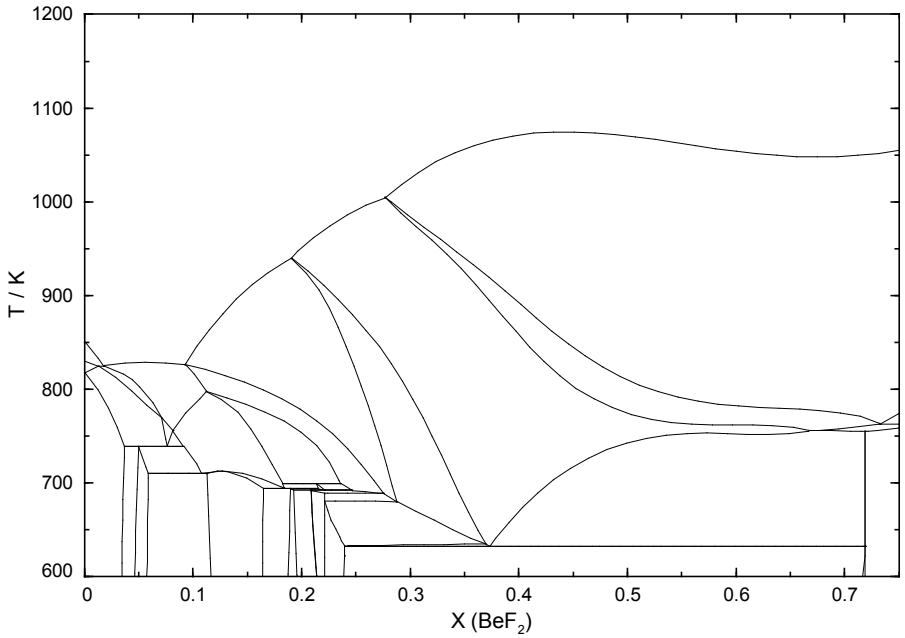

Figure 6.12: The calculated LiF-BeF_2 pseudo-bynary phase diagram with fixed concentration of UF_4 and ThF_4 set to 2.55 mol% and 19.95 mol% respectively.

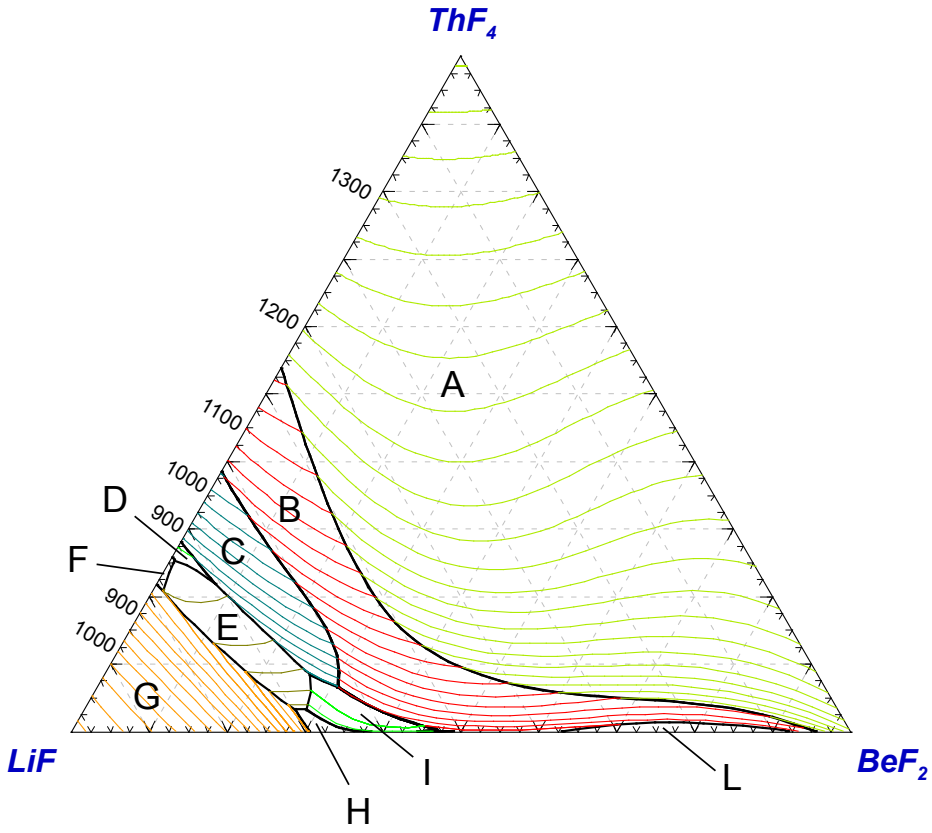

Figure 6.13: The calculated LiF-BeF_2-ThF_4 pseudo-ternary phase diagram with fixed concentration of UF_4 set to 2.55 mol%. Primary phase fields: A - (U,Th)F_4 (s.s.); B - Li(U,Th)$_4F_{17}$ (s.s.); C - Li(U,Th)$_2F_9$ (s.s.); D - Li$_7$(U,Th)$_6F_{31}$ (s.s.); E - (Li,Th, Be) F_x (s.s.); F - Li$_3$(U,Th)F_7 (s.s.); G - LiF; H - Li_2BeF_4; I - Li$_7$(U,Th)$_6F_{31}$ (s.s.) L - BeF_2.

to 10 mol% leads to a temperature drop of almost 70 K and at the same time the BeF_2 concentration increases from 5 mol% to 18 mol% .

6.5. CONCLUSIONS

In this work the thermodynamic description of the LiF-NaF-BeF_2-ThF_4-UF_4 system has been performed. Using the obtained thermodynamic database, the influence of the BeF_2 component in the candidate salts for the MSFR concept was studied. The optimization of the fuel has been performed with respect to its melting point identifying four different possible fuel compositions.

The calculations performed in this study have shown that the addition of BeF_2 to the molten salt fuel can lower the final melting temperature. However the reduction observed is rather low, 5 K for the NaF-free composition and 17 K for NaF-containing salt. The effect on the melting point may be more significant for compositions with lower content of ThF_4, which were not in the purpose of this work. In summary, taking into consideration the issues related to the presence of BeF_2 in the salt, addition of BeF_2 to the salt does not seem to be very profitable under the criteria previously defined.

The compositions which fullfill the set composition criteria are reported in Table 6.8 and some important properties (melting point, boiling point and vapour pressure) for those salts have been calculated. All the compositions selected exhibit good properties in terms of reactor safety. In fact the calculated boiling points are close to 2000 K and the vapour pressures are very low at operating temperature of MSR, which is believed to be 50 K higher than the melting point, as indicated in the Table.

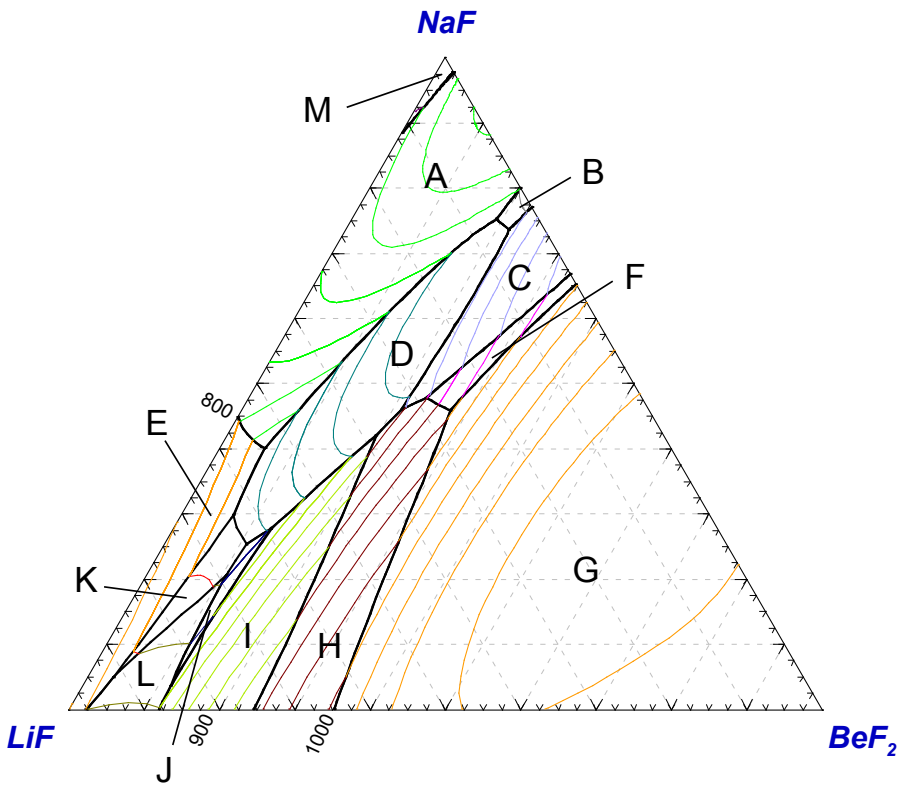

Figure 6.14: The calculated LiF-BeF_2-NaF pseudo-ternary phase diagram with fixed concentration of UF_4 and ThF_4 set to 2.55 mol% and 19.95 mol% respectively. Primary phase fields: A - $Na_2(U,Th)F_6$ (s.s.); B - $Na_7(U,Th)_6F_{31}$ (s.s.); C - $Na(U,Th)_2F_9$ (s.s.); D - $(Li,Na)_7Th_6F_{31}$ (s.s.); E - (Li,Na)F (s.s.); F - $Th_{10}Na_3BeF_{45}$; G - $(U,Th)F_4$ (s.s.); H - $Li(U,Th)_4F_{17}$ (s.s.); I - $Li(U,Th)_2F_9$ (s.s.); J - $Li_7(U,Th)_6F_{31}$ (s.s.); K - $Li_3(U,Th)F_7$ (s.s.); L - $(Li,Be,Th)F_x$; M - NaF.

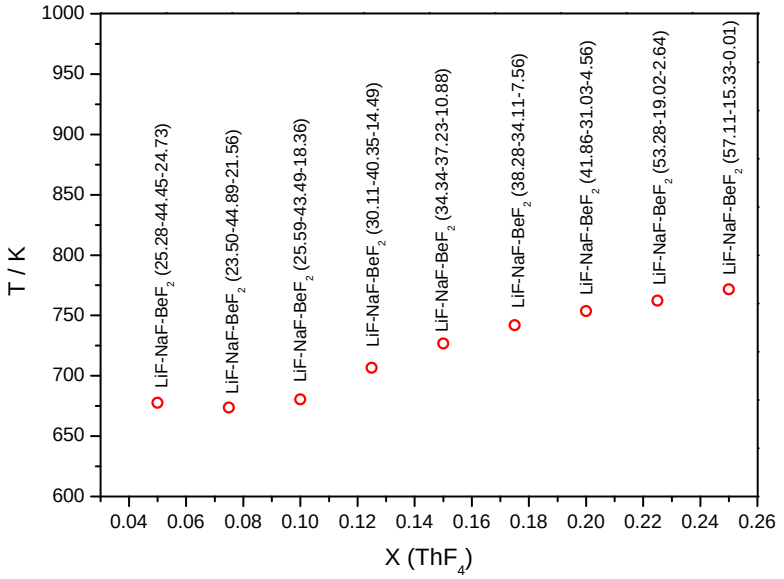

Figure 6.15: The calculated lowest eutectic temperature for the LiF-NaF-BeF_2 pseudo-ternary phase diagram with fixed concentration of UF_4 and ThF_4 plotted as a function of ThF_4 content. The composition of the solvent at the eutectic point is given for each point.

Table 6.8: The proposed fuel compositions and related fuel properties.

Composition	T melting	T boiling	log P(Pa)	P at T^*_{oper}
LiF-ThF_4-UF_4 (76.2-21.3-2.55)	829.6 K	2021.5 K	11.486-12719/(T/K)	$1.08{\cdot}10^{-3}$ Pa
LiF-BeF_2-ThF_4-UF_4 (75.7-1.8-19.95-2.55)	825.0 K	1991.2 K	10.895-11576/(T/K)	$4.67{\cdot}10^{-3}$ Pa
LiF-NaF-ThF_4-UF_4 (47.3-25.9-24.3-2.55)	770.4 K	2038.2 K	11.215-12578/(T/K)	$7.27{\cdot}10^{-5}$ Pa
LiF-NaF-BeF_2-ThF_4-UF_4 (41.8-31.1-4.6-19.95-2.55)	753.4 K	1978.5 K	11.806-12891/(T/K)	$4.08{\cdot}10^{-5}$ Pa

*T_{oper} is the operation temperature defined as 50 K higher than the melting point.

REFERENCES

[1] E. Capelli, O. Beneš, and R. J. M. Konings, *Thermodynamic assessment of the LiF-NaF-BeF_2-ThF_4-UF_4 system,* J. Nucl. Mater. **449**, 111 (2014).

[2] O. Beneš, M. Beilmann, and R. J. M. Konings, *Thermodynamic assessment of the LiF–NaF–ThF_4–UF_4 system,* J. Nucl. Mater. **405**, 186 (2010).

[3] S. Delpech, E. Merle-Lucotte, D. Heuer, M. Allibert, V. Ghetta, C. Le-Brun, X. Doligez, and G. Picard, *Reactor physics and reprocessing scheme for innovative molten salt reactor system,* J. Fluor. Chem. **130**, 11 (2009).

[4] O. Beneš and R. J. M. Konings, *Thermodynamic evaluation of the (LiF + NaF + BeF_2 + PuF_3) system: An actinide burner fuel,* J. Chem. Thermodyn. **41**, 1086 (2009).

[5] E. Capelli, O. Beneš, M. Beilmann, and R. J. M. Konings, *Thermodynamic investigation of the LiF-ThF_4 system,* J. Chem. Thermodyn. **58**, 110 (2013).

[6] R. E. Thoma and J. E. Ricci, *Fractional crystallization reactions in the system LiF-BeF_2-ThF_4*, Tech. Rep. ORNL-TM 2596 (1969).

[7] A. D. Pelton, P. Chartrand, and G. Eriksson, *The Modified Quasi-chemical Model: Part IV. Two sublattice quadruplet approximation,* Metall. Trans. **32A**, 1409 (2001).

[8] J. van der Meer, R. J. M. Konings, and H. A. J. Oonk, *Thermodynamic assessment of the LiF-BeF_2-ThF_4-UF_4 system,* J. Nucl. Mat. **357**, 48 (2006).

[9] R. E. Thoma, H. Insley, H. A. Friedman, and C. F. Weaver, *Phase equilibria in the systems BeF_2-ThF_4 and LiF-BeF_2-ThF_4,* J. Phys. Chem. **64**, 865 (1960).

[10] L. V. Jones, D. E. Etter, C. R. Hudgens, A. A. Huffman, T. B. Rhinehammer, N. E. Rogers, P. A. Tucker, and L. Wittenberg, *Phase equilibria in the ternary fused-salt system LiF-BeF_2-UF_4*, J. Am. Ceram. Soc. **45**, 79 (1962).

[11] C. F. Weaver, R. E. Thoma, H. Insley, and H. A. Friedman, *Phase Equilibria in Molten-Salt Breeder Reactor Fuels*, Tech. Rep. ORNL-TM-2896 (1960).

[12] F. J. Smith, L. M. Ferris, and C. T. Thompson, *Liquid-Vapor Equilibria in LiF-BeF_2 and LiF-BeF_2 -ThF_4 Systems*, Tech. Rep. ORNL-TM-4415 (1969).

[13] R. E. Thoma, *Phase Diagrams of Nuclear Reactor Materials*, Tech. Rep. ORNL-2548 (1959).

[14] R. E. Thoma, C. F. Weaver, H. Insley, and H. A. Friedman, *Phase equilibria in the system NaF/BeF_2/ThF_4*, Nucl. Sci. Eng. **19**, 406 (1964).

[15] G. D. Brunton, *The crystal structure of $Na_3BeTh_{10}F_{45}$*, Acta Cryst. **B29**, 2976 (1973).

[16] J. F. Eichelberger, C. R. Hundgens, L. V. Jones, G. Pish, T. B. Rhinehavver, P. A. Tucker, and L. J. Wittenberg, *Phase equilibria for the ternary fused-salt system NaF-BeF_2-UF_4*, J. Am. Ceram. Soc. **46**, 279 (1963).

[17] C. F. Weaver, R. E. Thoma, H. A. Friedman, and G. M. Hebert, *Phase equilibria in the system BeF_2-UF_4-ThF_4,* J. Am. Ceram. Soc. **44**, 146 (1961).

[18] E. Merle-Lucotte, D. Heuer, M. Allibert, X. Doligez, and V. Ghetta, *Minimizing the fissile inventory of the molten salt fast reactor,* Advances in Nuclear Fuel Management IV (ANFM 2009), LaGrange Park, IL, USA , (2009).

7

THERMODYNAMIC INVESTIGATION OF THE CaF_2-ThF_4 AND THE LiF-CaF_2-ThF_4 SYSTEMS

Elisa CAPELLI, Ondřej BENEŠ, Philippe E. RAISON, Markus BEILMANN, Carsten KÜENZEL, Rudy J.M. KONINGS

In this study we present the thermodynamic description of the binary CaF_2-ThF_4 system and the ternary LiF-CaF_2-ThF_4 system. In order to describe the general shape of the phase diagram, the phase equilibria of several intermediate compositions of the CaF_2-ThF_4 system have been measured for the first time in the present work using the DSC technique. These results have been combined with X-ray diffraction studies for the identification of the phases in equilibrium and for the determination of the structure of the $CaThF_6$ compound. Considering all the novel experimental data, the CaF_2-ThF_4 system has been assessed for the first time using the Calphad approach. Moreover, the ternary LiF-CaF_2-ThF_4 phase diagram has been extrapolated and optimized using the experimental data obtained in this study for the ternary mixtures. The model developed is in very good agreement with all the measurements performed and correctly predicted the lowest eutectic temperature and composition.

Parts of this chapter have been published in Journal of Chemical and Engineering Data **60**, 3166 (2015) [1].

7.1. INTRODUCTION

A comprehensive study of thermodynamic properties and phase equilibria of fused fluoride salts for Molten Salt Reactor (MSR) technology has been in progress at the Institute for Transuranium Element (ITU) for several years. The MSR is one of the six reactor concepts selected in the Generation IV programme as it meets the Gen IV goals in terms of sustainability, safety and reliability, proliferation resistance and economics. Research on the MSR is includes among others an innovative thorium-fuelled fast spectrum concept (MSFR)[2–4] and potential salt systems have been critically reviewed as fuel for this reactor[5]. The LiF-ThF_4 system is the reference fuel solvent and possible additives that could be considered (within certain concentrations limits) are NaF, BeF_2 and CaF_2 [6, 7], which may improve the properties of the binary solvent.

The addition of a new component in the fuel mixture must be evaluated considering different issues such as material compatibility and the fuel reprocessing scheme but one of the most important aspects is the prediction and evaluation of the thermodynamic and physical properties (neutron economy, melting temperature, vapour pressure, chemical stability at high temperature and actinide solubility). While in case of the BeF_2 and NaF additives, the thermodynamic description of the complete fuel salt has been already reported in literature [8–10], scoping studies of the LiF-CaF_2-ThF_4 are required to assess the feasability of this salt option. Moreover, it has been reported in a recent study [11], that LiF-CaF_2 melts can be used as an electrolyte for the electrodeposition of Nd and Th. Also in this case, physico-chemical properties of mixtures, such as LiF-CaF_2-ThF_4 melts, have to be determined in order to design a clean-up unit for the fuel salt.

In this work, we present the complete thermodynamic assessment of the LiF-CaF_2-ThF_4 ternary system. In order to describe this multi-component salt system, the thermodynamic description of all binary sub-systems is needed. Among them, the binary system CaF_2-ThF_4 is not reported in literature and only preliminary data are available [12]. Therefore, the first step of the study was an experimental investigation of the binary system CaF_2-ThF_4. The phase equilibria of several intermediate compositions have been measured using a Differential Scanning Calorimeter (DSC) to describe the general shape of the phase diagram The phase fields have been identified by X-Ray Diffraction (XRD). Moreover, the intermediate compound $CaThF_6$ has been synthesized and its crystal structure determined. All these experimental data have been used to assess for the first time the CaF_2-ThF_4 phase diagram. Furthermore, the ternary phase diagram of the LiF-CaF_2-ThF_4 system has been predicted using an adequate interpolation technique. Ternary parameters have been optimized using our novel experimental data on the ternary liquid solution to refine the thermodynamic assessment. The model predicts a lowest ternary eutectic at T = 809.9 K for the composition LiF-ThF_4-CaF_2 (66.6-29.0-4.4) which has been synthesized and measured. The agreement between the predicted and measured eutectic temperature, eutectic composition and heat of fusion is very good. Since none of these theree thermodynamic properties were used to tune the liquid model, the results validate the predictive ability of the thermodynamic assessment.

7.2. EXPERIMENT

7.2.1. MATERIALS

The samples used for all experiments were prepared from pure lithium fluoride LiF and calcium fluoride CaF_2, obtained from Alfa Aesar, and thorium fluoride ThF_4 obtained from Rhodia (France). Details on the provenance and the purity of each material are reported in Table 7.1. While CaF_2 was provided in anhydrous form, the LiF was subjected to a pre-treatment in order to remove the residual moisture, if present, from the powder. It consisted of a heating cycle at 623 K for several hours under inert argon atmosphere. A different heat treatment is required in the case of the ThF_4 component that shows an additional tendency to oxidize and form oxyfluorides. The purification was performed using NH_4HF_2 as fluorinating agent and it is described in details elsewhere [13]. After the purification of the pure components, samples were handled inside an argon glove box where the oxygen and water concentrations are monitored and kept low, typically below 5 ppm for both gases.

Several intermediate compositions of both CaF_2-ThF_4 and LiF-CaF_2-ThF_4 systems were prepared by mixing stoichiometric quantities of the pure materials. The powder was then filled into a specific nickel crucible, designed for our DSC instrument [14], which serves as a barrier between the corrosive fluorides vapours and the detector. In addition to the samples prepared for the DSC analysis, the $CaThF_6$ compound has been synthesized for the determination of its crystal structure using XRD. The synthesis was done by mixing stoichiometric quantities of the pure CaF_2 and ThF_4 materials and by heating the mixture in a closed container up to 1423 K for several hours in order to achieve the complete reaction. One of the samples (composition x_{CaF_2}=0.64) was subjected to a quenching procedure in order to determine the ratio between the stable phases at high temperature. The powder was compressed into a pellet, encapsulated inside a nickel crucible [15] and heated to 1273 K in a furnace under argon flow. After the temperature stabilization, the sample was dropped into liquid nitrogen and analysed with the XRD technique.

Table 7.1: Details on provenance and purity of all compounds used.

Compound	Provenance	Metallic purity	Further treatments
LiF	Alfa Aesar	99.99 w%[a]	Drying under Ar atmosphere
CaF_2	Alfa Aesar	99.99 w %[a] , ultradry	None
ThF_4	Rhodia	99.8^+ w%[b]	Purification described in [13]

[a] Purity grade as given by the supplier.
[b] Minimal estimated purity, based on XRD analysis.

7.2.2. DIFFERENTIAL SCANNING CALORIMETRY

The samples were analysed using a DSC instrument for the experimental determination of the phase equilibrium temperatures. The instrument is a SETARAM MD-HTC96 and it consists of two compartments, respectively the reference and the sample compartment, that are subjected to the same controlled temperature program. During the measurement, the heat flow and the temperature signals are detected by a series of interconnected S-type thermocouples placed around the compartments. First order phase transitions are registered by the instrument as a peak in the heat flow versus temperature signal providing information on the temperature and the heat of transition. A temperature calibration as function of temperature and heating rate has been performed before the measurements using several reference metals (In, Sn, Pb, Zn, Al, Ag, Cu).

In this study, we used a standard program consisting of four heating cycles up to 1523 K. The heating ramp was performed with constant heating rate of 10 K/min, while the cooling ramp was performed at different cooling rates for each cycle (5 K/min, 7 K/min, 10 K/min and 15 K/min). The transition temperatures were identified as the onset of the peak during heating to avoid problems of supercooling. However, in some DSC spectra (close to the eutectic), the liquidus transition is difficult to identify as it tends to form a broad shoulder and a complementary analysis on the cooling is also performed. The transition temperature is extrapolated to zero cooling rate by measuring the same transition at different cooling rates. After the first heating ramp, an isothermal sequence of 2 h was programmed in order to achieve the complete mixing of the starting materials in the liquid phase. It is important to notice that the maximum temperature reached by the instrument (1523 K) was below the melting point of pure CaF_2 (1691 K), therefore the mixing occured after the dissolution of CaF_2 in liquid ThF_4. This process can be rather slow and it is necessary to control whether the mixing reaction is complete or not. This was done by monitoring the variation of the temperature for the same transition in the subsequent cycles. A maximum variation of ±5 K was considered as acceptable (within the experimental uncertainty) and measurements that did not fullfill this criterion were discarded. For the LiF-ThF_4-CaF_2 ternary eutectic composition, the heat of the transition was also measured from the DSC curve by integration of the observed peak upon heating. The energy calibration is given by an internal standard of high purity (Al or Ag), as described in detail elsewhere [13].

7.2.3. X-RAY DIFFRACTION ANALYSIS

As part of the work on the determination of the CaF_2-ThF_4 phase diagram, X-ray diffraction studies have been performed. Using the XRD technique, two intermediate compositions (x_{CaF_2}=0.28 and x_{CaF_2}=0.64) have been investigated to determine the phases present. The $CaThF_6$ structure has also been identified.

The XRD pattern of all samples were measured at room temperature using a Bruker D8 X-ray diffractometer mounted in a Bragg-Brentano configuration with a curved Ge monochromator (1, 1, 1) and a ceramic copper tube (40 kV, 40 mA) equipped with a LinxEye position sensitive detector. As mentioned before, fluorides are hygroscopic and must be protected from air during the measurement. In case of the two-phase samples,

the powder was embedded into an epoxy resin which prevented the sample deterioration. On the other hand, the use of the resin increases significantly the background signal and makes the Rietveld analysis complicated. For this reason, the resin was not used in the case of the $CaThF_6$ sample and the possible sample deterioration was monitored by comparing the intensity and the position of the main peak in the spectra as function of time. After several cycles a peak shift was observed, therefore the subsequent measurements were not taken into account.

The data were collected by step scanning in the angle range (2θ) 7-120 at a step size of 0.013152 for the $CaThF_6$ sample and in the angle range (2θ) 10-120 at step size of 0.019729 for the other samples.

7.3. THERMODYNAMIC MODELING

Using the experimental data measured in this work, the binary CaF_2-ThF_4 phase diagram and the ternary LiF-CaF_2-ThF_4 phase diagram have been assessed for the first time. The optimization was done according to the Calphad method using the FactSage software [16], as described throughout the next sections.

7.3.1. PURE COMPOUNDS AND SOLID SOLUTION

The relative stability of compounds was analyzed using the following functions for each compound:

$$G^*(T) = \Delta_f H^0(298) - S^0(298)T + \int_{298}^{T} C_p(T)dT - T\int_{298}^{T}\left(\frac{C_p(T)}{T}\right)dT, \tag{7.1}$$

where $\Delta_f H^0(298)$ and $S^0(298)$ are respectively the standard enthalpy of formation and standard absolute entropy, both referenced to a temperature of 298.15 K, and $C_p(T)$ is the temperature function of the heat capacity at constant pressure. The thermodynamic data for all compounds used in this work are reported in Table 7.2. Except for $CaThF_6$ and the Li_2CaThF_8 compounds, the data have been taken from literature, respectively NIST-JANAF Tables [17] for LiF, Chartrand *et al.* [18] for CaF_2 and Capelli *et al.* [9] for ThF_4 and the LiF-ThF_4 intermediate compounds. In the case of the $CaThF_6$ and the Li_2CaThF_8 compounds, their thermodynamic properties ($\Delta_f H^0(298)$, $S^0(298)$ and $Cp(T)$) were estimated in this work. The heat capacity was calculated as weighted average from the heat capacity of their end-members, following the Neumann-Kopp rule. The other properties, $\Delta_f H^0(298)$ and $S^0(298)$, have been optimized in order to reproduce the experimental results as reported in Table 7.2. The entropy of formation from the end-members for $CaThF_6$ and Li_2CaThF_8 are respectively 10 J K^{-1} mol^{-1} and 5 J K^{-1} mol^{-1}.

In case of the CaF_2-ThF_4 phase diagram, the formation of a solid solution in the CaF_2 rich-side has been considered based on experimental evidence [19]. The Gibbs energy of this solid solution is described as follows:

$$\begin{aligned} g(T) = & x_{CaF_2}\cdot g_{CaF_2}(T) + x_{ThF_4}\cdot g_{ThF_4}(T) + x_{CaF_2}RTlnx_{CaF_2} \\ & + x_{ThF_4}RTlnx_{ThF_4} + \Delta g^{xs} \end{aligned} \tag{7.2}$$

Table 7.2: The $\Delta_f H^0(298.15)$ (kJ · mol^{-1}), $S^0(298.15)$ (J · K^{-1} · mol^{-1}) and C_p (J · K^{-1} · mol^{-1}) data of pure compounds used in this study.

Compound	$\Delta_f H^0(298.15)$	$S^0(298.15)$	C_p = a + b T + c T^2 + d T^{-2}			
			a	b T	c T^2	d T^{-2}
LiF (cr)	-616.931	35.66	43.309	$1.6312\cdot10^{-2}$	$5.0470\cdot10^{-7}$	$-5.691\cdot10^{5}$
LiF (l)	-598.654	42.962	64.183	-	-	-
ThF_4 (cr)	-2097.900	142.05	122.173	$8.3700\cdot10^{-3}$	-	$-1.255\cdot10^{6}$
ThF_4 (l)	-2103.654	101.237	170.0	-	-	-
CaF_2 (cr,α)[a]	-1225.912	68.572	122.8224	$2.848\cdot10^{-2}$	-	$-6.490\cdot10^{6}$
CaF_2 (cr,β)[b]	-1221.142	71.9217	122.8224	$2.848\cdot10^{-2}$	-	$-6.490\cdot10^{6}$
CaF_2 (l)[c]	-1186.068	92.566	161.2395	$2.118\cdot10^{-2}$	-	$-7.683\cdot10^{6}$
$LiThF_5$(cr)	-2719.490	181.89	165.482	$2.468\cdot10^{-2}$	$5.047\cdot10^{-7}$	$-1.824\cdot10^{6}$
Li_3ThF_7(cr)	-3960.259	236.1	282.100	$5.730\cdot10^{-2}$	$1.514\cdot10^{-6}$	$-2.962\cdot10^{6}$
$LiTh_2F_9$(cr)	-4822.329	324.29	287.655	$3.305\cdot10^{-2}$	$5.047\cdot10^{-7}$	$-3.079\cdot10^{6}$
$LiTh_4F_{17}$(cr)	-9021.140	609.0	532.001	$4.979\cdot10^{-2}$	$5.047\cdot10^{-7}$	$-5.589\cdot10^{6}$
$CaThF_6$ (cr)[d]	-3322.812	220.622	244.995	$3.685\cdot10^{-2}$	-	$-7.745\cdot10^{6}$
Li_2CaThF_8 (cr)[e]	-4571.074	285.94	331.613	$6.947\cdot10^{-2}$	$1.009\cdot10^{-6}$	$-8.883\cdot10^{6}$

[a] A transition between α and β phase occurs at 1424 K. T range (298.15 to 1424 K), additional C_p terms: $-72535.5\cdot T^{-1}$, $-4023.107\cdot T^{-0.5}$. In the T range (1424 to 2000 K) C_p (J · K^{-1} · mol^{-1})= 104.

[b] T range (298.15 to 1424 K), additional C_p terms: $-72535.5\cdot T^{-1}$, $-4023.107\cdot T^{-0.5}$. In the T range (1424 to 2000 K) C_p (J · K^{-1} · mol^{-1})= $107.989+1.046\cdot10^{-2}\cdot T$.

[c] T range (298.15 to 2000 K), additional C_p terms: $93543.1\cdot T^{-1}$, $-5633.815\cdot T^{-0.5}$. In the T range (1000 to 4000 K) C_p (J · K^{-1} · mol^{-1})= 99.914.

[d] T range (298.15 to 1424 K), additional C_p terms:$72535.5\cdot T^{-1}$, $-4023.107\cdot T^{-0.5}$. In the T range (1424 to 2000 K) C_p (J · K^{-1} · mol^{-1})=$226.173+8.37\cdot10^{-3}\cdot T-1.255\cdot10^{6}\cdot T^{-2}$.

[e] T range (298.15 to 1424 K), additional C_p terms:$72535.5\cdot T^{-1}$, $-4023.107\cdot T^{-0.5}$. In the T range (1424 to 2000 K) C_p (J · K^{-1} · mol^{-1})=$312.791+4.099\cdot10^{-2}\cdot T-2.393\cdot10^{6}\cdot T^{-2}+1.009\cdot10^{-6}\cdot T^{2}$.

where x_{CaF_2} and x_{ThF_4} are the mole fractions of the pure CaF_2 and ThF_4 components respectively, g_{CaF_2} and g_{ThF_4} are the standard Gibbs energy of the same compounds, R is the universal gas constant and ΔG^{xs} is the excess Gibbs energy of mixing. The latter term has been optimized in this work, using the sublattice model [20] and considering the cationic species involved (Ca^{2+}, Th^{4+}) on the first sublattice and the anionic species (F^-) on the second sublattice. The following relation has been obtained to describe the excess Gibbs energy:

$$\Delta g^{xs} = y_{Ca^{2+}} \cdot y^2_{Th^{4+}} \cdot 5800 \ \mathrm{J \cdot mol^{-1}}. \tag{7.3}$$

where the y terms are site fractions of the given species. We note here that compensatory effects, such as cationic vacancies, are not considered in this model. Since there are no evidences in literature on the formation of solid solutions in the LiF-ThF_4 and LiF-CaF_2 systems, none were considered in this study.

7.3.2. LIQUID SOLUTION

Considering a liquid solution, the excess Gibbs energy of mixing is described by the modified quasi-chemical model proposed by Pelton *et al* [21]. This model is well suited for the description of ionic liquids as it permits to select the composition of maximum short range ordering by varying the ratio between two parameters: the cation-cation coordination numbers $Z^A_{AB/FF}$ and $Z^B_{AB/FF}$ (in the present case with fluorine as the only type of anion). Moreover, this model was used for the description of all the other systems in our database, thus it allows its extension without compatibility issues.

The short range ordering is defined by the quadruplet approximation and the model treats the second-nearest neighbour interactions, cation-cation and anion-anion. Since fluorine is the only anion in the mixture no excess Gibbs energy is associated to the anion-anion (F-F) interaction. Let A and B be two generic cations and F the fluorine anion, the formation of the generic second-nearest neighbour pair (A-F-B) is given by the following reaction:

$$(A-F-A)+(B-F-B) = 2(A-F-B) \qquad \Delta g_{AB/F} \tag{7.4}$$

where $\Delta g_{AB/F}$ is the Gibbs energy change related to the pair formation. It is an empirical parameter of the model, which may be composition dependent, and it can be expanded in polynomial form such as:

$$\Delta g_{AB/F} = \Delta g^0_{AB/F} + \sum_{i \geq 1} g^{i0}_{AB/F} \chi^i_{AB/F} + \sum_{j \geq 1} g^{0j}_{AB/F} \chi^j_{BA/F} \tag{7.5}$$

where $\Delta g^0_{AB/F}$ and $g^{ij}_{AB/F}$ are composition independent coefficients while the dependence on composition is given by the $\chi_{AB/F}$ terms, defined as function of the cation-cation pair mole fractions X_{AA}, X_{BB}, X_{AB} [21]. In order to respect the charge-neutrality in the system, the following relation in terms of cation-cation coordination numbers ($Z^A_{AB/FF}$ and $Z^B_{AB/FF}$) and absolute cationic and anionic charges (q_A, q_B,..) must be fullfilled.

$$\frac{q_A}{Z^A_{AB/FF}} + \frac{q_B}{Z^B_{AB/FF}} = \frac{q_F}{Z^F_{AB/FF}} + \frac{q_F}{Z^F_{AB/FF}}. \tag{7.6}$$

While the charges are fixed by the chemistry of the cations and anion, the coordination numbers $Z^A_{AB/FF}$ and $Z^B_{AB/FF}$ (reported in Table 7.3) give the flexibility to select the composition of strongest short range ordering. At this point, the excess Gibbs energy tends to have its minimum, which is very likely coupled with the tendency to show the lowest melting point. Therefore, as first approximation the expected composition of the eutectic in the binary phase diagram was used to select the coordination numbers. We note here that more knowledge on the structure in a fluoride melt or on the Gibbs energy function would be helpful to improve the description. $Z^F_{AB/FF}$ is then automatically fixed by the charge-neutrality condition.

The Gibbs energy parameters for the $(Ca_{1-x}Th_x)F_{2+2x}$ liquid solution optimized in this work are given below as well as the Gibbs energy parameters for the $(Li_{1-x}Th_x)F_{1+3x}$ and $(Li_{1-x}Ca_x)F_{1+x}$ liquid solutions, taken from Capelli *et al.* [9] and Chartrand *et al.* [18] respectively.

$$\begin{aligned}\Delta g_{CaTh/FF} = &-19552.36 + 12.56T + \chi_{CaTh/F}\,(75362.4 - 43.96T)\\ &+ \chi_{ThCa/F}\,(-56658.67 + 33.49T) \quad \mathrm{J\cdot mol^{-1}}\end{aligned} \tag{7.7}$$

$$\begin{aligned}\Delta g_{LiTh/FF} = &-10883 + \chi_{LiTh/F}\,(-6697 + 2.93T)\\ &+ \chi_{ThLi/F}\,(-20930 + 19.25T) \quad \mathrm{J\cdot mol^{-1}}\end{aligned} \tag{7.8}$$

$$\Delta g_{LiCa/FF} = -2183.5 - 1.3591T + \chi_{LiCa}\,595.7 - \chi_{CaLi}\,790.8 \quad \mathrm{J\cdot mol^{-1}} \tag{7.9}$$

The Gibbs energy of the hypotetical cubic ThF_4 end-member in the CaF_2-ThF_4 solid solution had to be destabilized to avoid the formation of solid solution at the ThF_4 side according to:

$$g_{ThF_4}(s.s.) = g_{ThF_4} + 2000\ \mathrm{J\cdot mol^{-1}} \tag{7.10}$$

Using the models and the parameters established for all the stable phases in the binary phase diagrams, the ternary phase diagram LiF-ThF_4-CaF_2 has been extrapolated. The interpolation was based on the asymmetric Kohler/Toop model, in which LiF was choosen as asymmetric component due to the higher ionic nature compared to the others. In order to reproduce the experimental data measured for the ternary mixture, the following ternary parameter has been introduced for the ternary liquid phase:

$$\Delta g^{001}_{CaTh(Li)/FF} = -27627.6\ \mathrm{J\cdot mol^{-1}} \tag{7.11}$$

Table 7.3: Cation-cation coordination numbers of the liquid solution.

A	B	$Z^A_{AB/FF}$	$Z^B_{AB/FF}$
Li^+	Li^+	6	6
Ca^{2+}	Ca^{2+}	6	6
Th^{4+}	Th^{4+}	6	6
Li^+	Ca^{2+}	3	6
Li^+	Th^{4+}	2	6
Ca^{2+}	Th^{4+}	1.5	6

7.4. RESULTS

7.4.1. CaF_2-ThF_4 PHASE DIAGRAM

According to the available literature, there are no published data on the phase equilibria of the CaF_2-ThF_4 system. The only information available concerns the stability of the intermediate compound $CaThF_6$ [22, 23] and the formation of a solid solution in the CaF_2 rich side [19]. In order to determine the general shape of the phase diagram, several intermediate compositions have been prepared as described in the Experiment section and measured using the DSC for the determination of the equilibrium temperatures. The obtained values are listed in Table 7.4. These data were used to assess the binary phase diagram, as shown in Figure 7.1. Due to the temperature limit of the instrument, transitions occuring at temperature above 1523 K could not be measured and the shape of the liquidus line at high content of CaF_2 could not be determined exactly. Two invariant equilibria have been experimentally identified as the average of the values measured at different compositions, one eutectic at T=1224.4±6 K and one peritectic at T=1332.7±9 K. Both temperatures have been exactly reproduced in the phase diagram. Moreover, the composition of the eutectic point has been experimentally determined at x_{CaF_2}=0.293 by the analysis of the DSC output which shows a single peak during both heating and cooling process.

As already observed by Laval *et al.* [19], a solid solution is formed between the two end-members for high concentration of CaF_2. Based on neutron diffraction studies, they determined the maximum solid solubility of ThF_4 in CaF_2 at x_{ThF4}=0.185 at the peritectic temperature. In our study, several compositions with high content of CaF_2 have been measured. Samples having composition in the range $0.5 \leq x_{CaF_2} \leq 0.805$ have shown a transition corresponding to the peritectic temperature while samples having composition in the range above $x_{CaF_2} \geq 0.812$ do not show any transition. This represents a change in the phase fields at the peritectic temperature within the detection limit of the DSC (near the solubility limit the enthalpy effect is very small). According to this observation, the maximum solid solubity at the peritectic temperature has been fixed at x_{CaF_2}=0.81, which is in close agreement with the results of Laval *et al.* [19].

The calorimetric data on the phase equilibria have been combined with the analysis of the stable phases for the different phase fields. In the range between $0 \leq x_{CaF_2} \leq 0.5$, the stable phases below the eutectic temperature are $CaThF_6$ and ThF_4 while in the range between $0.5 \leq x_{CaF_2} \leq 0.81$ below the peritectic temperature the $CaThF_6$ intermediate compound and $Ca_{1-x}Th_xF_{2+2x}$ solid solution are in equilibrium. This was confirmed by the XRD analysis of two samples having compositions in the two different ranges x_{CaF_2}=0.28 and x_{CaF_2}=0.64, respectively. The experimental powder patterns are shown in Figure 7.2, where they are compared with the single-phase spectra of the pure components as reported by literature. ThF_4 and $Ca_{1-x}Th_xF_{2+2x}$ data have been taken from Benner *et al.* [24] and Laval *et al.* [19] respectively, while the data for the $CaThF_6$ compound have been taken from this work, as described in the next section. Although, a quantitative determination of the phases was not possible and the relative intensities have not been scaled, the patterns clearly show the characteristic peaks of the predicted phases.

Table 7.4: Phase diagram equilibria of the CaF_2-ThF_4 system measured in this study at p = 0.1 MPa by DSC. The transition temperatures T are reported as function of molar fraction x_{CaF_2}.

x_{CaF_2}	T / K	Equilibrium	x_{CaF_2}	T / K	Equilibrium
0.032	1235.4	Eutectic	0.360	1225.4	Eutectic
	1373.6	Liquidus		1298.3	Liquidus
0.086	1235.2	Eutectic	0.394	1222.9	Eutectic
	1348.5	Liquidus		1311.5	Liquidus
0.162	1226.6	Eutectic	0.441	1220.9	Eutectic
	1333.0	Liquidus		1326.8	Liquidus
0.184	1224.0	Eutectic	0.461	1218.3	Eutectic
	1315.7	Liquidus		1335.8	Liquidus
0.220	1216.9	Eutectic	0.484	1212.2	Eutectic
	1274.7	Liquidus		1350.6	Liquidus
0.247	1226.0	Eutectic	0.501	1219.4	Eutectic
	1271.8	Liquidus		1358.5	Liquidus
0.264	1227.3	Eutectic	0.507	1318.3	Peritectic
	1263.5	Liquidus		1362.9	Liquidus
0.271	1228.8	Eutectic	0.548	1332.7	Peritectic
	1249.6	Liquidus	0.640	1340.6	Peritectic
0.285	1225.0	Eutectic	0.789	1331.9	Peritectic
	1240.0	Liquidus	0.805	1339.6	Peritectic
0.285	1224.3	Eutectic	0.812	no transition below 1523 K	
	1251.8	Liquidus	0.831	no transition below 1523 K	
0.293	1224.8	Eutectic	0.850	no transition below 1523 K	
0.309	1225.3	Eutectic	0.958	no transition below 1523 K	
	1249.8	Liquidus			
0.334	1225.3	Eutectic			
	1272.8	Liquidus			

Standard uncertainty u are $u(T)$=5 K and $u(x)$= 0.001.

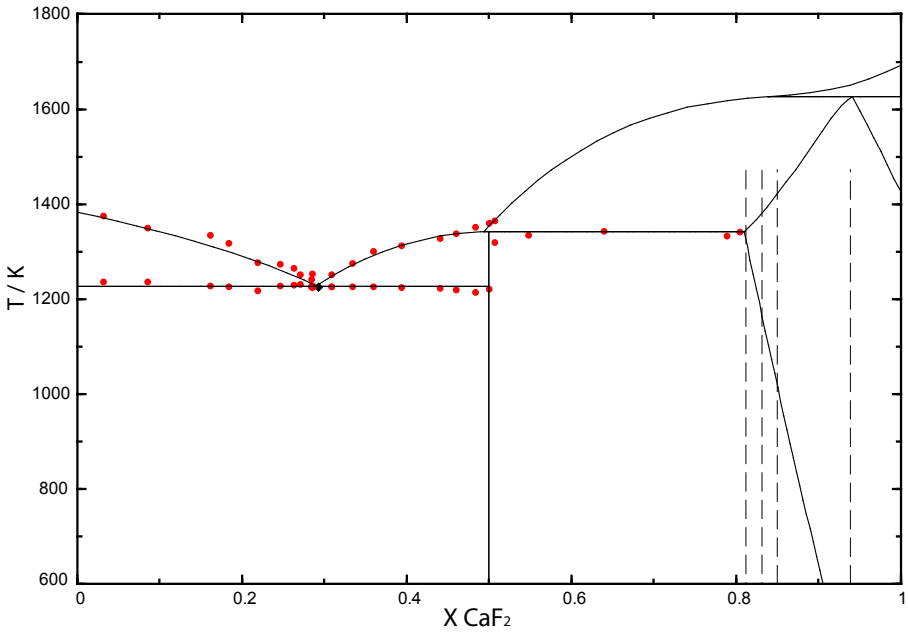

Figure 7.1: The binary phase diagram of the CaF_2-ThF_4 system assessed in this study. (•) Experimental data measured in this work.

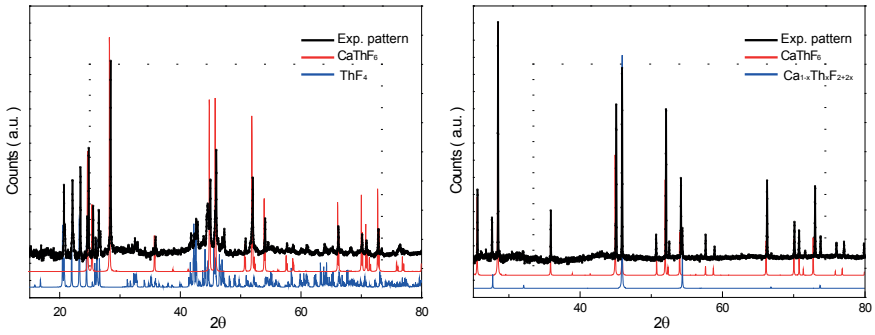

Figure 7.2: Experimental powder patterns obtained in this work for the compositions x_{CaF_2}=0.28 (left graph) and x_{CaF_2}=0.64 (right graph). The spectra are compared with the literature data for ThF_4 [24], $CaThF_6$ (this study) and $Ca_{1-x}Th_xF_{2+2x}$ [19].

7.4.2. $CaThF_6$ COMPOUND

The formation of the intermediate compound $CaThF_6$ in the CaF_2-ThF_4 system is well known and was reported in early studies by Zachariasen [22] and by Keller *et al.* [23]. Both authors reported this compound to be isostructural with the LaF_3 compound and they determined the lattice parameters. However, the atomic positions are not given in these works and therefore we have synthesized the $CaThF_6$ compound and measured its XRD pattern.

Structural analysis was performed by the Rietveld method with the Fullprof2k suite [25]. As starting point, we considered the lattice parameters reported by Keller *et al.* [23] and the atomic positions of the LaF_3 structure, in which the La^{3+} site have been substituted with Ca^{2+} and Th^{4+}, each having a occupancy factor of 0.5. Different structures for the LaF_3 have been reported in literature with different space group and atomic positions [26–28]. In this work, the trigonal structural model (space group P -3 c 1), as determined by Zalkin *et al.* [28], was used as it represents the currently accepted structure cite85Max, 07Lo.

The shape of the peaks was described by a Pseudo-Voigt function and the background was fitted based on linear interpolation between a set of about 99 background points with refinable heights. The comparison between the calculated and the measured pattern is shown in Figure 7.3. The compound crystallizes in the trigonal crystal system and the refined lattice parameters are $a = b = 6.981(1)$ Å and $c = 7.185(1)$ Å. The results of the structural analysis are summarized in Table 7.5 and Table 7.6 and a sketch of the unit cell is given in Figure 7.4.

7.4.3. LIF-CaF_2-ThF_4 PHASE DIAGRAM

The ternary LiF-ThF_4-CaF_2 phase diagram was calculated based on the assessed subbinary systems (LiF-CaF_2, LiF-ThF_4 and CaF_2-ThF_4) according to the Kohler/Toop formalism. The existence of a ternary compound with stoichiometry Li_2CaThF_8 was reported by Védrine *et al.* [29] and has been considered in this work. In absence of evidence of any other ternary intermediate compound, this was the only one considered in our assessment. The thermodynamic properties of this compound ($\Delta_f H^0(298.15)$, $S^0(298.15)$, C_p) are not known. Therefore they have been optimized in this work in a way to reproduce at best our experimental data. According to our model, the compound have a semicongruent melting point decomposing at 888 K to liquid and the solid solution $Ca_{1-x}Th_xF_{2+2x}$.

For the assessment of the phase diagram, several ternary compositions of the LiF-ThF_4-CaF_2 system have been measured in this study using the DSC. The results are reported in Table 7.7 and they have been used to optimize the ternary parameters of the liquid solution. The comparison between the model and the experimental data points is shown in Figure 7.5, where the LiF-ThF_4 pseudo-binary phase diagram with fixed concentrations of CaF_2 of 5 mol%, 10 mol% and 13 mol% are compared with the measured phase equilibrium temperatures. All diagrams show a very good agreement.

Table 7.5: Structural parameters and refined atomic positions in the $CaThF_6$ compound obtained in this study.

Symmetry and space group			trigonal P -3 c 1 (165)				
Lattice parameters							
a (Å)	b (Å)	c (Å)	α	β	γ	Volume (Å^3)	Ref.
6.981(1)	6.981(1)	7.185(1)	90	90	120	303.24	This work
6.994	6.994	7.121					[23]
6.971	6.971	7.175					[22]
Refined atomic position (R_{wp}: 9.48; R_p: 6.04; R_{exp}: 6.60; χ^2: 2.07)							
Atom	Ox.state	Wyckoff	x	y	z	Occupancy	B (Å)
Ca	+2	6c	0.332(4)	0	0.25	0.5	0.51
Th	+4	6c	0.332(4)	0	0.25	0.5	0.51
F1	-1	2a	0.34(1)	0.293(9)	0.100(2)	1	1*
F2	-1	4b	0.3333	0.6666	0.23(1)	1	1*
F3	-1	6c	0	0	0.25	1	1*

*Not refined.
Uncertainty is expressed by 2 standard deviation, as calculated with the Fullprof2k suite [25].

Table 7.6: Distances in the $CaThF_6$ structure.

Atom pairs	Distances
Ca/Th - F1	2.68(4); 2.68(4); 2.533(8); 2.533(8); 2.28(2) 2.28(2); 2.78(2) and 2.78(2)
Ca/Th - F2	2.334(2) and 2.334(2)
Ca/Th - F3	2.32(1)

Uncertainty is expressed by 2 standard deviation, as calculated with the Fullprof2k suite [25].

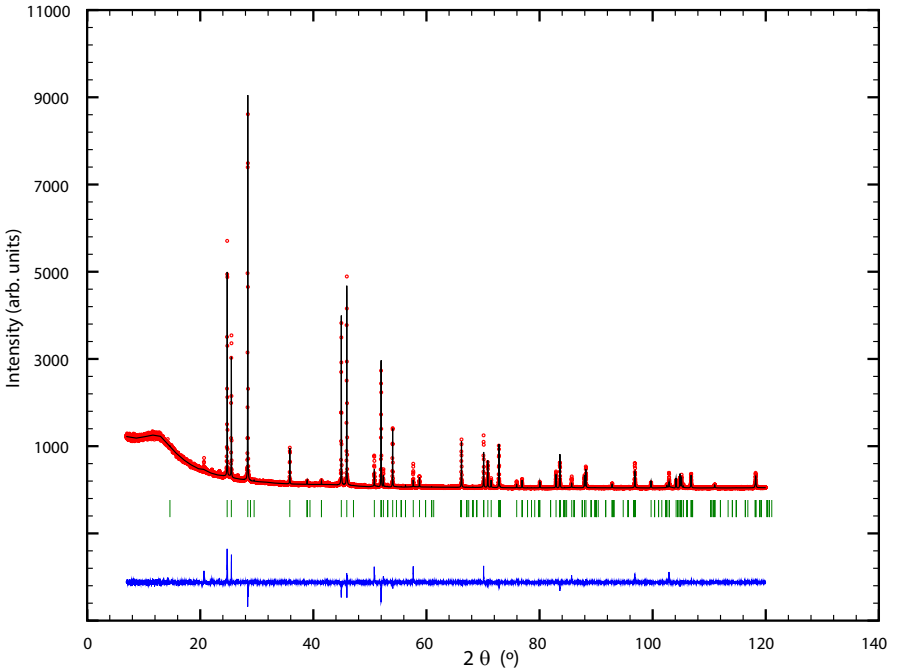

Figure 7.3: Comparison between the observed (in red) and calculated (in black) X-ray diffraction pattern of $CaThF_6$ compound. The difference between the experimental and calculated intensities is reported in blue and the Bragg reflections are marked in green.

Table 7.7: Phase diagram equilibria of the LiF-CaF_2-ThF_4 system measured in this study at p = 0.1 MPa by DSC. The transition temperatures T are reported as function of composition (molar fractions x_{LiF}, x_{CaF_2}, x_{ThF_4}).

x_{LiF}	x_{CaF_2}	x_{ThF_4}	T / K	Equilibrium
0.667	0.053	0.281	805.0	Eutectic
			834.0	Liquidus
0.700	0.050	0.250	819.5	Decomposition of Li_3ThF_7
			852.5	Liquidus
0.725	0.100	0.175	812.9	Decomposition of Li_3ThF_7
			837.7	Decomposition of Li_2CaThF_8
			901.6	LiF melting
			1167.8	Liquidus
0.630	0.130	0.240	812.8	Decomposition of Li_3ThF_7
			840.0	LiF melting
			1180.0	Liquidus

Standard uncertainty u are $u(T)$= 5 K and $u(x)$= 0.001.

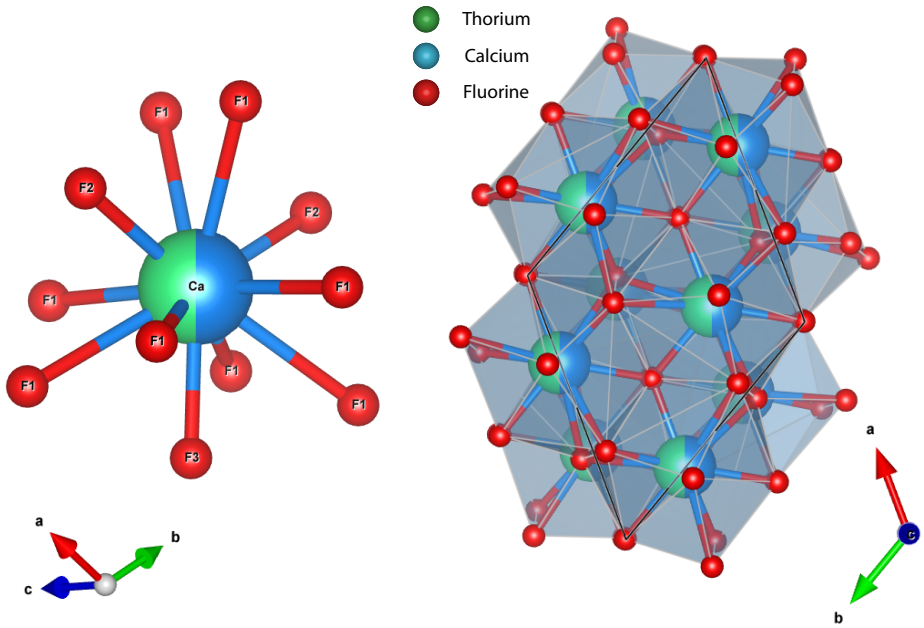

Figure 7.4: Crystal structure of $CaThF_6$.

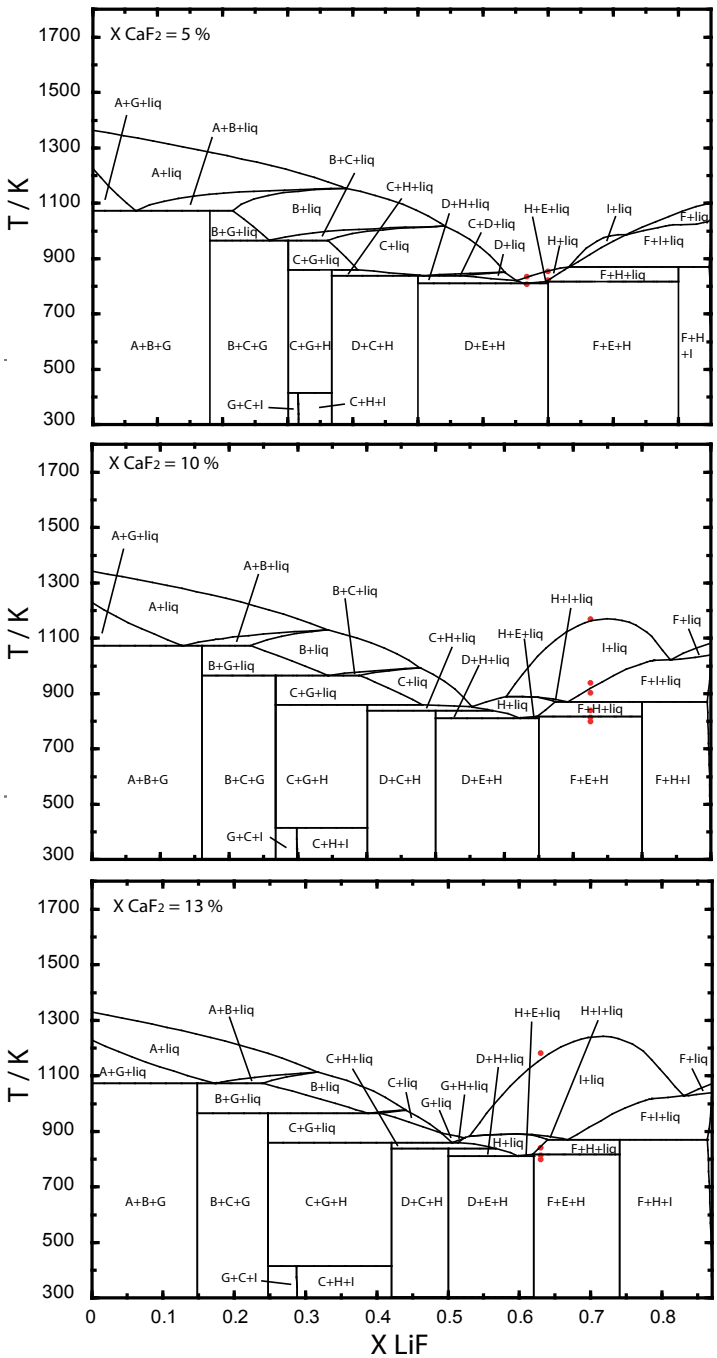

Figure 7.5: The LiF-ThF_4 pseudo binary phase diagram having fixed compostion of CaF_2 of 5%, 10% and 13%, respectively. Phase fields:(A) ThF_4 (B) $LiTh_4F_{17}$ (C) $LiTh_2F_9$ (D) $LiThF_5$ (E) Li_3ThF_7 (F) LiF (G) $CaThF_6$ (H) Li_2ThCaF_8 (I) $Ca_{1-x}Th_xF_{2+2x}$ (s.s.). (•) Experimental data measured in this work.

The liquidus projection of the assessed LiF-ThF_4-CaF_2 phase diagram is shown in Figure 7.6 with indicated primary crystallization fields. Eight invariant equilibria and one saddle point have been identified and they are listed in Table 7.8. The lowest eutectic was found at T = 810. 7 K for the composition LiF-ThF_4-CaF_2 (66.9-28.8-4.3). This composition has been synthesized (exact composition: LiF-ThF_4-CaF_2 (66.1-29.4-4.5)) and measured using DSC as shown in Figure 7.7. The measurement confirmed the eutectic composition as a single peak was observed both during cooling and heating. Moreover, the experimentally determined eutectic temperature was found at T =805.7 K in close agreement to the predicted value,l within the instrument's uncertainty. Furthermore, the heat of the transition has been measured and the value found ΔH_{fus}=13.4 ±1.0 kJ·mol^{-1} is in close agreement with the value predicted by the model ΔH_{fus}=14.3 kJ·mol^{-1}.

7.5. CONCLUSIONS

n this work, a thermodynamic investigation of the CaF_2-ThF_4 and LiF-CaF_2-ThF_4 systems have been performed. The phase diagrams of both systems have been assessed for the first time using the quasi-chemical model for the liquid solution and the two sublattice model for the solid solution. The assessment has been based on novel experimental data on binary and ternary mixtures obtained in this study. The DSC technique has been used for the identification of the phase equilibria in the system while the XRD technique allowed the determination of the stable phases. Moreover, the structural parameters of the $CaThF_6$ compound have been determined by Rietveld analysis. It was shown that the model is able to correctly predict the properties of the ternary mixture such as the eutectic composition and temperature. Therefore it can be considered as a valuable tool to determine the physico-chemical properties of the LiF-CaF_2-ThF_4 mixture for different applications.

Table 7.8: Invariant equilibria and saddle points found in the LiF-ThF_4-CaF_2 system.

x_{LiF}	x_{CaF_2}	x_{ThF_4}	T/ K	Equilibrium	Crystal phases in equilibrium
0.260	0.196	0.544	1072.1	Quasi-peritectic	ThF_4, $LiTh_4F_{17}$, $CaThF_6$
0.415	0.150	0.435	965.0	Quasi-peritectic	$LiTh_4F_{17}$, $LiTh_2F_9$, $CaThF_6$
0.619	0.093	0.288	889.3	Saddle point	Li_2ThCaF_8, $Ca_{1-x}Th_xF_{2+2x}$ (s.s.)
0.525	0.132	0.343	880.5	Quasi-peritectic	$CaThF_6$, Li_2ThCaF_8, $Ca_{1-x}Th_xF_{2+2x}$ (s.s.)
0.732	0.050	0.218	869.55	Quasi-peritectic	Li_2ThCaF_8, LiF, $Ca_{1-x}Th_xF_{2+2x}$ (s.s.)
0.514	0.123	0.363	858.4	Quasi-peritectic	$CaThF_6$, Li_2ThCaF_8, $LiTh_2F_9$
0.596	0.075	0.329	837.3	Quasi-peritectic	$LiTh_2F_9$, $LiThF_5$, Li_2ThCaF_8
0.711	0.035	0.254	815.5	Quasi-peritectic	Li_3ThF_7, LiF, Li_2ThCaF_8
0.669	0.043	0.288	810.7	Eutectic	$LiThF_5$, Li_3ThF_7, Li_2ThCaF_8

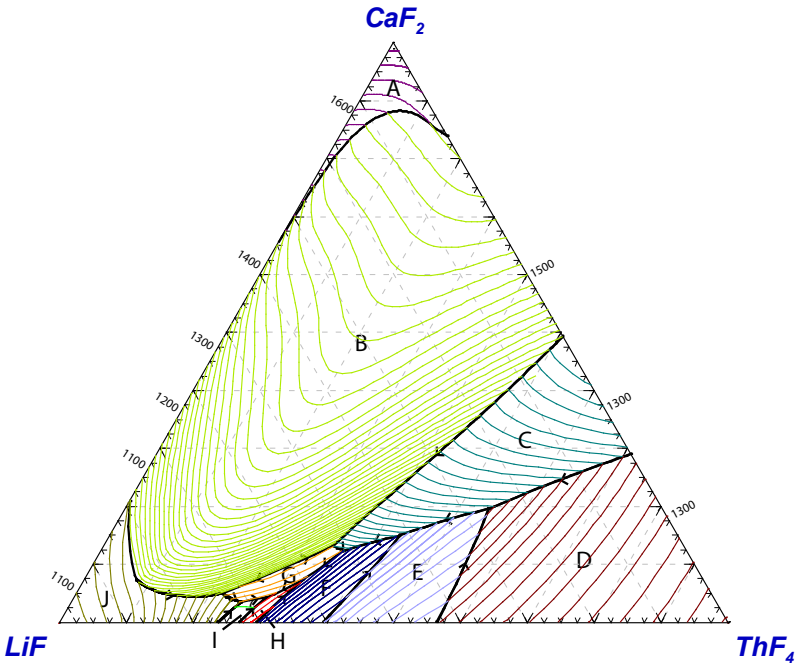

Figure 7.6: The liquidus projection of the assessed LiF-CaF_2-ThF_4 system. Primary cristallization fields: (A) CaF_2; (B) $Ca_{1-x}Th_xF_{2+2x}$ (s.s.); (C) $CaThF_6$; (D) ThF_4; (E) $LiTh_4F_{17}$; (F) $LiTh_2F_9$; (G) Li_2ThCaF_8; (H) $LiThF_5$; (I) Li_3ThF_7; (J) LiF.

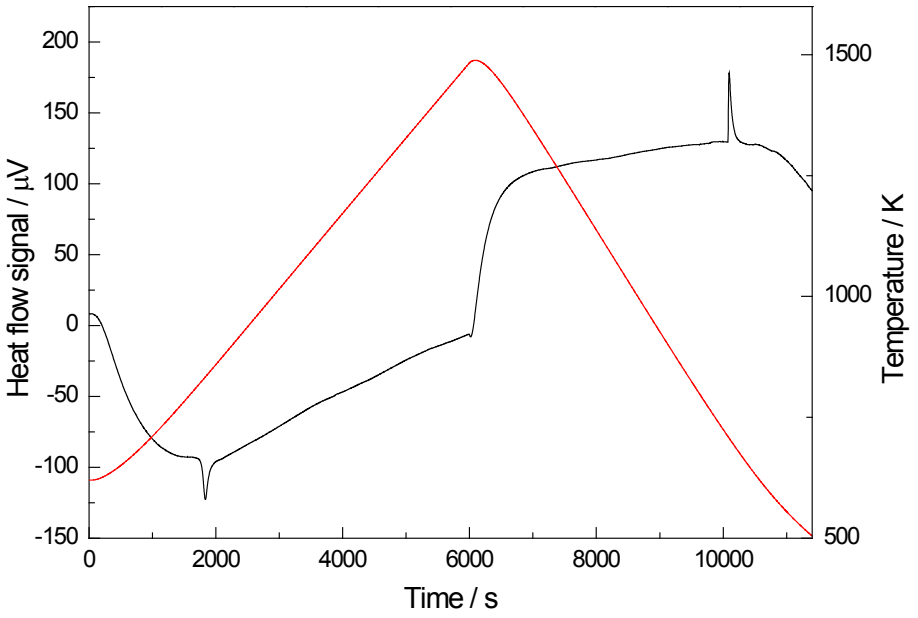

Figure 7.7: The DSC output of the measurement of the ternary eutectic in the system LiF-CaF_2-ThF_4.

ACKNOWLEDGEMENTS

This work was supported by the EVOL project in the 7th Framework Programme of the European Commision (Grant agreement No.249696). The authors would like to thank D. Bouxière and G. Pagliosa for the collection of the X-ray data.

REFERENCES

[1] E. Capelli, O. Beneš, P. E. Raison, M. Beilmann, C. Künzel, and R. J. M. Konings, *Thermodynamic investigation of the CaF_2-ThF_4 and the LiF-CaF_2-ThF_4 systems,* J. Chem. Eng. Data (2015), doi: 10.1021/acs.jced.5b00347.

[2] S. Delpech, E. Merle-Lucotte, D. Heuer, M. Allibert, V. Ghetta, C. Le-Brun, X. Doligez, and G. Picard, *Reactor physics and reprocessing scheme for innovative molten salt reactor system,* J. Fluor. Chem. **130**, 11 (2009).

[3] A. Nuttin, D. Heuer, A. Billebaud, R. Brissot, C. L. Brun, E. Liatard, J. M. Loiesaux, L. Mathieu, O. Meplan, E. Merle-Lucotte, H. Nifenecker, and F. Perdu, *Potential of thorium molten salt reactors: detailed calculations and concept evolution with a view to large scale energy production,* Prog. Nucl. Energ. **46**, 77 (2005).

[4] L. Mathieu, D. Heuer, R. Brissot, C. L. Brun, E. Liatard, J. Loiseaux, O. Meplan, E. Merle-Lucotte, A. Nuttin, J. Wilson, C. Garzenne, D. Lecarpentier, and E. Walle, *The Thorium Molten Salt Reactor: Moving on from the MSBR,* Prog. in Nucl. En. **48**, 664 (2006).

[5] O. Beneš and R. J. M. Konings, *Thermodynamic properties and phase diagrams of fluoride salts for nuclear applications,* J. Fluorine Chem. **130**, 22 (2009).

[6] C. Renault, S. Delpech, E. Merle-Lucotte, R. J. M. Konings, M. Hron, and V. Ignatiev, *The Molten Salt Reactor: R&D status and perspectives in europe,* Proceedings of FISA, Prague, Czech Repubblic (2009).

[7] C. Renault, M. Horn, and D. E. Holcomb, *The molten salt reactor MSR in generation IV: Overview and perspectives,* GIF Symposium, Paris, France (2009).

[8] O. Beneš, M. Beilmann, and R. J. M. Konings, *Thermodynamic assessment of the LiF–NaF–ThF_4–UF_4 system,* J. Nucl. Mater. **405**, 186 (2010).

[9] E. Capelli, O. Beneš, and R. J. M. Konings, *Thermodynamic assessment of the LiF-NaF-BeF_2-ThF_4-UF_4 system,* J. Nucl. Mater. **449**, 111 (2014).

[10] C. F. Weaver, R. E. Thoma, H. Insley, and H. A. Friedman, *Phase Equilibria in Molten-Salt Breeder Reactor Fuels*, Tech. Rep. ORNL-TM-2896 (1960).

[11] P. Chamelot, L. Massot, C. Hamel, C. Nourry, and P. Taxil, *Feasibility of the electrochemical way in molten fluorides for separating thorium and lanthanides and extracting lanthanides from the solvent,* J. Nucl. Mat. **360**, 64 (2007).

[12] M. Beilmann, O. Beneš, E. Capelli, V. Reuscher, R. J. M. Konings, and T. Fanghänel, *Excess heat capacity in liquid binary alkali-fluoride mixtures,* Inorg. Chem. **52**, 2404 (2013).

[13] E. Capelli, O. Beneš, M. Beilmann, and R. J. M. Konings, *Thermodynamic investigation of the LiF-ThF_4 system,* J. Chem. Thermodyn. **58**, 110 (2013).

[14] O. Beneš, R. J. M. Konings, S. Wurzer, M. Sierig, and A. Dockendorf, *A DSC study of the $NaNO_3$–KNO_3 system using an innovative encapsulation technique,* Thermochim. Acta **509**, 62 (2010).

[15] O. Beneš, R. J. M. Konings, C. Künzel, M. Sierig, A. Dockendorf, and L. Vlahovic, *The high-temperature heat capacity of the (Li, Na)F liquid solution,* J. Chem. Thermodyn. **41**, 899 (2009).

[16] C. W. Bale, P. Chartrand, S. A. Degterov, G. Eriksson, K. Hack, R. BenMahfoud, J. Melançon, A. D. Pelton, and S. Petersen, *Factsage thermochemical software and databases,* CALPHAD **26**, 189 (2002).

[17] M. W. Chase Jr.(ed.), *NIST-JANAF Thermochemical Tables Fourth Edition,* J. Phys. Chem. Ref. Data, Monograph **9**, (1998).

[18] P. Chartrand and A. D. Pelton, *Thermodynamic evaluation and optimization of the LiF-NaF-KF-MgF_2-CaF_2 system using the modified quasi-chemical model,* Metall. Trans. **32A**, 1385 (2001).

[19] J. P. Laval, A. Mikou, B. Frit, and J.Pannetier, *Neutron diffraction study of the anion-excess fluorite-related Ca_{1-x} Th_x F_{2+2x} solid solution,* J. Solid State Chem. **61**, 359 (1986).

[20] A. D. Pelton, *A database and sublattice model for molten salts,* CALPHAD **12**, 127 (1988).

[21] A. D. Pelton and P. Chartrand, *The Modified Quasi-chemical Model: Part II. Multicomponent solutions,* Metall. Trans. **32A**, 1355 (2001).

[22] W. H. Zachariasen, *Crystal chemical studies of the 5f-series of elements. XII.New compounds representing known structure types,* Acta Cryst. **2**, 388 (1949).

[23] C. Keller and M. Salzer, *Ternäre fluoride des typs Me^{II} $Me^{IV}F_6$ mit LaF_3 struktur,* J. Inorg. Nucl. Chem. **29**, 2925 (1967).

[24] G. Benner and B. G. Mueller, *Zur kenntnis binärer fluoride des ZrF_4 typs: HfF_4 und ThF_4,* Z. anorg. allg. Chem. **588**, 33 (1950).

[25] J. Rodriguez-Carvajal, *Recent advances in magnetic structure determination by neutron powder diffraction,* Physica B **192**, 55 (1993).

[26] C. DeRango, G. Tsoucaris, and C. Zelwer, *Determination de la structure du fluorure de lanthane LaF_3,* Comptes rendus hebd. séances acad. sci. Paris **263**, 64 (1966).

[27] M. Mansmann, *Zur kristallstruktur von lanthantrifluorid,* Z. anorg. allg. Chem. **331**, 98 (1964).

[28] A. Zalkin, D. H. Templeton, and T. E. Hopkins, *The atomic parameters in the lanthanum trifluoride structure,* Inorg. Chem. **5**, 1466 (1966).

[29] A. Védrine, L. Baraduc, and J.-L. Cousseins, *Sur une nouvelle famille de composes $M^{II}M^{IV}Li_2F_8$ de structure apparentee a celle de la scheelite,* Mat. Res. Bull. **8**, 581 (1973).

8

DISCUSSION AND CONCLUSIONS

Once we rid ourselves of traditional thinking
we can get on with creating the future.

James Bertrand

The MSR is a very promising concept for the next generation of nuclear energy systems. Due to the liquid nature of the fuel, it has radically different properties from the current operating nuclear reactors and could potentially lead to significant advances in nuclear safety. The MSR can be designed as a thermal spectrum reactor or as a fast spectrum reactor providing in both cases excellent safety features. Moreover, it is well fitted to the thorium cycle and represents an interesting option for both nuclear breeding and nuclear waste reduction.

The research described in this thesis focuses on the thermodynamic description of molten salt mixtures for the MSFR fuel, a concept currently being investigated in Europe. The main goal was to provide a reliable model of the most relevant fuel systems as candidates for this technology and to compile a multi-component thermodynamic database. This was achieved by combining experimental work and thermodynamic modeling. New experimental data on fluoride mixtures, including phase equilibrium temperatures, vapour pressure, enthalpy of mixing and heat capacity, were collected and are presented in this work. A substantial effort has been made to optimize the purity of the single salt components and to develop dedicated experimental procedures compatible with fluoride salts at high temperature. This experimental work provides the basis for the development of the thermodynamic database through a modeling approach. The importance of a thermodynamic model for the design and safety assessment of new reactor technologies has been demonstrated in this thesis. It is a very important tool that allows the evaluation of the performance of several salt mixtures predicting their

Parts of this chapter have been published in GLOBAL proceeding.

physico-chemical properties. The optimum fuel composition can be selected by defining appropriate screening criteria, in our case the lowest liquidus temperature in the system compatible with the fuel composition requirements. As second step, the performance and the safety limits of the salt mixture are evaluated taking into consideration additional thermodynamic properties, such as vapour pressure and boiling point.

The developed thermodynamic database includes the most important systems for the MSFR technology, however its relevance is not limited to this context. Molten salt have various applications both in the nuclear and conventional industry in which they are currently under investigation for heat transfer and heat storage purposes.

8.1. SUMMARY OF RESULTS AND DISCUSSION

The first section of this thesis shows the improvements achieved in the description of the binary LiF-ThF_4 system. Nowadays, it is considered as the key system for the MSFR technology and therefore it is crucial to have an accurate description of its thermodynamic behaviour. The purification of the single components, in particular ThF_4, was an essential first step for the study of more complex systems. ThF_4 was purified using NH_4HF_2 as fluorinating agent and characterized by DSC and XRD analysis. Both techniques confirmed the high purity of the sample, which is particularly important for a reliable determination of its basic thermodynamic properties. The high temperature heat capacity of both the crystalline state and the liquid state was measured by drop calorimetry and the results are presented here for the first time.

The phase diagram of the binary LiF-ThF_4 system has been re-assessed in this work based on new experimental data. The enthalpy of mixing of the liquid solution and several phase equilibria points were measured using the DSC. The phase diagram as optimized in this study consists of five invariant equilibria; two eutectics and three peritectics. Four intermediate compounds were found to be stable, namely Li_3ThF_7, $LiThF_5$, $LiTh_2F_9$ and $LiTh_4F_{17}$. Among these compounds, the most important is probably the Li_3ThF_7, which shows the lowest melting point in the system, thus it was synthesized and its enthalpy of fusion experimentally determined.

The vapor pressure of the fuel mixture determines its volatility with respect to temperature and thus is very important for the reactor safety. In order to investigate this property, several samples were prepared by mixing stoichiometric quantities of the two end-members LiF and ThF_4. The measurements were performed using the KEMS technique from 1000 K to 1400 K and four main gaseous species were found to be present in the mixed systems, namely LiF, Li_2F_2, Li_3F_3 and ThF_4. The total vapour pressure over the liquid solution was evaluated as function of temperature for all the measured compositions. Based on these measurements the thermodynamic activities of LiF and ThF_4 in the $Li_xTh_{1-x}F_{4-3x}$ liquid solution were also determined. The measured vapour pressures are very low in the temperature range of the MSFR operation and they are in good agreement with the pressure predicted by the thermodynamic model.

In conclusion, different properties have been measured for this key binary system improving the general understanding on its thermodynamic behaviour, as shown in Fig-

ure 8.1. Taking advantage of different sets of experimental data increases dramatically the precision of the model and improves its capability to provide reliable predictions of the unknown properties. As an example, based on the assessment of the binary LiF-ThF_4 system, a value for the ThF_4 heat capacity was suggested and afterwards confirmed by experiments. Vapour pressure and thermodynamic activities were not used to tune the thermodynamic model. Therefore, the results validate the predictive ability of the thermodynamic assessment. The minimum liquidus temperature in the system was found at 832 K for X_{ThF_4}=23.8%.

For the start-up of the reactor the addition of fissile material is needed. Two main fuel options were considered in this work, one for the MSFR concept started with plutonium and the second for the MSFR concept started with uranium. In the first case, the reference salt is a mixture of LiF–ThF_4-PuF_3-UF_4. In order to predict the influence of the fissile components on the melting behaviour of the LiF-ThF_4 solvent, the thermodynamic assessment of the quaternary LiF-ThF_4-UF_4-PuF_3 system has been performed. In fact, it must be noted that a small amount of UF_4 must always be present in the salt to control its redox potential via the UF_4/UF_3 ratio. The work has been carried out under the two main assumptions that the pair compounds CeF_3/PuF_3 and UF_4/ThF_4 can be considered as proxy compounds due to their very similar thermodynamic properties. As an example, CeF_3 and PuF_3 have almost identical melting points: 1703 K and 1698 K, respectively. This similarity has been used both for describing the thermodynamic functions and to simplify the experimental procedure. Combining different experimental results on solubility and ternary phase equilibrium, the thermodynamic assessment of the quaternary system LiF–ThF_4-PuF_3-UF_4 was obtained.

The first fuel option was determined considering a fix concentration of UF_4 of 1 mol% (minimum required) and plotting the pseudo ternary phase diagram of the LiF–ThF_4-PuF_3 system. The lowest eutectic was identified for the composition LiF–ThF_4-PuF_3-UF_4 (75.4-20.6-3.0-1.0) at T=819 K, which represents an interesting option for the MSFR fuel. However, this analysis considers only the melting behaviour of the mixture, which should be coupled with neutronic calculations to establish whether it also fulfills the reactor physics criteria as well as non-proliferation issues. This could lead to the necessity of partially substitute the ThF_4 with UF_4 (in order to increase the fissile concentration and mantain enrichment to reasonable values) and could influence the thermodynamic properties of the final fuel mixture. For this reason, we investigated the influence of partial substitution of ThF_4 by UF_4 on the most important fuel properties. It was concluded that within the range of compositions compatible with MSFR, the impact on melting point, boiling point and vapour pressure is relatively small. Lastly, compositions with higher concentration of PuF_3 may also be of interest. This option maximizes the waste reduction but the melting point of the salt is higher. In this case, it is also important to guarantee that the concentration of trivalent elements is safely below the solubility limit at the operation temperature in order to avoid precipitation and local concentration of fissile material.

The LiF-UF_4-ThF_4 is the reference salt composition for the MSFR configuration started with uranium. In addition to these "required" components, the presence of other compounds may be advantageous to optimize the physico-chemical properties of the

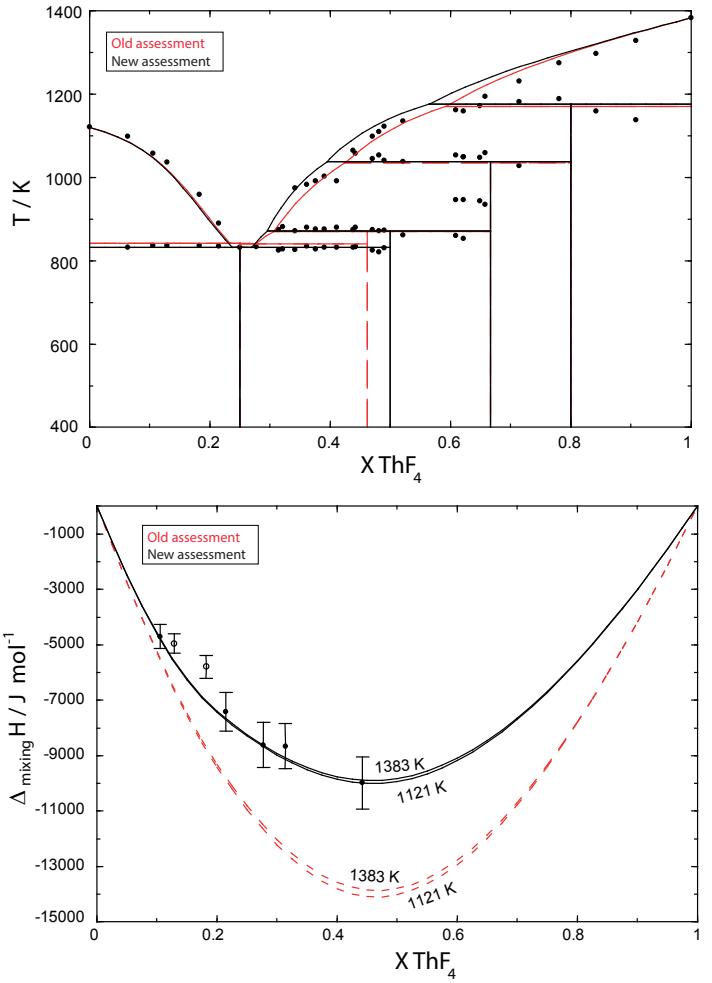

Li_3ThF_7 enthalpy of fusion:	
Experiment:	$\Delta_{fus}H = 54.8 \pm 8$ kJ/mol
Literature (*Gilbert*,1962)	$\Delta_{fus}H = 58.4$ kJ/mol
Old assessment:	$\Delta_{fus}H = 87.2$ kJ/mol
New assessment:	$\Delta_{fus}H = 58.8$ kJ/mol

Figure 8.1: Comparison between the LiF-ThF_4 assessment, the previous version and the experimental data. Top to bottom: Phase diagram of LiF-ThF_4 system; Enthalpy of mixing of the LiF-ThF_4 liquid solution; and enthalpy of fusion of the Li_3ThF_7 compound.

fuel salt. One of the most studied additives for the moderated concept is BeF_2, which has a very low neutron capture cross section and reduces the melting temperature of the fuel mixture. Since the MSFR concept is a non-moderated reactor with not so tight neutron economy, atoms with higher capture cross sections, such as NaF and CaF_2, can also be considered. However, it must be noted that the presence of additives may complicate the reprocessing chemistry or increase the viscosity of the salt. To evaluate the influence of NaF and BeF_2 addition on the melting behaviour of the reference salt mixture, we have performed the full thermodynamic assessment of the LiF-NaF-BeF_2-ThF_4-UF_4 system. Using all the data available in literature, two binary systems (in addition to the already assessed systems) and five ternary systems have been newly assessed. Using the thermodynamic database developed, we identified the most promising compositions with respect to the melting behaviour and we calculated their thermodynamic properties. Table 8.1 lists the proposed fuel compositions. The concentration of fissile material was fixed for all the options to 2.55 mol% in agreement with neutronic recommendations (see Chapter 6 for details). Afterwards, we studied the behaviour of different fuel options ((i) no additives, (ii) addition of BeF_2 only , (iii) addition of NaF only and (iv) addition of BeF_2 and NaF) and the compositions having the lowest liquidus temperature were selected. All the compositions selected exhibit good properties in terms of reactor safety. In fact the calculated boiling points are closed to 2000 K and the vapour pressures are very low.

CaF_2 is also an interesting additive for the MSFR. It has a high thermodynamic stability and the addition of CaF_2 to the salt matrix would increase the fraction of heavier elements and limit the moderation effect. Finally, a mixture of LiF and CaF_2 is expected to be used for the salt reprocessing [1], therefore addition of CaF_2 would have no negative influence on the reprocessing process. Given these possible advantages, we decided to investigate the effect of CaF_2 addition on the melting behaviour of the basic system LiF-ThF_4. Before studying the ternary system, a preliminary investigation on the binary sub-system CaF_2-ThF_4 was needed as no experimental data were found in literature. The phase diagram was described by coupling the measurement of phase equilibria points using the DSC with diffraction studies for the identification of the phases in equilibrium. Two invariant equilibria have been identified, one eutectic at T=1224 K and one peritectic at T=1333 K. The formation of a solid solution in the ThF_4-rich side was confirmed and the $CaThF_6$ compound structure was determined by Rietveld analysis. As second step, the ternary phase diagram of the LiF-CaF_2-ThF_4 system has been extrapolated and the ternary parameters of the liquid solution have been optimized using our novel experimental data on the ternary mixture. The model predicts a lowest ternary eutectic at T=811 K for the composition LiF-ThF_4-CaF_2 (66.9-28.8-4.3) which has been synthesized and measured at T=806 K. The agreement between the model and the experiments in terms of eutectic temperature, eutectic composition and heat of fusion is very good and confirms reliability of the thermodynamic assessment. This composition option is also interesting for the MSFR fuel. The melting point is somewhat lower compared to the binary mixture and the calculated thermodynamic properties are also very good (see Table 8.1). An interesting path of investigation to improve the available dataset would be the extension to the quaternary system LiF-CaF_2-ThF_4-UF_4 and the evaluation of simultaneous addition of different components.

To summarize the results on the influence of additional components in the fuel matrix, Table 8.1 compares the proposed fuel compositions. As explained in the main body of this thesis they were selected seeking for the lowest liquidus temperature in the systems, compatible with the fuel requirements. The boiling point and the calculated pressure above the liquid mixture at the operation temperature (defined as 50 K higher than the liquidus point) are also compared as they are important parameters for the safety assessment. Considering solely the thermodynamic properties, addition of further components (NaF, BeF_2 or CaF_2) is advantageous as it results in a decrease of the minimum operation temperature for the reactor. However, these results should be considered in a larger context. For example, the presence of BeF_2 in the melt has some important drawbacks, mainly related to its chemistry, toxicity, and neutronic features [2] and there is an incentive to keep its content to the minimum. Considering these issues and the low reduction in the final melting point of the mixture compared to the basic mixture, addition of only BeF_2 does not seem to be very profitable. Less data are available in literature on NaF and CaF_2 as additive. The addition of these compounds looks more promising, however in both cases neutronic feasibility and suitability for the on-line reprocessing must also be confirmed.

8.2. MAIN OUTCOMES

The main outcomes of this study can be summarized as follows:

- The experimental routines for measuring fluoride samples at high temperature have been optimized. This includes mainly the purification of the single components, the handling, preparation and purity analysis of the samples and the development of dedicated experimental procedures compatible with encapsulated sample.
- The experimental results obtained significantly contribute to the database on fluoride salts. Different sets of thermodynamic data were obtained including binary and ternary phase equilibrium points, vapour pressure, thermodynamic activities, enthalpy of fusion, enthalpy of mixing and heat capacity. In addition, structural studies have also been performed.
- The existing thermodynamic database on molten salts have been extended and currently includes most of alkaline, alkali-earth and actinide fluorides. In total, six binary systems and eight ternary systems have been newly assessed in this thesis and included in the database.
- Thermodynamic calculations were performed using the developed database and several fuel options have been identified based on their physico-chemical properties. The proposed fuel compositions are reported in Table 8.1.

Concluding, the present work has been successful in identifying a set of fuel options, which can be considered as reference for the MSFR technology. It represents a concrete step towards the final choice of the MSFR fuel.

Table 8.1: The proposed fuel compositions and related fuel properties.

Composition	Liquidus temperature	Boiling temperature	P at T^*_{oper}
	Basic mixture		
$LiF\text{-}ThF_4$ (76.2-23.8)	832 K	2027 K	$8.56{\cdot}10^{-4}$ Pa
	MSFR started with plutonium		
$LiF\text{-}ThF_4\text{-}UF_4\text{-}PuF_3$ (78.0-16.0-1.0-5.0)	867 K	2035 K	$5.33\cdot10^{-3}$ Pa
$LiF\text{-}ThF_4\text{-}UF_4\text{-}PuF_3$ (75.3-20.6-1.0-3.1)	819 K	2032 K	$7.26{\cdot}10^{-4}$ Pa
	MSFR started with uranium		
$LiF\text{-}ThF_4\text{-}UF_4$ (76.2-21.3-2.55)	830 K	2022 K	$1.08{\cdot}10^{-3}$ Pa
$LiF\text{-}BeF_2\text{-}ThF_4\text{-}UF_4$ (75.7-1.8-19.95-2.55)	825 K	1991 K	$4.67{\cdot}10^{-3}$ Pa
$LiF\text{-}NaF\text{-}ThF_4\text{-}UF_4$ (47.3-25.9-24.3-2.55)	770 K	2038 K	$7.27{\cdot}10^{-5}$ Pa
$LiF\text{-}NaF\text{-}BeF_2\text{-}ThF_4\text{-}UF_4$ (41.8-31.1-4.6-19.95-2.55)	753 K	1979 K	$4.08{\cdot}10^{-5}$ Pa
$LiF\text{-}CaF_2\text{-}ThF_4$ ** (66.9-4.3-28.8)	811 K	2017 K	$4.12{\cdot}10^{-4}$ Pa

* T_{oper} is the operation temperature defined as 50 K higher than the melting point.
** Preliminary result without UF_4 addition.

8.3. OUTLOOK

Research on the characterization of molten fluoride salts must be continued in the future to validate and extend the knowledge on the MSR fuel behaviour. This is required to ensure the safe operation of such a reactor and to predict its behaviour during irradiation and in the long-term perspective.

The present work has been successful in improving the description of the thermodynamic properties of the most relevant compounds, however there is still room for improvement. For instance, in absence of literature data heat capacities of liquid solutions are usually assumed to be "ideal" and estimated on the basis of the empirical Neumann-Kopp rule. In contrast to this assumption, recent studies [3, 4] have shown that for binary fluoride systems the deviation from ideality can be significant, up to 40%. Further studies in this direction are suggested to improve the description of liquid mixtures. In order to be able to predict the thermodynamic properties of more complex liquids, studies of the local structure of molten salt mixture would also be of great interest.

The present thesis consider only "fresh" fuel scenario, i.e. at the beginning of the reactor operation time. During irradiation fission products are formed by the fission reaction and accumulate in the fuel matrix. The effect of this composition change on the melting behaviour, solubility limit and vapour pressure of the fuel must be carefully evaluated. This could be achieved extending the thermodynamic database to the main fission products. In addition, the demonstration of the retention capacity of the salt for fission products that are volatile in LWR fuels (e.g. Cs, I) would be of primary importance.

Finally, in order to give an ultimate answer on the optimum fuel composition, different criteria should be considered simultanueously, the most relevant being the physicochemical properties, the core physics and the chemistry of the salt.

REFERENCES

[1] P. Chamelot, L. Massot, C. Hamel, C. Nourry, and P. Taxil, *Feasibility of the electrochemical way in molten fluorides for separating thorium and lanthanides and extracting lanthanides from the solvent,* J. Nucl. Mat. **360**, 64 (2007).

[2] L. Mathieu, D. Heuer, R. Brissot, C. L. Brun, E. Liatard, J. Loiseaux, O. Meplan, E. Merle-Lucotte, A. Nuttin, J. Wilson, C. Garzenne, D. Lecarpentier, and E. Walle, *The Thorium Molten Salt Reactor: Moving on from the MSBR,* Prog. in Nucl. En. **48**, 664 (2006).

[3] M. Beilmann, O. Beneš, E. Capelli, V. Reuscher, R. J. M. Konings, and T. Fanghänel, *Excess heat capacity in liquid binary alkali-fluoride mixtures,* Inorg. Chem. **52**, 2404 (2013).

[4] E. Capelli, O. Beneš, and R. J. M. Konings, *Excess heat capacity of the $(Li_{1-x}Ca_x)F_{1+x}$ liquid solution determined by differential scanning calorimetry and drop calorimetry,* J. Chem. Thermodynam. **81**, 160 (2015).

SUMMARY

The Molten Salt Reactor (MSR) is an innovative future reactor technology with excellent performance in terms of safety and reliability, sustainability, proliferation resistance and economics. The very unique feature of this reactor concept is the liquid nature of the fuel which offers numerous advantages concerning the reactor safety. Nowadays, the research in Europe is focused on a promising design, the Molten Salt Fast Reactor (MSFR), that combines the generic assets of molten salt as liquid fuel with those related to fast neutron reactors and thorium fuel cycle. For the design of the reactor and in order to determine its safety limits, it is extremely important to have an accurate description of the physico-chemical properties of the fuel salt (such as the melting point, the boiling point and the vapour pressure). Moreover, a thorough knowledge of the fuel behaviour is required for the selection of the optimal composition. Potential fuel mixtures have been critically reviewed as fuel for the MSFR and the thermodynamic description of the most important systems will be presented in this work, starting from the basic LiF-ThF_4 system to more complex systems, such as LiF-ThF_4-PuF_3-UF_4, LiF-NaF-BeF_2-ThF_4-UF_4 and LiF-CaF_2-ThF_4.

The key system for the MSFR fuel is the binary mixture LiF-ThF_4. An extensive study on the thermodynamic properties of this system has been conducted and the improvements achieved in its description are reported in this thesis. The purification of the single components, in particular ThF_4, was an essential first step for the study of more complex systems. ThF_4 was purified using NH_4HF_2 as fluorinating agent and characterized by DSC and XRD analysis. Both techniques confirmed the high purity of the sample, which is particularly important for a reliable determination of its basic thermodynamic properties. The high temperature heat capacity of both the crystalline state and the liquid state was measured by drop calorimetry and the results are presented here for the first time.

The phase diagram of the binary LiF-ThF_4 system has been re-assessed in this work based on new experimental data. In order to describe the general shape of the binary system, the phase equilibria of some selected compositions have been measured. Moreover, the enthalpy of mixing of the LiF-ThF_4 liquid solution has been obtained using a novel method designed for the DSC technique. The phase diagram as optimized in this study consists of five invariant equilibria; two eutectics and three peritectics. Four intermediate compounds were found to be stable, namely Li_3ThF_7, $LiThF_5$, $LiTh_2F_9$ and $LiTh_4F_{17}$. Among these compounds, the most important is probably the Li_3ThF_7, which shows the lowest melting point in the system. It was synthesized and its enthalpy of fusion experimentally determined.

The vapor pressure of the fuel salt is also very important for the reactor safety as it determines its volatility with respect to temperature. In order to investigate this prop-

erty, several samples were prepared by mixing stoichiometric quantities of the two end-members LiF and ThF_4. The measurements were performed using the KEMS technique from 1000 K to 1400 K and four main gaseous species were found to be present in the mixed systems, namely LiF, Li_2F_2, Li_3F_3 and ThF_4. The total vapour pressure over the liquid solution was evaluated as function of temperature for all the measured compositions. Based on these measurements the thermodynamic activities of LiF and ThF_4 in the $Li_xTh_{1-x}F_{4-3x}$ liquid solution were also determined. The measured vapour pressures are very low in the temperature range of the MSFR operation and they are in good agreement with the pressure predicted by the thermodynamic model.

In conclusion, taking advantage of different sets of experimental data, the LiF-ThF_4 model has been improved. Vapour pressure and thermodynamic activities were not used to tune the thermodynamic model but agree well. Therefore, the results validate the predictive ability of the thermodynamic assessment.

For the start-up of the reactor an addition of fissile material is needed. One of the initial fissile choices in the MSFR concept is PuF_3. In order to predict the influence of this component on the melting behaviour of the LiF-ThF_4 solvent, the thermodynamic assessment of the LiF-ThF_4-PuF_3 system has been performed and the model has been confirmed by a series of experiments, using CeF_3 as proxy compound to PuF_3. In addition to the ternary mixture, UF_4 must also be present in the fuel to control the redox potential of the salt via the UF_4/UF_3 ratio. Therefore, the model was extended by addition of UF_4 describing the complete quaternary system LiF-ThF_4-PuF_3-UF_4.

The possibility of including an additional component in the MSFR fuel is currently under discussion. The additive may improve the physico-chemical properties of the fuel salt, as for example reducing its melting point. In the early designs, the only considered additive was BeF_2, which has a very low capture cross section. However, in the non-moderated concept other compounds such as NaF and CaF_2 could also be considered. The thermodynamic assessment of the LiF-NaF-BeF_2-ThF_4-UF_4 system has been performed in this thesis. Using all the data available in literature, two binary systems and five ternary systems have been newly assessed and different fuel options have been compared. To evaluate the influence of CaF_2 component, new experimental data were required. The binary phase diagram CaF_2-ThF_4 was described by coupling the measurement of phase equilibria points by DSC with diffraction studies for the identification of the phases in equilibrium. Based on the binary sub-systems, the LiF-CaF_2-ThF_4 ternary system has been extrapolated and optimized using newly measured experimental data on ternary mixtures.

The results of the present thesis have been used to improve the thermodynamic description on fluoride salts, including the fuel candidates for the MSFR. It has been shown that the model developed in this work is able to correctly reproduce all the experimental data measured and therefore can be considered as a valuable tool to predict the salt characteristic under normal and off-normal conditions of the MSR. Finally, a set of reference fuel options was identified based on their physico-chemical properties. The compositions reported represent the best candidates for the reactor fuel and can be used to define the operation reactor parameters and further develop the MSFR concept.

SAMENVATTING

De gesmoltenzoutreactor (MSR) is een innovatieve reactor technologie voor de toekomst met uitzonderlijke kenmerken wat betreft veiligheid, betrouwbaarheid, duurzaamheid, proliferatie bestendigheid en economie. De meest unieke eigenschap van de reactor is de vloeibare toestand van de splijtstof, waardoor diverse voordelen ontstaan met betrekking tot reactor veiligheid. Momenteel richt het onderzoek in Europa zich op een veelbelovend ontwerp, de snelle gesmoltenzoutreactor (MSFR), die de generieke voordelen van gesmolten zout als splijtstof combineert met die van snelle reactoren en van de thorium spijtstofketen. Voor het ontwerp van de reactor en in het bijzonder voor het bepalen van de veiligheidslimieten, is het belangrijk om over een nauwkeurige beschrijving van de fysisch-chemische eigenschappen van het splijtstofzout (zoals smeltpunt, kookpunt en dampspanning) te beschikken. Bovendien is kennis van deze eigenschappen noodzakelijk voor de selectie van de beste zoutsamenstelling. Mogelijke nieuwe zoutmengsels voor de MSFR worden in dit proefschrift geanalyseerd en de thermodynamische beschrijving van de belangrijkste systemen wordt gepresenteerd, te beginnen bij het LiF-ThF_4 systeem, en vervolgens complexere systemen zoals LiF-ThF_4-PuF_3-UF_4, LiF-NaF-BeF_2-ThF_4-UF_4 en LiF-CaF_2-ThF_4.

Als brandstof voor de MSFR bezet het binaire mengsel LiF-ThF_4 een sleutelpositie. Een uitgebreide studie van de thermodynamische eigenschappen van dit systeem werd uitgevoerd, en de verbeteringen in de beschrijving worden in dit proefschrift gepresenteerd. De zuivering van de betreffende verbindingen, in het bijzonder ThF_4, was een essentieële stap voor de studie van complexere systemen. ThF_4 werd gezuiverd met NH_4HF_2 als fluorinatiemiddel en geanalyseerd met behulp van DSC en röntgendiffractie. Beide technieken bevestigden de hoge zuiverheid van het materiaal, wat in het bijzonder van belang is voor de nauwkeurige bepaling van de thermodynamische eigenschappen van het materiaal. De hoge-temperatuur soortelijke warmte in zowel de kristallijne als in de vloeibare vorm werden gemeten met behulp van valcalorimetrie, en deze unieke resultaten worden hier voor het eerst gepresenteerd.

Het fasediagram van het LiF-ThF_4 systeem werd in dit proefschrift op basis van nieuwe experimentele gegevens opnieuw geëvalueerd en gemodeleerd. Om de vorm het binaire systeem goed te beschrijven werden fasenevenwichten voor geselecteerde samenstellingen gemeten. Ook werden de mengenthalpie van de LiF-ThF_4 vloeibare fase gemeten met een nieuw ontwerp voor de DSC. Het fasediagram, dat door middel van de optimalisatie werd verkregen, toont vijf invariante evenwichten: twee eutectica en drie peritectica. Vier verbindingen zijn stabiel in het systeem: Li_3ThF_7, $LiThF_5$, $LiTh_2F_9$ en $LiTh_4F_{17}$. Li_3LiF_7 is hiervan de belangrijkste en heeft het laagste smeltpunt. Deze verbinding werd gesynthetiseerd en het smeltpunt werd gemeten.

De dampspanning van het splijtstofzout is eveneens erg belangrijk voor de reactorveiligheid, aangezien het de relatie tussen vluchtigheid en temperatuur bepaalt. Om deze eigenschap van het zout te bepalen werden door middel van het mengen van stoichiometrische hoeveelheden van de eindleden LiF en ThF_4 verschillende monsters gemaakt. De metingen werden tussen 1000 en 1400 K met de KEMS uitgevoerd en vier gasvormige verbindingen werden waargenomen, LiF, Li_2F_2, Li_3F_3 en ThF_4. De totale dampspanning boven de vloeibare fase werd als functie van temperatuur en samenstelling bepaald. Op basis van deze metingen werd eveneens de thermodynamische activiteit van LiF en ThF_4 in de vloeibare oplossing $LiF_xTh_{1-x}F_{4-3x}$ bepaald. The gemeten dampspanning is zeer laag in het temperatuurbereik van de MSFR en is in goede overeenstemming met de dampspanning, die door middel van het thermodynamisch model is verkregen.

Het kan worden geconcludeerd, dat met behulp van de verschillende experimentele gegevens het LiF- ThF_4 systeem is verbeterd. De experimentele gegevens voor dampspanning en de thermodynamische activiteit werden niet gebruikt om het thermodynamisch model te optimaliseren, maar zijn wel in goede overeenstemming. De resultaten valideren dus het voorspellend vermogen van het thermodynamisch model.

Voor het opstarten van de reactor is het toevoegen van een splijtbaar materiaal noodzakelijk. Een van de eerste keuzes voor de MSFR is PuF_3. Om de invloed van deze toevoeging op het smeltgedrag van het LiF- ThF_4 systeem te bepalen, werd een thermodynamische evaluatie van het LiF-ThF_4-PuF_3 systeem uitgevoerd en het model gevalideerd met een serie experimenten met CeF_3 als simulant van PuF_3. In aanvulling op het ternaire mengsel, moet ook UF_4 aanwezig zijn in het splijtstofzout om de redox eigenschappen van het zout te controleren via de UF_4/UF_3 verhouding. Daarom werd het model verder uitgebreid met UF_4, om het complete quaternaire systeem LiF-ThF_4-PuF_3-UF_4 te beschrijven.

De mogelijkheid om aanvullende componenten aan het splijtstofzout toe te voegen wordt momenteel geanalyseerd. Deze aanvullingen kunnen de fysisch-chemische eigenschappen van het splijtstofzout verbeteren, bijvoorbeeld het verlagen van het smeltpunt. In de eerste ontwerpen was BeF_2 de enige aanvullende component die werd beschouwd, aangezien het een zeer lage vangstdoorsnede voor neutronen heeft. Echter in niet-gemodereerde concepten kunnen andere verbindingen, zoals NaF en CaF_2, worden overwogen. De thermodynamische evaluatie van het LiF-NaF-BeF_2-ThF_4-UF_4 systeem werd in het kader van dit proefschrift uitgevoerd. Op basis van de gegevens die in de literatuur beschikbaar zijn, werden twee binaire systemen en vijf ternaire systemen opnieuw geëvalueerd en verschillende splijtzout samenstellingen vergeleken. Om de invloed van CaF_2 te bepalen, waren aanvullende experimentele gegevens nodig. De beschrijving van het binaire system CaF_2-ThF_4 werd verkregen door het koppelen van DSC metingen van de fasenevenwichten en röntgendiffractie om de fasen in het systeem te identificeren. Op basis van de binaire systemen werd het ternaire systeem verkregen en aan de hand van experimentele gegevens voor het ternaire systeem verder geoptimaliseerd.

De resultaten, die in dit proefschrift worden gepresenteerd, werden gebruikt om de thermodynamisch beschrijving van fluoride zouten te verbeteren, inclusief de mogelijke samenstelling voor het MSFR splijtstofzout. Het werd aangetoond, dat het in dit

proefschrift ontwikkelde model in staat is om alle experimentele gegevens correct weer te geven en kan daarom als een waardevol instrument worden beschouwd om het zoutgedrag tijdens normaal bedrijf en tijdens ongevalssituaties in een MSR te voorspellen. Ten slot werd op basis van hun fysisch-chemische eigenschappen een stel splijtstofzout samenstellingen geïdentificeerd. Diegene, die in dit proefschrift worden gepresenteerd, zijn de beste mogelijkheden voor het splijtstofzout en kunnen worden gebruikt om de bedrijfscondities te bepalen en het MSFR concept verder te ontwikkelen.

CURRICULUM VITÆ

Elisa CAPELLI

12-10-1987 Ponte S. Pietro (BG), Italy

EDUCATION

2016 Ph.D.
Faculty of Applied Sciences
Delft University of Technology, Delft, Netherlands.

Thesis: Thermodynamic characterization of salt components for Molten Salt Reactor fuel
Promotor: Prof. dr. R.J.M. Konings

2009-2012 Master degree in Nuclear Engineering
Politecnico di Milano, Milano, Italy

2006-2009 Bachelor degree in Physics Engineering
Politecnico di Milano, Milano Italy

2001-2006 Chemistry High School
Istituto Tecnico Industriale di Stato "G. Natta", Bergamo, Italy

AWARDS

2015 ENEN (European Nuclear Education Network) PhD Prize
for the Best Presentation of relevant Research in Nuclear fields

PROFESSIONAL EXPERIENCE

2012-2015	Grantholder European Commission, Joint Research Centre Institute for Transuranium Elements Karlsruhe, Germany.
2011-2012	Trainee European Commission, Joint Research Centre Institute for Transuranium Elements Karlsruhe, Germany.

LIST OF PUBLICATIONS

10. **E. Capelli**, O. Beneš, R. J. M. Konings, *Heat capacity of ThF_4 from T=400* K *to T= 1550* K, in preparation, (2015).

9. **E. Capelli**, O. Beneš, J.-Y. Colle, R. J. M. Konings, *Determination of the thermodynamic activities of LiF and ThF_4 in the $Li_xTh_{1-x}F_{4-3x}$ liquid solution by Knudsen Effusion Mass Spectrometry*, Physical Chemistry Chemical Physics **17**, 30110 (2015) .

8. **E. Capelli**, O. Beneš, P. E. Raison, M. Beilmann, C. Künzel , R. J. M. Konings, *Thermodynamic investigation of the CaF_2-ThF_4 and LiF-CaF_2-ThF_4 systems* , Journal of Chemical and Engineering Data **60**, 3166 (2015).

7. B. Claux, O. Beneš, **E. Capelli**, P. Souček, R. Meier, *On the fluorination of PuO_2 by NH_4HF_2*, submitted to Journal of Fluorine Chemistry, (2015).

6. **E. Capelli**, O. Beneš , R. J. M. Konings, *Thermodynamic assessment of the LiF-ThF_4-PuF_3-UF_4 system*, Journal of Nuclear Materials **462**, 43 (2015).

5. **E. Capelli**, O. Beneš , R. J. M. Konings, *Excess heat capacity of the $(Li_{1-x}Ca_x)F_{1+x}$ liquid solution determined by differential scanning calorimetry and drop calorimetry*, Journal of Chemical Thermodynamics **81**, 160 (2015).

4. **E. Capelli**, O. Beneš , R. J. M. Konings, *Thermodynamic assessment of the LiF-NaF-BeF_2-ThF_4-UF_4 system*, Journal of Nuclear Materials **449**,111 (2014).

3. **E. Capelli**, O. Beneš , R. J. M. Konings, *Thermodynamic investigation of the LiF-ThF_4 system*, Journal of Chemical Thermodynamics **58**,110 (2013).

2. M. Beilmann, O. Beneš, **E. Capelli**, V. Reuscher, R. J. M. Konings, and Th. Fanghänel, *Excess heat capacity in liquid binary alkali-fluoride mixtures*, Inorganic chemistry **52**, 2404 (2013).

1. O. Beneš, D. Sedmidubský, M. Beilmann, O. S. Vălu, **E. Capelli**, M. Salanne, S. Nichenko, R.J.M. Konings, *A comprehensive study of the heat capacity of CsF from 5* K *to 1400* K, Journal of Chemical Thermodynamics **57**, 92 (2013).

ACKNOWLEDGEMENTS

"All things begin and end, as stories." The time I spent at ITU, first as trainee and starting my PhD after, was great. And at the end of this story, I really feel like I want to express my gratitude to many people that have helped me during these years. I could not have succeeded without the invaluable support of a several.

The work performed in this thesis was supported by the European Commission in the Framework of the EVOL project of the 7th Framework Programme. I would like to thank the former and the present director of the Institute of Transuranium Elements, Prof. Dr. Fanghänel and Dr. Betti, to have given me the possibility to perform this project. I would also like to thank the TU Delft for giving me the possibility with this work to candidate for PhD at the Faculty of Applied Sciences.

I acknowledge all the doctoral committee members for the precious time and comments.

I owe my gratitude to Prof. Dr. Rudy Konings, who has been the promotor and a supervisor of this thesis. I appreciate all the contributions of time and ideas as well as the nice discussions, which have made my PhD stimulating.

An heartfelt and special thanks goes to Dr. Ondřej Beneš. He was not only my supervisor at ITU, but a mentor and friend. He has challenged, motivated and encouraged me in so many ways during this years. Through his eyes I could see the good even in the worst results. For sharing his knowledge with me, for the several scientific discussions, for the confidence and for the time spent together, I am forever grateful. Thank you, Ondrej!

All the colleagues of the Materials Research unit have contributed immensely to my personal and professional time at ITU, a source of friendships as well as good advice and collaboration. Jean-Yves Colle and Mark Sierig deserve a special mention for their precious support in the lab, I could always count on some technical advices and collaboration. In particular, thanks to Jean-Yves for his expertise and the help during the KEMS measurements and to Mark for his enthusiasm and help during the welding of the crucibles. I am also thankful for the collaboration in the lab and the discussions to Konstantinos Boboridis, Alex Dockendorf, Dario Manara, Mohamed Naji, Anna Smith, Luka Vlahovic, and to the Laser Flash group, for tolerating my frequent bag-in/bag-out. I would also like to mention and thank the microscopy group, Thierry Wiss, Bert Cremer and Markus Ernstberger for the SEM/EDX analysis. Last, but not least, thanks to Petra for the help with all the administrative issues and for having a patient answer to all my innumerous questions.

It was a great pleasure to collaborate with many great people, not only in the Materials Research Unit. I am indebted to Dr. Philippe Raison for several discussions that

helped me to build my knowledge on XRD and the Rietveld analysis. I would like to thank Daniel Bouexiére and Giorgio Pagliosa for performing the XRD measurements and Laura Martel for the NMR measurements. A special thanks also to Dr. Pavel Souček and Roland Meier, for the nice work together and the samples.

A warm thank you to the secretaries of the Department of Radiation Science and Technology and of the Faculty of Applied Sciences at TU Delft, Thea Miedema and Ans van Schaik, for the help and assistance concerning the administrative issues.

For introducing me to ITU and for his constant interest, I would like to thank Prof. Dr. Lelio Luzzi.

My time at ITU was made enjoyable in large part due to the many friends that became part of my life. I wish to offer my most heartfelt thanks to all of them. To the Italian Trainee Group 2011, Luca, Andrea, Fidelma and Valentina, and to the new entries, Davide and Sara. To Tsveti, Jhonny, Laura, Vaclav, Emily, Sylvain and Valentino, thanks *******! To the members of the climbing club for sharing with me some nice climbing sessions. To my officemates, Fidelma and Mohamed for the nice office environment.

A big thank you to Fabiola, who shared with me this experience and became one of my best friends. We have shared so many moments and experiences, that I cannot imagine my life in ITU and in general the last three years without her friendship and support.

Of course no acknowledgments would be complete without giving thanks to my parents and my brother for their unconditional support. Last but definitely not least Gian, I have managed to complete my thesis only thanks to his constant support, motivation and patience. I don't have words to express my gratitude.

Elisa Capelli